JAERI-Review
99-028

JAERI TANDEM & V.D.G. ANNUAL REPORT 1998 APRIL 1, 1998-MARCH 31, 1999

December 1999

Department of Materials Science

日本原子力研究所
Japan Atomic Energy Research Institute

本レポートは、日本原子力研究所が不定期に公刊している研究報告書です。
入手の問合わせは、日本原子力研究所研究情報部研究情報課（〒319-1195　茨城県那珂郡東海村）あて、お申し越し下さい。なお、このほかに財団法人原子力弘済会資料センター（〒319-1195　茨城県那珂郡東海村日本原子力研究所内）で複写による実費領布を行っております。

This report is issued irregularly.
Inquiries about availability of the reports should be addressed to Research Information Division, Department of Intellectual Resources, Japan Atomic Energy Research Institute, Tokai-mura, Naka-gun, Ibaraki-ken 319-1195, Japan.

編集兼発行　日本原子力研究所

JAERI－Review 99－028

JAERI TANDEM & V.D.G.
Annual Report
1998
April 1, 1998 – March 31,1999

Department of Materials Science※

Tokai Research Establishment
Japan Atomic Energy Research Institute
Tokai-mura, Naka-gun, Ibaraki-ken

(Received November 2,1999)

This annual report describes research activities which have been performed with the JAERI tandem accelerator and the Van de Graaff accelerator from April 1, 1998 to March 31, 1999. Summary reports of 38 papers, and lists of publication, personnel and cooperative research with universities are contained.

Keywords: JAERI Tandem, V.D.G., Nuclear Structure, Nuclear Reactions, Nuclear Theory, Atomic Physics, Solid State Physics, Radiation Effects in Materials, Progress Report.

※ Editors: Suehiro TAKEUCHI, Hiroshi IKEZOE, Satoshi CHIBA, Msasao SATAKA, Yuichiro NAGAME,Satoshi TAKEMORI, and Akira IWAMOTO

JAERI－Review 99－028

原研タンデム、バンデグラフ加速器 １９９８年度年次報告

日本原子力研究所東海研究所
物質科学研究部※

（１９９９年１１月２日受理）

本年次報告書は、東海研究所の原研タンデム及びバンデグラフ加速器で、１９９８年４月１日から１９９９年３月３１日までの間に行われた研究活動をとりまとめたものである。

(1) 加速器の運転と開発研究　(2)核構造　(3)核反応　(4)核理論　(5)原子分子物理・固体物理及び材料の放射効果の５部門にまたがる 38 編の研究報告、公表された文献、関与した職員及び大学等との協力研究のリストを収録している。

東海研究所：〒319-1195　茨城県那珂郡東海村白方白根２－４
※（編集者）竹内末広・池添　博・千葉　敏・左高正雄・永目諭一郎
竹森聡司・岩本　昭

Contents

1. Accelerator Operation and Development. 1
1.1 Tandem Accelerator and Booster Operation. 3
1.2 Utilization of Tandem Accelerator and Booster. 4
1.3 ECR Plasma Processing of Superconducting Resonator Surfaces. 5
1.4 Acceleration Results of In-terminal ECR Ion Source. 7
2. Nuclear Structure. 9
2.1 Excited States of the Neutron-rich Nucleus ^{168}Dy. 11
2.2 Excited States in the Doubly Magic ^{68}Ni and Its Neighbour ^{69}Cu. 13
2.3 High Spin States of ^{155,156}Gd. 15
2.4 Coulomb Excitation of 9$^-$ Isomer in ^{180}Ta. 16
2.5 Mean-square Nuclear Charge Radius of ^{144}Ce. 18
2.6 Half-life of ^{235}Am. 20
2.7 Application of the Method of Multidimensional Spectrum to Analytical Chemistry. 22
2.8 Three-nucleon Cluster Structure in the A=19 Mirror Nuclei; ^{19}F and ^{19}Ne. 23
2.9 $(\nu g_{9/2}^{-2})_8^+$ Isomers in $^{82}Se_{48}$ and $^{80}Ge_{48}$ Populated by Deep-inelastic Collisions. 25
2.10 In-beam γ-ray Study of ^{79,80}Kr. 27
2.11 High-spin States in ^{180}Os. 29
3. Nuclear Reactions. 31
3.1 Energy Dependence of the Two-Neutron Transfer Reaction in the Ni+Ni System Around the Coulomb Barrier. 33
3.2 Nucleon Interaction and Collective Structure of ^{12}C by the Soft-rotator Model. 35
3.3 Sub-barrier Fusion of Deformed Nuclei in the Reactions of ^{60}Ni+^{154}Sm and ^{32}S+^{182}W. 37
3.4 Measurement of Fusion Cross Section for ^{32}S+^{182}W. 40
3.5 Preequilibrium Fission Following Fusion of ^{32}S+^{182}W. 42
3.6 Measurement of Fusion- and Evaporation Residue Cross Sections for ^{28}Si+^{198}Pt. 44
3.7 Source Preparation for γ-ray Emission Probability Measurement of Proton-rich Nuclei. 46

3.8 Deformation Degrees of Scissioning Nuclei..... 47
4. Nuclear Theory..... 49
4.1 Systematic Studies of Fission Saddle-point Shapes..... 51
5. Atomic Physics, Solid State Physics and
Radiation Effects in Materials..... 53
5.1 Ejected Electron Spectra from High Energy Highly
Charged Oxygen Ions in Collisions with Helium Atoms..... 55
5.2 High-resolution Zero-Degree Electron Spectroscopy (V)..... 57
5.3 Emission of Secondary Ions from Conductive Materials
Bombarded with Heavy Ions..... 60
5.4 The Effect of Splayed Columnar Defects on Transport
Characteristics in $YBa_2Cu_3O_y$ Thin Film..... 62
5.5 Introduction of Columnar Defects in Bi-2212
Single Crystals by High-energy Heavy-Ion Irradiation..... 64
5.6 Novel Asymmetric Critical State in $YBa_2Cu_3O_{7-\delta}$
with Columnar Defects..... 66
5.7 Josephson Plasma Resonance in Heavy Ion
Irradiated $Bi_2Sr_2CaCu_2O_{8+\delta}$ Single Crystals..... 68
5.8 Influence of Ion Velocity on Damage Efficiency in
the $Bi_2Sr_2CaCu_2O_x$ Single Crystal Irradiated with Au Ions..... 71
5.9 Structure of Defects Induced by High-Energy Heavy Ions
in High-Tc Superconductor..... 73
5.10 Superconductivity and Weak Localization in
Multi-layered Ge/Nb Films..... 75
5.11 Effects of **Electronic Excitation on Radiation Annealing**
in Iron by Energetic Ion Irradiations..... 78
5.12 Radiation Defects in Nanocrystalline Materials 80
5.13 Study of Irradiation Embrittlement Mechanism
with High Energy Ions..... 81
5.14 Tolerance of Single Event Burnout in Power MOSFETs
Caused by High-Energy Ions..... 84
6. Publication in Journal and Proceedings, and contribution to
Scientific Meetings..... 87
7. Personnel and Committees..... 111
8. Cooperative Researches..... 119

目　次

1. 加速器の運転状況および開発..... 1
1.1 タンデム加速器とブースターの運転..... 3
1.2 タンデム加速器とブースターの利用..... 4
1.3 超伝導空洞表面のＥＣＲプラズマ処理..... 5
1.4 ターミナル内 ECR イオン源の加速試験結果..... 7
2. 原子核構造..... 9
2.1 中性子過剰核 ^{168}Dy の励起準位..... 11
2.2 二重閉殻 ^{68}Ni と隣接核 ^{69}Cu の励起状態..... 13
2.3 ^{155,156}Gd の高スピン状態..... 15
2.4 ^{180}Ta の 9⁻アイソマーのクーロン励起 16
2.5 ^{144}Ce の平均２乗核荷電半径..... 18
2.6 ^{235}Am の半減期..... 20
2.7 多重ガンマ線スペクトルの分析化学への応用..... 22
2.8 A=19 鏡映核 ^{19}F, ^{19}Ne における３核子クラスター構造..... 23
2.9 深部非弾性散乱による $^{82}Se_{48}$, $^{80}Ge_{48}$ の$(\nu g_{9/2}^{-2})_8^+$アイソマー..... 25
2.10 ^{79,80}Kr のインビームγ線分光..... 27
2.11 ^{180}Os の高スピン状態..... 29
3. 原子核反応..... 31
3.1 クーロン障壁近傍での Ni+Ni の系の２中性子移行反応の
入射エネルギー依存性..... 33
3.2 Soft-rotator モデルによる ^{12}C の核子入射反応及び
集団構造の研究..... 35
3.3 ^{60}Ni+^{154}Sm 及び ^{32}S+^{182}W 反応における変形核サブバリアー
融合反応..... 37
3.4 ^{32}S+^{182}W の融合断面積の測定..... 40
3.5 ^{32}S+^{182}W の融合反応における非平衡核分裂..... 42
3.6 ^{28}Si+^{198}Pt の融合および蒸発残留核断面積の測定..... 44
3.7 陽子過剰核のγ線放出率測定のための線源作製..... 46
3.8 分離点原子核の変形度..... 47
4. 原子核理論..... 49
4.1 核分裂鞍部点の形の系統的研究..... 51
5. 原子分子物理、固体物理及び材料の照射効果..... 53
5.1 高速の酸素多価イオンと He 原子の衝突による放出電子分光.... 55

5.2 0度電子分光による高励起Si, Sイオンからの
放出電子スペクトル(V)..... 57
5.3 高エネルギー重イオン衝突による伝導材料からの
二次イオン放出..... 60
5.4 $YBa_2Cu_3O_y$薄膜の輸送特性に対するスプレー柱状欠陥導入
の効果..... 62
5.5 高エネルギー重イオン照射によるBi-2212単結晶への
円柱状欠陥の導入..... 64
5.6 柱状欠陥を導入した$YBa_2Cu_3O_{7-\delta}$における
新しい非対称臨界状態..... 66
5.7 重イオン照射された$Bi_2Sr_2CaCu_2O_{8+\delta}$単結晶における
ジョセフソンプラズマ共鳴..... 68
5.8 $Bi_2Sr_2CaCu_2O_x$単結晶を用いたAuイオン照射における損傷効率
へのイオン速度の影響..... 71
5.9 高エネルギー重イオン照射による高温超伝導体の欠陥構造..... 73
5.10 Ge/Nb多層薄膜における超伝導と弱局在..... 75
5.11 高エネルギーイオン照射による鉄の照射アニーリングへの
電子励起効果..... 78
5.12 ナノクリスタルにおける照射欠陥の研究..... 80
5.13 高エネルギーイオン照射を用いた脆性機構の研究..... 81
5.14 高エネルギーイオンによるPower MOSFETの
シングルイベントバーンアウト耐性..... 84
6. 雑誌および国際会議等の刊行物、学会報告..... 87
7. 関連課室、職員および委員会..... 111
8. 共同・協力研究..... 119

PREFACE

This report covers research and development activities using the tandem accelerator and its superconducting booster at JAERI, Tokai, for the period from April 1, 1998 to March 31, 1999. During this period, the tandem accelerator was operated over 3,700 hours and delivered stable beams to the experiments in the fields of accelerator developments, nuclear structure, nuclear reactions, atomic physics, solid state physics and radiation effects in materials. The superconducting booster was utilized for 42 days on 10 experimental subjects of nuclear structure and reactions. Sixteen research programs have been carried out in collaborations with about a hundred researchers from universities and research institutes.

A compact electron cyclotron resonance ion source (ECRIS) installed in the high voltage terminal has come into operation for experiments. Beams of proton, oxygen, nitrogen, argon, krypton, and xenon were accelerated. Upgrading the system in two directions is under way; one is to get a metallic ion beam using a metal-organic compound and the other is to produce more highly charged heavy-ion beams using a bigger high-performance ECRIS.

In the field of nuclear science, the new neutron deficient americium isotope ^{233}Am produced in ^{233}U(^{6}Li,6n) reaction has been identified with the gas-jet coupled JAERI-ISOL system. Using the deep inelastic collisions of ^{70}Zn on ^{198}Pt, new isomers of ^{68}Ni and ^{69}Cu have been found. Gamma-ray detector array GEMINI has been successfully applied to analytical chemistry, where the method revealed to have the ability of detecting the materials of concentration down to the order of 10^{-9}. In the field of materials science, radiation damage study on light water pressure vessel steel has been started by using heavy-ion beams for Fe-Cu model alloys. The study on secondary ion emission after the irradiation of materials by high energy heavy-ions showed that the electronic excitation plays an important role in conductive materials as well as in insulators.

A symposium on "Heavy-Ion Science in the Energy Region of Tandem Accelerator" was held on Jan. 12 and 13, 1999 at Mito Joyo-Geibun hall. Twenty five talks and fifty one posters which covered the whole activities of JAERI Tandem and Booster accelerators were presented. There were lively discussions among researchers of nuclear science and materials science.

Akira Iwamoto
Deputy Director
Department of Materials Science

This is a blank page.

1. Accelerator Operation and Development

This is a blank page.

1.1 TANDEM ACCELERATOR AND BOOSTER OPERATION

ACCELERATORS OPERATION GROUP

Tandem Accelerator and Booster: The operations of the tandem accelerator for experiments were performed as scheduled in the past one year. There were three short periods of scheduled maintenance. The running time was 3706 hours. The summary of the operation from April 1, 1998 to March 31, 1999 is as follows.

1) Time distribution in terms of terminal voltages (Tandem accelerator)

>16 MV	9 days	5.8 %
15-16	74	48.1
14-15	28	18.1
13-14	3	2.0
12-13	7	4.6
11-12	5	3.3
10-11	21	13.6
9-10	5	3.3
8-9	0	0
<8	2	1.2

Booster operation

^{58}Ni	-310 MeV	9 days
^{70}Zn	565	4
^{76}Ge	635	8
^{90}Zr	390	1
^{136}Xe	500	1

The tandem accelerator had 6 unexpected tank openings in this fiscal year due to troubles of the control system and the vacuum system on the tandem accelerator which were considered to be affected by the new arrangement for the ECR ion source. Thirty-one days of the scheduled machine time were canceled for these troubles. The super-conducting booster was utilized for 23 days for 8 experimental subjects. The booster ran steadily at field gradients below 4.5MV/m. During these times, the tandem booster and its helium refrigeration systems were operated 2 periods during 2 scheduled machine time periods excluding a brief stop by scheduled maintenance. The helium refrigeration systems were in operation for 87 days from May 11, 93 days from September 16 in 1998.

From the beginning of August to the middle of September, the helium compressor systems had an overhaul maintenance which was the first time since their installation it in 1993, and oil absorption materials and moisture filtering system were changed and reactivated to maintain the helium gas qualities.

1.2 UTILIZATION OF TANDEM ACCELERATOR AND BOOSTER

T. YOSHIDA and S. KANDA

The utilization of the tandem accelerator facility was carried out for 154 days for various experiments in three scheduled machine times in the FY 1998. But, 12 research programs, 31 days were canceled due to troubles of the tandem accelerator.
The collaboration research programs for the FY 1998 were examined at late November in 1997, and 16 subjects were accepted by the rprogram committee. These programs accounted for approximately 67% of the whole machine time. Seventeen ion species were utilized in the 3 experimental periods as follows. Especially, we installed the electron cyclotron resonance (ECR) ion source in the high voltage terminal of tandem accelerator and we got some inert gas ions and low charge state, high current nitrogen, oxygen and hydrogen ions successfully. The ECR ion source test report are described in the accelerator developing section of this report.

1) Time distribution in terms of projectiles

$^{1}H(^{2}H)$	12 days	^{64}Zn	8 days
$^{6,7}Li$	8	^{74}Ge	12
$^{12,13}C$	1	^{79}Br	1
$^{16,18}O$	11	^{90}Zr	1
^{31}P	6	^{107}Ag	3
$^{32,33}S$	29	^{127}I	5
$^{35,37}Cl$	3	^{136}Xe	3
^{45}Sc	2	^{197}Au	11
$^{58,60}Ni$	30		

The experimental terms allotted in the three periods were 81 days in May 11 to August 9, 85 days in September 24 to January 21 in 1999 and 21 days in March 11 to end of March. The last term was continued to 1st machine time period in FY 1999. The summary of allotted time to various experimental subjects is as follows.

Research field	allotted days	total number of subjects
Nuclear physics	83	26
Atomic and Solid-state physics	48	36
Nuclear chemistry	19	8
Material research	7	5
Accelerator development	6	6

1.3 ECR PLASMA PROCESSING OF SUPERCONDUCTING RESONATOR SURFACES

S. TAKEUCHI

Some of the superconducting resonators in the tandem-booster are infected with "Q-disease" that is attributed to hydrogen pollution in the niobium superconductor during electro-chemical surface treatments and precipitation of hydrides at around 120K during precooling process. Such degradation in Q-factors lowers the accelerating gradients to a level as low as 3 MV/m from 5 MV/m which is usually available for healthy resonators. A fast cool-down technique through the precipitation temperatures of 130-90K can be taken as an expedient method of reducing the Q-degradation at each time of precooling[1]. For an ideal cure of the Q-disease, hydrogen needs to be outgassed from the niobium. The resonators used in the tandem booster are composed of a niobium center conductor and an outer conductor made of niobium-copper composite plates. Heating can be applied to the center conductor part, but not to a whole resonator. As a possible hydrogen outgassing method without heating, ECR(abbr. of electron cyclotron resonance) plasma processing has been investigated. ECR plasma processing is a dry cleaning method and brings no hydrogen pollution. Therefore, it can be hopefully applied to booster resonators not only for hydrogen outgassing and but also for re-surface-treatments.

It is expected for an outgassing mechanism that alpha-phase hydrogen atoms which are free from trapping by niobium or impurity atoms have a chance to arrive at the surface as a result of diffusion and to be kicked out by ion sputtering. If the sputtering probability is assumed to be 100 % in a calculation, hydrogen content can be reduced to 10% in 2 hours for a 2.5 mm thick wall or in 30 hours for a 10 mm thick wall[2]. The superconducting resonators consist of 2-2.5 mm and 9-10 mm thick niobium walls. It may take much more than 30 hours to have a substantial effect of outgassing. Ions in ECR plasma have low kinetic energies for moderate rf input, so that physical sputtering is very weak, but chemical sputtering can be strong if we use a gas which contains chemically active atoms. For example, hydrogen gas has been used for outgassing oxygen from the walls of nuclear fusion apparatus[3]. We need to find a gas effective for hydrogen outgassing.

In FY 1998, an ECR plasma processing apparatus was set up and the first experiment was done with a spare resonator. The experimental set-up is illustrated in Fig. 1. A resonator was placed in a solenoid, pumped by a turbo-molecular pump and fed with 2.45 GHz rf wave. The magnetic field at the ECR condition is in the vicinity of 0.088 T.

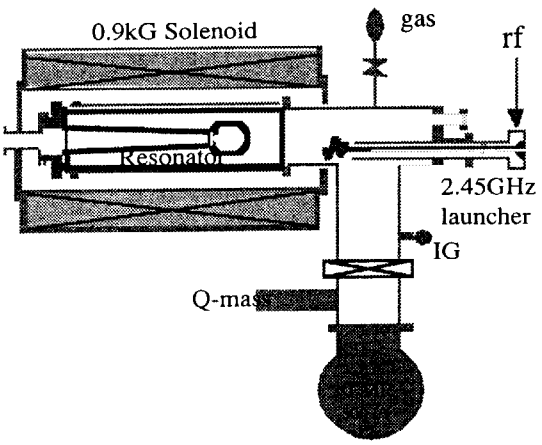

Fig. 1. Set-up for ECR plasma surface processing

ECR plasma was formed at a pressure of 3 - 5 $\times 10^{-3}$ Pa for every gas. First two experiments were done in FY 1998 with hydrogen and helium gases using a spare resonator. After each ECR processing, the resonator was moved into a testing cryostat and Q-values were measured at 4.2K for the two cases of fast(40-60K/h) and slow(10-12K/h) precoolings from 130K to 90 K. We had a decrease in Q after a hydrogen processing. After a helium processing with 100W RF input for 60 hours, we had 30% and 50 % increases in Q for the fast and slow precoolings, respectively. This is a promising result for curing Q-disease.

From now on, we will investigate the ECR plasma processing with various gases using the spare resonator and with niobium samples instead of real resonators, to see hydrogen outgassing and cleaning effects, and measure characteristics of plasma with different gases as a function of rf input power.

References

[1] S. Takeuchi and M. Matsuda, Proc. of the Eighth Workshop on RF Superconductivity, Abano Terme(1997)pp237-247.
[2] S. Takeuchi, Proc. of the 2nd Superconducting Linear Accelerator Meeting in Japan, Tsukuba (1999), to be published.
[3] for example: S. Kato, N. Noda, H. Oyama, K. Akaishi, T. Senju, K. Kanako, O. Motojima, J. Sakamoto and A. Iiyoshi, J. Nucl. Mater. 162-164(1989)pp763-768.

1.4 ACCELERATION RESULTS OF IN-TERMINAL ECR ION SOURCE

M. MATSUDA, S. TAKEUCHI and C. KOBAYASHI[1]

The in-terminal ECR ion source (TECRIS) was installed in the high voltage terminal of the tandem accelerator in April, 1998. Some troubles were occurred by electric discharges and high pressure insulation gas for electric devices and vacuum leak. As a result of mending, however, acceleration tests have been successfully carried out with beams of H^+, N^{2+}, $O^{3+, 5+}$, $Ar^{8+, 9+}$ and $Xe^{12+, 13+}$ ions. Furthermore, it was proven to provide beams for the machine time schedule from the in-terminal ECR ion source.

After the first acceleration tests of H and Ar ions, occasional electric discharges were occurred in fault of the power supplies of Einzel lens, electrostatic steerer, bias voltage and two 45-degree magnets. These power supplies were exchanged by different type devices and inserted electrical surge filters for each of signal and power lines. The high voltage shield box had a hall in order to pass through a wave-guide, and the hall was covered with aluminum plate for completely electrical shield and insertion insulated wave-guide. The cold line of secondary wiring of the insulating transformer was directly connected to the high voltage shield box. As a result of these measures, fatal damages of power supplies were not occurred, but small troubles, for instance, could not read monitor output, were sometimes occurred. However, since it is difficult to make these troubles clear, we have to take trial and error method.

Some improvements were made in ion source and injector system. The electrostatic steerer was improved in its performance; old type power supplies, which were controlled only one side electrode voltage and the other was fixed, were replaced for both side electrode controllable system. Since the penning discharge in the extraction insulator duct caused ceramic insulator deterioration, the new extraction insulator duct with three 5mm inner ditches was in place of it. As a result of acceleration tests, the aperture located in entrance of acceleration tube (VA TH-1) was spread from 4.8mmϕ to 6.0mmϕ in order to improve beam transmission.
Gas feeding system is shown in Figure 1. The number of gas lines of the source gas feeding system was increased to three from two in order to increase beam species. One of the three gas line was used a thermo-mechanical-leak valve connected to motor driven slidac for the gas flow control. Other two gas lines were used shut-off calibrated leak source valves which dead volume was limited to 0.0001cc in order to get good vacuum immediately after closing valve and simplified operation. These valves were driven by solenoid magnet.

The results of acceleration experiments for H, N, O, Ar and Xe ion are presented in Table 1.

Table 1. The result of acceleration experiments

Ion species	Charge State	Current [eμA]	Energy [MeV]	Ion species	Charge State	Current [eμA]	Energy [MeV]
H	1	2.3	14	Ar	8	3.4	104
H	1	1.8	15.6	Ar	9	0.24	126
N	2	1.0*	28	Ar	9	0.67	126
O	3	1.5*	42	^{132}Xe	12	1.3	192
O	5	0.15	70	^{132}Xe	13	0.17	182
Ar	6	2.1	84	^{132}Xe	13	0.47	208
Ar	8	2.3	112	^{132}Xe	12→23	0.067	306**

*: Limited by radiation safety, **: using 2nd foil

In these experiments, the extraction and pre-acceleration voltages were 15kV and 80kV, respectively except for Xe ions. For Xe ions, the pre-acceleration voltage was set to 50kV, because the maximum field strength of the injection magnet was not high enough to bend the ions accelerated by 80kV. H^+ ions were

[1] Nihon Advanced Technology. Co.

generated by out-gas from vacuum chamber. Compared with conventional negative ion sources, TECRIS could produce the low energy and high intensity nitrogen and oxygen beams. It was proven that noble gas ions (Ar and Xe) were successfully accelerated, and these beam energies and intensities were equal to the neighboring mass ions from negative ion source. It was confirmed 2nd stripper could be able to increase beam energy up to about 300MeV for Xe beam. The beam profiles were very sharp at the object and image points of the analyzing magnet, since energy spread and beam scattering are smaller than the use of foil stripper.
Some problems were found. The resolution of digital to analog converter for post 45-degree injection magnet (BM TI-1) and electrostatic quadrupole triplet (EQ TH-2) are not so enough. As for EQ TH-2 power supplies, their accuracy and linearity are low, since the range required for TECRIS is less than 5% of full output.

On the other hand, metal ion extracted examination was performed at test bench by using a MIVOC (Metal Ions from Volatile Compounds) method [3]. Extracted current of Fe^{9+} and Fe^{10+} were 7e A and 2e A, respectively. However, it was difficult to select desired beam, because extracted beams often contained another ions from plasma chamber and gas lines smeared with volatile compounds.

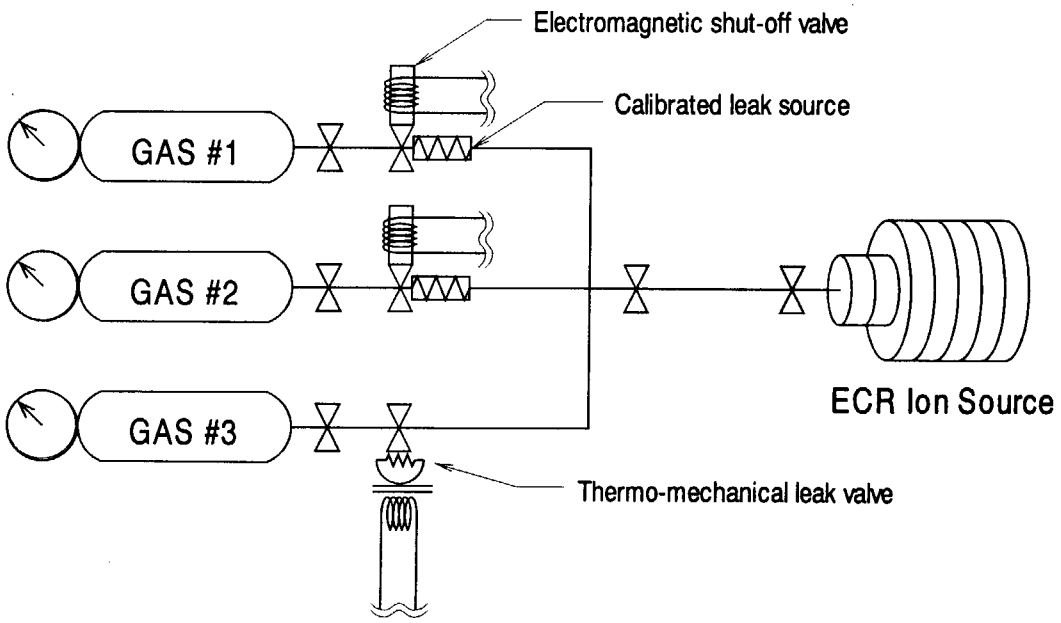

Figure 1. Gas feeding system for Terminal ECR ion source

References
[1] M. Matsuda et al., JAERI TANDEM & V.D.G. Annual Report 1996 pp7-8
[2] M. Matsuda et al., JAERI TANDEM & V.D.G. Annual Report 1997 pp10-12
[3] T. Nakagawa et al., Nucl. Instrum. & Methods A396 (1997) 9-12

2. Nuclear Structure

This is a blank page.

2.1 EXCITED STATES OF THE NEUTRON-RICH NUCLEUS ^{168}Dy

M. ASAI, S. ICHIKAWA, K. TSUKADA, M. SAKAMA[1], M. SHIBATA[2],
Y. KOJIMA[3], A. OSA, I. NISHINAKA, Y. NAGAME and K. KAWADE[2]

Neutron-rich nuclei with the mass $A > 160$ lie in the well deformed region near the midshell of both wide proton and neutron open shells. Experimental studies for these nuclei are, however, still limited to the vicinity of stable nuclei because of difficulties in their productions and observations. Despite recent progress in experimental techniques [1-4], in this mass region the most neutron-rich nuclei whose excited states have been experimentally established are the ones with only two neutrons in excess over the most neutron-rich even-even stable nuclei with only a few exceptions [2]. In the present work, we have identified excited states of ^{168}Dy, with four neutrons in excess over the most neutron-rich stable nucleus ^{164}Dy, through the β^- decay of ^{168}Tb, and discuss nuclear deformation around the midshell region.

The nucleus ^{168}Tb was produced through the proton-induced fission of ^{238}U. A stack of eight ^{238}U targets was bombarded with a 20 MeV proton beam of about 1 μA intensity. Fission products were transported into an ion source of the JAERI-ISOL by gas-jet stream, and mass-separated as monoxide ions [5]. Gamma-ray singles, β-γ and γ-γ coincidence measurements were performed.

Figure 1 shows a β-coincident γ-ray spectrum for the mass 168 + 16 fraction. Dy KX rays originating from the β^- decay of ^{168}Tb were clearly observed, and 74.96, 173.37, and 227.03 keV γ rays with half-lives similar to that of Dy KX rays were also found. These γ rays were coincident with Dy KX rays and coincident each other. Therefore, it is concluded that these three γ rays originate from the β^- decay of ^{168}Tb. The 74.96 and 173.37 keV γ rays were assigned to the $2_1^+ \rightarrow 0_1^+$ and $4_1^+ \rightarrow 2_1^+$ transitions in the ground state band, respectively. The 227.03 keV γ ray is probably incorporated between the 4^- state in the octupole band and the 3^+ state in the γ band. Details are described in Ref. [6].

Figure 2(a) shows excitation energies of the 2_1^+ states in even-even Gd, Dy, Er, Yb, Hf, and W isotopes. The 2_1^+ energy of Dy isotopes takes the minimum at ^{164}Dy, and then rises at ^{166}Dy. This tendency has been interpreted that the maximum deformation occurs at $N = 98$ (^{164}Dy) in Dy isotopes as suggested in Ref. [7]. However, the present result revealed that the 2_1^+ state again decreases in energy at ^{168}Dy. The energy of the 4_1^+ states also shows the same tendency. This indicates that the second energy minimum exists around $N \approx 104$ like Er, Yb, and Hf isotopes, which is reasonably explained as the maximum deformation at the $N = 104$ neutron midshell. In contrast to the 2_1^+ energy, the energy ratio between the 4_1^+ and 2_1^+ states $E(4_1^+)/E(2_1^+)$ for Dy isotopes increases smoothly with neutron number toward the $N \approx 104$ neutron midshell as shown in Fig. 2(b). Thus the energy minimum at $N = 98$ is considered to be a rather irregular behavior. This implies the existence of some local effect to enhance nuclear deformation around ^{164}Dy.

[1]Department of Chemistry, Tokyo Metropolitan University
[2]Department of Energy Engineering and Science, Nagoya University
[3]Faculty of Engineering, Hiroshima University

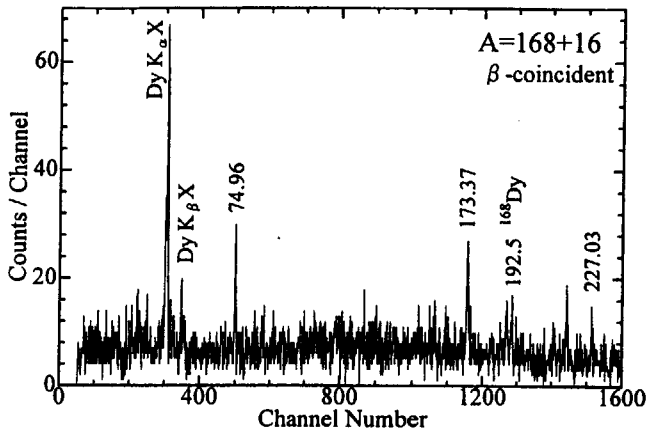

Fig. 1. Beta-coincident γ-ray spectrum for the mass 168 + 16 fraction.

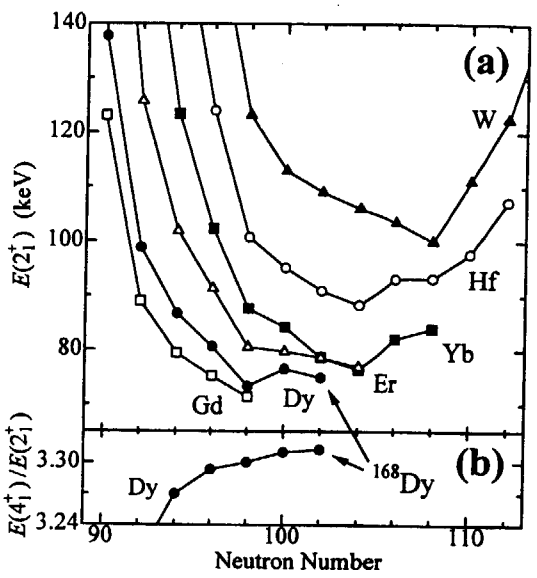

Fig. 2. (a) Level energies of the first 2^+ states in even-even Gd, Dy, Er, Yb, Hf, and W isotopes. (b) Energy ratios between the 4_1^+ and 2_1^+ states $E(4_1^+)/E(2_1^+)$ for even-even Dy isotopes.

References

1) R. C. Greenwood, R. A. Anderl, J. D. Cole and H. Willmes, Phys. Rev. C **35** (1987) 1965.
2) K. Rykaczewski, K.-L. Gippert, N. Kaffrell, R. Kirchner, O. Klepper, V. T. Koslowsky, W. Kurcewicz, W. Nazarewicz, E. Roeckl, E. Runte, D. Schardt, W.-D. Schmidt-Ott and P. Tidemand-Petersson, Nucl. Phys. **A499** (1989) 529.
3) J. H. Hamilton *et al.*, Prog. Part. Nucl. Phys. **38** (1997) 273.
4) C. Y. Wu, M. W. Simon, D. Cline, G. A. Davis, A. O. Macchiavelli and K. Vetter, Phys. Rev. C **57** (1998) 3466.
5) S. Ichikawa, M. Asai, K. Tsukada, A. Osa, T. Ikuta, N. Shinohara, H. Iimura, Y. Nagame, Y. Hatsukawa, I. Nishinaka, K. Kawade, H. Yamamoto, M. Shibata and Y. Kojima, Nucl. Instrum. Methods Phys. Res. A **374** (1996) 330.
6) M. Asai, S. Ichikawa, K. Tsukada, M. Sakama, M. Shibata, Y. Kojima, A. Osa, I. Nishinaka, Y. Nagame, K. Kawade and T. Tachibana, Phys. Rev. C **59** (1999) 3060.
7) S. A. Kerr, F. Hoyler, K. Schreckenbach, H. G. Borner, G. Colvin, P. H. M. Van Assche and E. Kaerts, *Proc. 5th Int. Symp. on Capture Gamma-ray Spectroscopy and Related Topics - 1984, Knoxville* (AIP, New York, 1985), p. 416.

2.2 EXCITED STATES IN THE DOUBLY MAGIC ^{68}Ni AND ITS NEIGHBOUR ^{69}Cu

T. ISHII, M. ASAI, A. MAKISHIMA[1], I. HOSSAIN[2], M. OGAWA[2], J. HASEGAWA[2], M. MATSUDA, and S. ICHIKAWA

In deep-inelastic collisions of 8 MeV/nucleon ^{70}Zn projectiles with ^{198}Pt, we have found the $(\nu g_{9/2}^2 \nu p_{1/2}^{-2})_{8+}$ isomer in ^{68}Ni. The γ rays from isomers with $T_{1/2} \gtrsim 1$ ns were measured with an improved isomer-scope [1] which detects the projectile-like fragments by $\Delta E - E$ telescopes. The γ-ray spectra sorted by nickel and copper isotopes are shown in Fig. 1(a) and (b), respectively. Figure 1(c) shows the γ-γ spectrum coincident with the low-lying transitions in ^{68}Ni. These three spectra are also sorted by setting the time window of $20 < t_{PLF-\gamma} < 100$ ns to reduce the γ rays from short-lived isomers. A decay scheme of the 8^+ isomer in ^{68}Ni is shown in Fig. 2. The lifetime of this isomer was derived to be 23(1) ns from the $t_{PLF-\gamma}$ coincidence data. From the partial half-life for the $8^+ \rightarrow 6^+$ transition, the effective charge of 1.5(1)e was obtained for the $g_{9/2}$ neutron, using $\langle g_{9/2} \mid r^2 \mid g_{9/2} \rangle = 22$ fm^2.

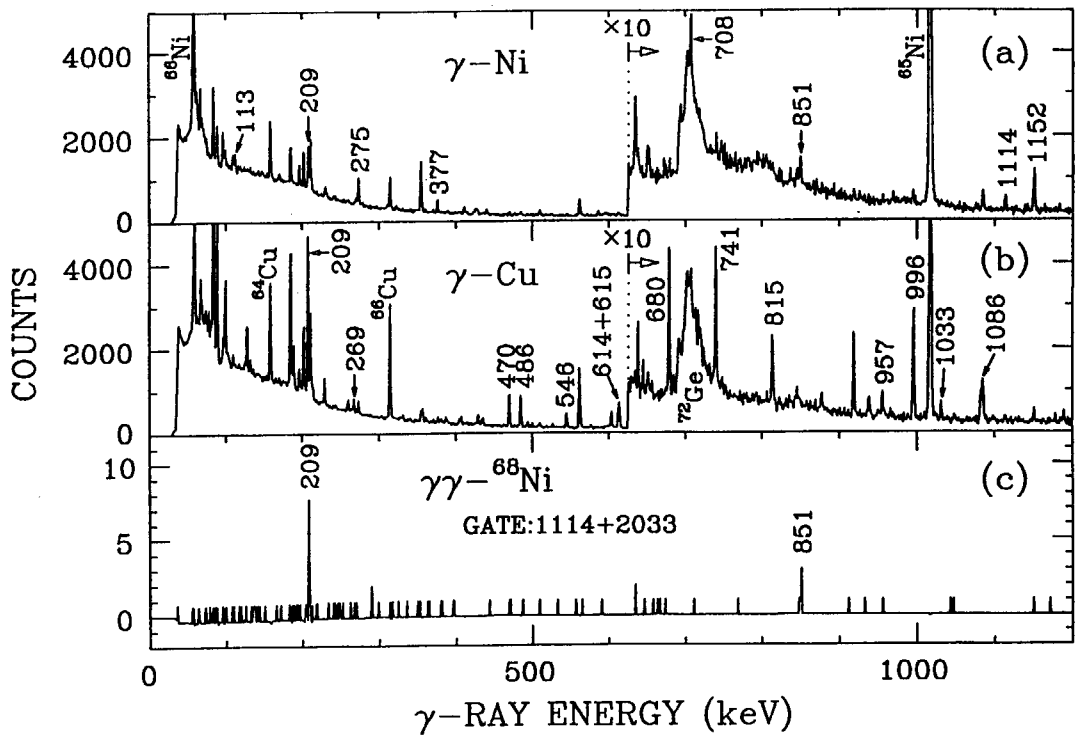

FIG. 1. (a) A γ-ray spectrum of Ni isotopes. The γ-ray energies are depicted for ^{68}Ni. (b) A γ-ray spectrum of Cu isotopes. The γ-ray energies are depicted for ^{69}Cu. (c) A γ-γ spectrum in coincidence with the 1114 and 2033 keV γ rays in ^{68}Ni. These three spectra were obtained from the ΔE-E-γ(-γ) coincidence data, by setting a $t_{PLF-\gamma}$ window of 20 – 100 ns and sorting by atomic numbers.

[1]Department of Liberal Arts and Sciences,National Defense Medical College
[2]Department of Energy Sciences, Tokyo Institute of Technology

In ^{69}Cu, two new isomers were found in the same reaction above; a $19/2^-$ isomer with 22(1) ns at 3691 keV, and a $(17/2^+)$ isomer with 39(6) ns at 3827 keV. The decay properties of the former isomer can be calculated quite accurately by a parameter-free shell model calculation using the residual interactions taken from the energy levels observed in ^{68}Ni and ^{68}Cu. The calculated levels are shown on the right-hand side in Fig. 2. The $B(E2; 19/2^- \rightarrow 15/2^-)$ value, 63(3) e^2fm^4, can be also explained. Using $e_\nu = 1.5e$ obtained from the present work and $e_\pi = 2.0e$ of an assumed value, this shell model calculation gives 56 e^2fm^4, in good agreement with the experiment.

The proton $2p - 1h(f_{7/2}^{-1})$ excitation across the $Z = 28$ shell was also found, as shown on the left-hand side in the ^{69}Cu decay scheme. The interpretation of this $\pi(2p - 1h)$ configuration is mainly based on the fact that the $7/2^-$ state at 1711 keV has a large spectroscopic factor in the proton pick-up reactions [2,3]. The $\Delta I = 2$ level spacings in this band are close to those in the two-valence-proton nucleus $^{70}_{30}$Zn. Furthermore, the $E2$ transitions in this band compete with the $M1$ transitions. These facts suggest that this band has large collectivity as ^{70}Zn, indicative of the softness of the $N = 40$ shell closure at $Z = 29$.

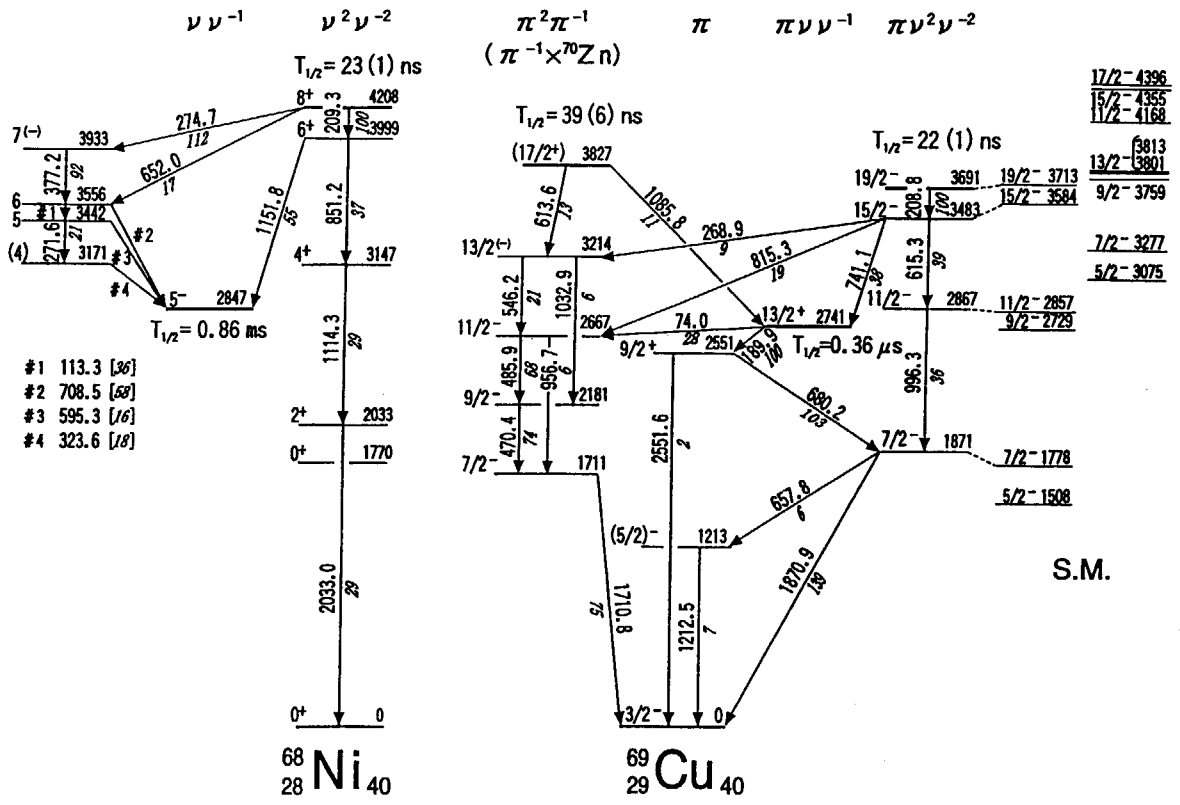

FIG. 2. Decay schemes of the isomers in ^{68}Ni and ^{69}Cu. The relative γ-ray intensities are depicted in italics. The experimental levels in ^{69}Cu denoted by $\pi\nu^2\nu^{-2}$ are compared to the shell model calculation; the calculated yrast levels are shown next to the experimental ones.

References

[1] T. Ishii *et al.*, Nucl. Instrum. Methods Phys. Res. **A395** (1997) 210.
[2] B. Zeidman and J.A. Nolen, Jr, Phys. Rev. C **18** (1978) 2122.
[3] F. Ajzenberg-Selove *et al.*, Phys. Rev. C **24** (1981) 1762.

2.3 HIGH SPIN STATES OF ^{155,156}Gd

T.HAYAKAWA, M.OSHIMA, Y.HATSUKAWA, J.KATAKURA, H.IIMURA, M.MATSUDA, S.MITARAI[1], R.SHIMIZU[1], T.SHIZUMA[2], M.SUGAWARA[3] and H.KUSAKARI[4]

High-spin states of ^{155,156}Gd nucleus have been investigated using the ^{150}Nd(^{12}C, αxn) reaction. The target was a self-supporting ^{150}Nd metallic foil enriched to 96.1 % with 2 mg/cm^2 thickness. Gamma-rays were deteced with an array of 11 HPGe detectors with BGO Compton suppressers. Two rotational bands of ^{155}Gd have been observed and extended up to $(51/2^+)$ and $45/2^+$. New band has been observed (Band 3). Ground rotational band of ^{156}Gd has been also extended up to 22^+. Fig. 1 shows the partial level scheme.

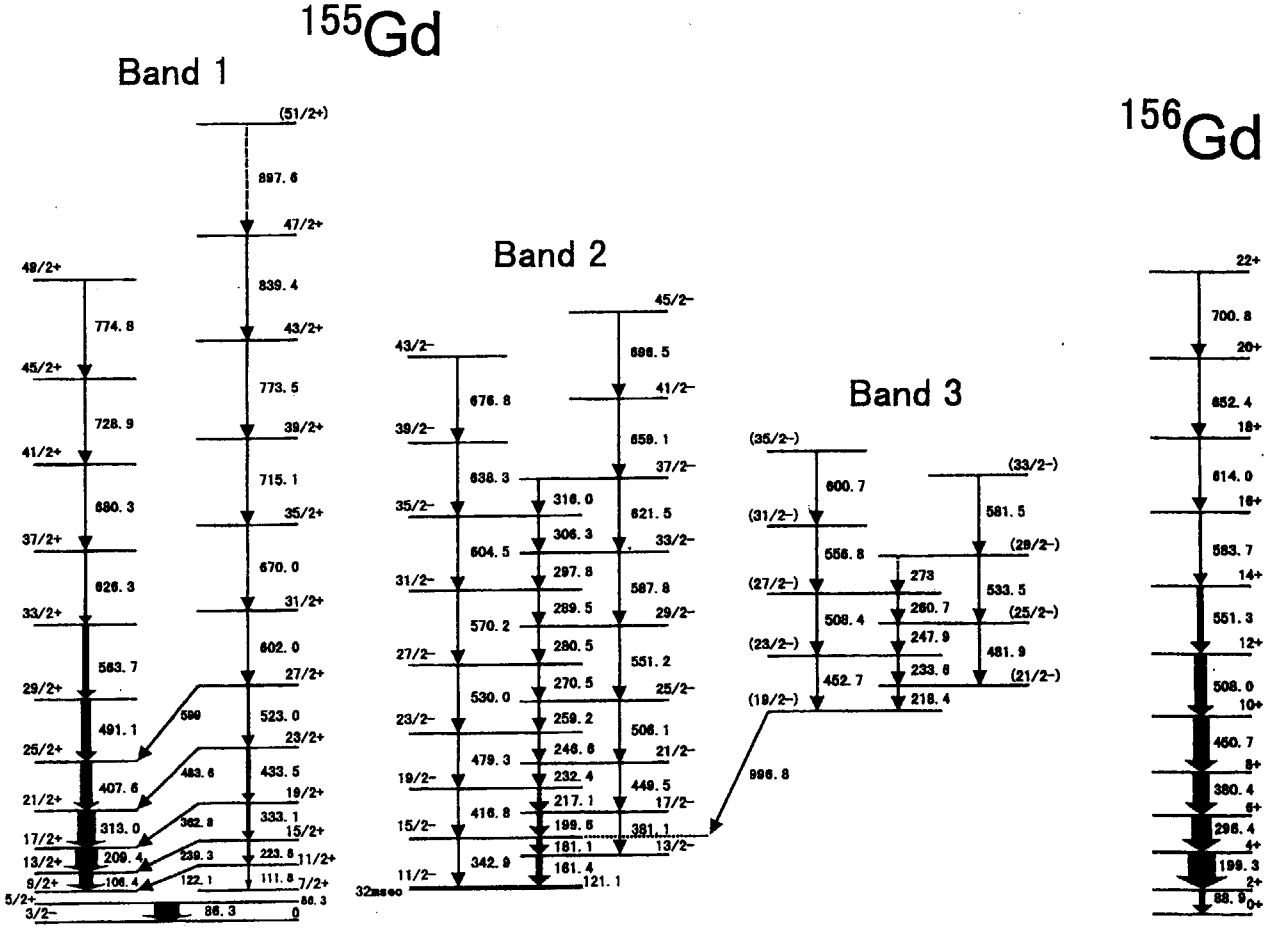

Fig. 1

[1]Kyushu University, Hakozaki, Hukuoka 812-8581, Japan
[2]University of Tsukuba, Tsukuba, Ibaraki 305-8577, Japan
[3]Chiba University, Inage, Chiba 263-8522, Japan
[4]Chiba Institute of Technology, Narashino, Chiba 275-8588, Japan

2.4 COULOMB EXCITATION OF 9⁻ ISOMER IN ^{180}Ta

H. KUSAKARI[1], M. OSHIMA, T. HAYAKAWA, M. SUGAWARA[2],
Y. HATSUKAWA, H. IIMURA, T. NAOI[1] and M. SUGIE[1]

The 75 keV 9⁻ excited state of ^{180}Ta is an isomer with an extremely long life of $T_{1/2} > 1.2\times10^{15}$ years, and it seems to have K = 9. Its decay to the 1^+ ground state or the 2^+ first excited state at 40 keV is strongly forbidden. Recent investigations in ^{180}Ta have been reported by Schlegel et al.[1], Schumann et al.[2] and Dracoulis et al.[3]. We have investigated Coulomb excitation of the 9⁻ isomer in ^{180}Ta using a 225 MeV ^{58}Ni beam from the JAERI tandem accelerator. Natural abundance of ^{180}Ta is 0.012 % in Ta. The target used in this experiment was isotopically enriched to 5.7 %. Radiation following the decay of the ground sate fed by Coulomb excitation of the 9⁻ isomer of ^{180}Ta was measured. The method of the present investigation is explained in Fig. 1. Yields of 54.6 keV X-rays ($K\alpha_2$) and 55.8 keV X-rays ($K\alpha_1$) of the daughter nucleus ^{180}Hf were measured (see Fig. 2), and the population of the ground state fed by the induced decay of the 9⁻ isomer of ^{180}Ta was obtained experimentally with the ambiguity of 8 %. The measurement of yields of 54.6 keV and 55.8 keV X-rays was repeated at the time interval of two hours, and they were checked to follow the decay curve with the half-life of 8.152 h for the ground state of ^{180}Ta. In our Coulomb excitation experiment, 27 events/sec of induced transition for 3×10^{15} nuclei in the 9⁻ isomeric state occurred. This rate of event is 4.7×10^8 times of the spontaneous decay rate of the 9⁻ isomer. It corresponds to the shortening of the effective half-life to about 2.6×10^6 years from the original half-life $T_{1/2} > 1.2\times10^{15}$ years.

We could obtain the absolute value of Coulomb excitation cross section of 9⁻ isomer using the above value of population and also the values of beam intensity and target thickness. The preliminary result of the present experiment shows that the Coulomb excitation cross section of the 9⁻ isomer of ^{180}Ta with a 225 MeV ^{58}Ni beam is as follows:

$$\sigma_{CEX} = 1.6 \pm 0.3 \quad [\text{mb}]$$

The above error (19 %) is mainly from uncertainties in the absolute values of beam intensity and target thickness. In the present Coulomb excitation, there are possibilities of the direct feeding to the ground state and other paths. In the latter, the path via the 7⁻ state at 685 keV or the 8⁻ state at 856 keV seems to be most probable if we assume the weak K mixing for the 9⁻ isomer and the relevant level; these levels have similar configurations[3]. In this case, B(E2) value of the transition from the 9⁻ isomer in ^{180}Ta is estimated as 0.01－0.04 Weisskopf unit.

---

[1] Faculty of Education, Chiba University.

[2] Chiba Institute of Technology.

References

1) C.Schlegel et al., Phys. Rev. **C50** (1994) 2198.

2) M.Schumann et al. , Phys. Rev. **C58** (1998) 1790.

3) G.D. Dracoulis et al., Phys. Rev. **C58** (1998) 1444.

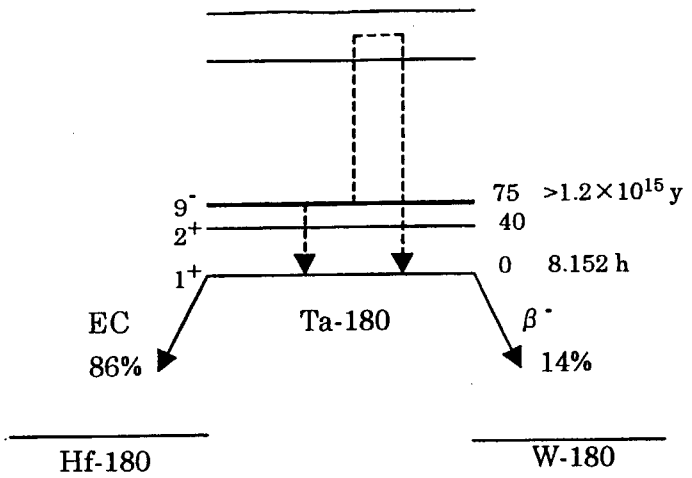

Fig. 1 Coulomb excitation of the 9⁻ isomer in ^{180}Ta and the decay to ^{180}Hf and ^{180}W.

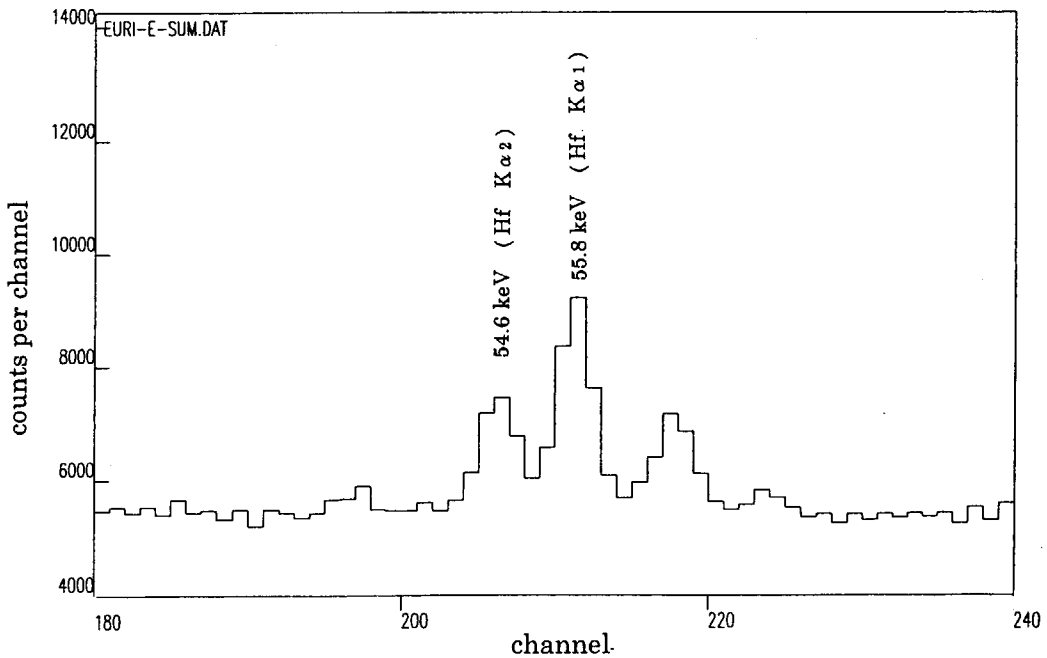

Fig. 2 X-ray spectrum in the decay of ^{180}Ta after Coulomb excitation of the 9⁻ isomer with a 225 MeV ^{58}Ni beam.

2.5 MEAN-SQUARE NUCLEAR CHARGE RADIUS OF ^{144}Ce

Y. ISHIDA[1], H. IIMURA, S. ICHIKAWA, AND T. HORIGUCHI[2]

Precise and systematic studies of the isotope shift (IS) of optical transitions provide the information on changes in the mean-square nuclear charge radius (MSCR). That study in the region of light rare-earth elements is of interest because it gives an opportunity to investigate the effect of neutron shell closure at N=82. Also, other nuclear structural changes are expected for the neutron-rich isotopes in this region [1]. Especially, it is well known that a drastic shape transition occurs between the neutron numbers of N=88 and 90 in the isotopic chains of Nd (Z=60) and Sm (Z=62), while not in Ba (Z=56) and Cs (Z=55) ones [2]. Therefore, it is quite interesting how the change in the MSCR of Ce (Z=58) isotopes behaves. As an extension of our previous study for Ce stable isotopes [3], we measured the IS for ^{144}Ce ($T_{1/2}$=284.9 d) by collinear laser-ion-beam spectroscopy and determined the change in the MSCR.

Two types of samples were prepared in this work: a sample with natural abundance and a radioactive one. The isotope ^{144}Ce was prepared from the spent fuel of the JRR-3 reactor at the Japan Atomic Energy Research Institute. The purification of ^{144}Ce was carried out by using the solvent extraction technique to remove the other fission products and uranium.

The experimental setup is almost the same as our previous one [3]. A single-mode tunable dye laser (Coherent 699-29) with rhodamine 110 dye was pumped by an Ar^+ laser (Coherent INNOVA-100-20). A part of the laser beam was used for the polarization spectroscopy of $^{127}I_2$ which provides an absolute frequency reference with a simple optical arrangement. A temperature-stabilized confocal Fabry-Pérot interferometer (FPI, Burleigh CFT-500) was used to calibrate the relative frequency of spectral lines. Each of the transmitted photons through either the FPI or the $^{127}I_2$ polarization spectrometer was detected by a photomultiplier tube (PMT, Hamamatsu R374). Ce ions were produced by a surface ionization ion source, accelerated to 40 keV, and mass separated by an analyzing magnet. The counterpropagating laser beam excited the Ce ions to the upper levels. The laser-induced fluorescence (LIF) was collected by an ellipsoidal mirror and detected by a cooled PMT (Hamamatsu R2256). The interaction region was defined with a cage kept at a constant potential of −3 kV, and accelerated ions were Doppler tuned to resonance with the laser frequency only inside the cage. Signals from three PMT's were simultaneously counted during the laser frequency scanning, and recorded by multichannel scalers controlled by a personal computer.

The 534.93-nm transition from the $4f(^2F)5d^2(^1G)\ ^2I_{11/2}$ level at 5969.01 cm^{-1} to the $4f5d(^1G)6p\ ^2H_{9/2}$ level at 24663.05 cm^{-1} in Ce^+ was measured in this work. The lower long-lived state at 5969.01 cm^{-1}, from which electric dipole transitions to much lower levels are allowed only with small transition probabilities, is thermally populated. The 24663.05-cm^{-1} level mostly decays to the levels near the ground state emitting the photon of wavelength about 440 nm. The relative frequency between each Ce peak and one of the $^{127}I_2$ peaks was determined by

[1] KEK, Tanashi Branch
[2] Department of Clinical Radiology, Hiroshima International University

comparison with the FPI spectrum. The observed shift in the peaks of the Ce spectra is due to a combination of IS and different Doppler shifts. To obtain the IS, the contribution of the Doppler shift was subtracted from the observed shift by measuring the acceleration voltage.

Table 1. Isotope shifts determined from the measurements in the 534.93-nm line of Ce^+.

Isotope shifts (MHz)			
136－140	138－140	142－140	144－142
89.9(55)	26.0(42)	140.1(28)	108.5(89)

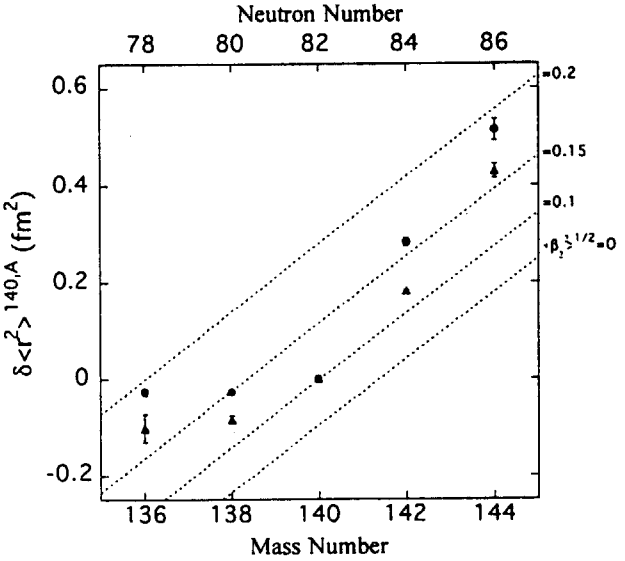

Fig. 1. Changes in the MSCR for the Ce isotopes (A=136, 138, 142, and 144) from this work (circle). Those from the $B(E2)$ (triangle) are also shown for comparison. The root-mean-square values of the quadrupole deformation parameter β_2 are indicated by parallel dotted lines, of which the gradients are given by the droplet model.

The experimental results of IS's for ^{144}Ce and stable isotopes are listed in Table 1. The uncertainties include statistical and systematic errors. The IS is composed of the mass shift (MS) and the field shift (FS). The FS is induced by the finite nuclear charge distribution. The MS and the FS can be separated from the IS through the King-plot analysis. The change in mean-square charge radii between ^{142}Ce and ^{144}Ce was determined from the FS, and was obtained to be $\delta\langle r^2\rangle^{142,144} = 0.232(20)$ fm^2. Figure 1 shows our experimental $\delta\langle r^2\rangle^{140,A}$ including those of stable isotopes for which the weighted averages are taken from our previous values [3] and the present ones. For comparison, Fig. 1 indicates the $\delta\langle r^2\rangle$ from the reduced $E2$ transition probability $B(E2)$ [4–7]. To resolve the discrepancies in Fig. 1 and to deepen our understanding of the structures of Ce isotopes, it is strongly desired to extend this study to the more neutron-rich side including ^{146}Ce (N=88) and ^{148}Ce (N=90).

References

1) E. W. Otten, in *Treatise on Heavy-Ion Science*, edited by D. A. Bromley (Plenum, New York, 1989), Vol. 8, p. 515.
2) J. Billowes and P. Campbell, J. Phys. G **21** (1995) 707.
3) Y. Ishida, H. Iimura, S. Ichikawa, and T. Horiguchi, J. Phys. B **30** (1997) 2569.
4) Yu. P. Gangrsky, S. G. Zemlyanoi, N. N. Kolensnikov, B. K. Kul'djanov, K. P. Marinova, B. N. Markov, V. S. Rostovskii, Yu. G. Teterev, Hoang Thi Kim Hue, and Chan Kong Tam, Sov. J. Nucl. Phys. **50** (1989) 757.
5) S. Raman, C. H. Malarkey, W. T. Milner, C. W. Nestor, Jr., and P. H. Stelson, At. Data Nucl. Data Tables **36** (1987) 1.
6) G. Lo Bianco, K. P. Schmittgen, K. O. Zell, and P. v. Brentano, Z. Phys. A **332** (1989) 103.
7) M. Moszynski and H. Mach, Nucl. Instrum. Methods A **277** (1989) 407.

2.6 HALF-LIFE OF ^{235}Am

M. SAKAMA[1], K. TSUKADA, M. ASAI, S. ICHIKAWA, Y. OURA[1], M. SHIBATA[2], A. OSA, I. NISHINAKA, Y. NAGAME, K. KAWADE[2] and H. NAKAHARA[1]

The present work on the half-life determination of ^{235}Am is a part of our series of the decay studies for neutron-deficient actinide isotopes with the Gas-jet coupled JAERI on-line isotope separator (ISOL) [1]. In the region of neutron-deficient actinide isotopes, there remain many identified isotopes which are still uncertain about the decay properties, especially in Am, Cm and Bk, because those isotopes decay dominantly through electron-capture (EC) and the α-decay probabilities are expected to be very small.

The isotope ^{235}Am was produced via the ^{235}U(^{6}Li,6n) reaction. A stack of twenty targets of ^{235}U set in a multiple-target chamber was bombarded with a 60 MeV ^{6}Li beam of about 300-particle-nA intensity. Reaction products recoiling out of the targets, which are attached to PbI_2 materials as aerosol clusters, were swept out of the chamber into a Teflon capillary (1.4 mm i.d., 8 m length) with the He gas (1.2 or 1.4 l/min). The products were transported through double skimmer structure (2 mm ϕ and 4 mm ϕ) into the thermal ion-source of the ISOL. The atoms of interest, ^{235}Am, were ionized by the surface ionization method at 2450 K and the ions were mass-separated by a magnet immediately. The mass-separated ions were implanted in an aluminum coated Mylar tape and periodically transported to a measuring position equipped with a low-background n-type HPGe detector. The data of x/γ-ray singles and x/γ-γ coincidence were recorded event by event together with the time information.

Calibration of the mass number was made by using the isotopes of ^{143m}Sm produced in the ^{141}Pr(^{6}Li,4n) reaction, ^{237}Am in ^{235}U(^{6}Li,4n), and ^{208}Pb which is a component of the cluster materials of the aerosol. The mass resolution of $M/\Delta M = 850$ was achieved for the isotope ^{208}Pb at the focal plane. The overall efficiency for ^{237}Am becomes approximately 0.5% which is 2 times higher than the previous one [2] and the signal-to-noise ratio (S/N) in the x/γ-ray spectrum was about 3.5 times larger than that in Ref. [3].

The x/γ-ray spectrum obtained at the mass-235 fraction is shown in Fig. 1. These Pu $K_{\alpha 1,2}$ and Pu $K_{\beta 1,3}$ x rays should only originate from the electron capture decay (EC) of ^{235}Am, indicating that ^{235}Am was produced. In addition to these Pu K x rays, Np $K_{\alpha 1,2}$ x rays from the EC decay of ^{235}Pu which should be the daughter of ^{235}Am were clearly observed in the figure. Within the statistical error in this work, however, no γ rays coincident with the Pu K x rays were detected. Half-lives of the Pu $K_{\alpha 1}$ and $K_{\alpha 2}$ x rays were deduced to be 9.3±0.5 and 9.3±1.4 min, respectively, as shown in Fig. 2, and that of the Np K_{α} x ray was about 30 min consistent with the half-life of ^{235}Pu. From weighted average of these values, the half-life of ^{235}Am was determined to be 9.3±0.7 min. With respect to proving the present Pu K x rays to be originated from ^{235}Am, the contribution from the isotopes ^{234}Am and ^{236}Am which are located near the mass 235 is negligible because of the high mass resolution of the ISOL.

The present half-life is compared in Table 1 with the theoretical predictions calculated with the gross theory (GT2) [4], the semi-gross theory (SGT) [5] and the microscopic proton-neutron quasiparticle random-phase approximation (pn-QRPA) [6]. The theoretical half-

[1]Department of Chemistry, Tokyo Metropolitan University
[2]Department of Energy Engineering and Science, Nagoya University

lives of GT2 and SGT are nearly the same as the present value within the factor of 1.

In the present study the ^{235}Am atoms were successfully mass-separated with ISOL and the Pu K x rays associated with the EC decay of Am were directly measured with the good S/N ratio, indicating that precise determination of the half-life of ^{235}Am was done.

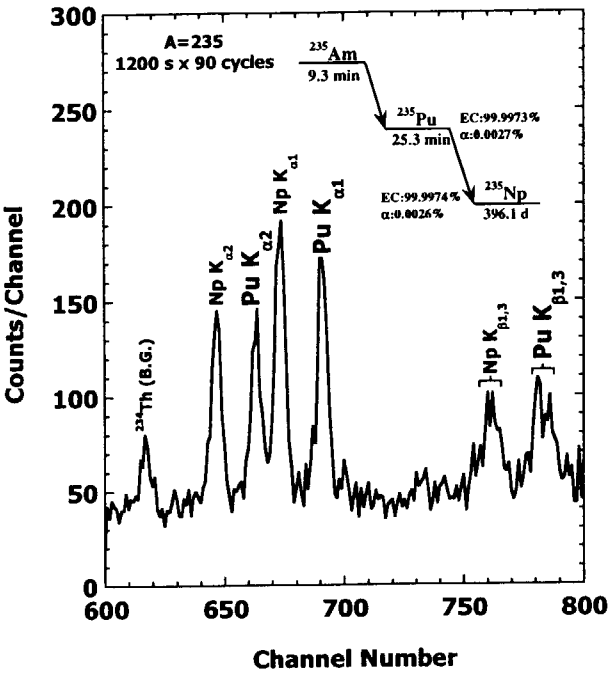

Figure 1. X/γ-ray spectrum observed at the mass-235 fraction.

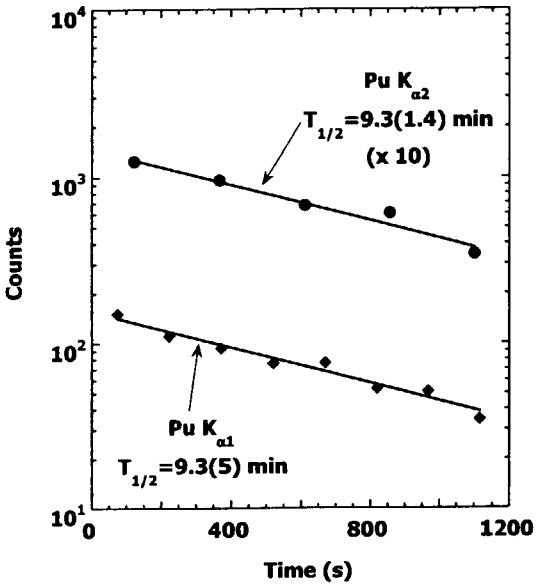

Figure 2. Decay curves for Pu $K_{\alpha 1,2}$ x rays from the EC decay of ^{235}Am.

Table 1. Comparison between the experimental and calculated values of EC-decay half-lives on ^{235}Am.

Present result	GT2[a] [4]	SGT[a] [5]	*pn*-QRPA[b] [6]
9.3±0.7 min	6.95 min	7.31 min	3.0 min

[a] Q_{EC}=2.56 MeV
[b] Q_{EC}=2.31 MeV

References

1) S. Ichikawa *et al.*, Nucl. Instrum. Methods B **126** (1997) 205.
2) M. Sakama *et al.*, JAERI 98-**017** (1998) 37.
3) K. Tsukada *et al.*, Phys. Rev. C **57** (1998) 2057.
4) T. Tachibana *et al.*, Prog. Theor. Phys. **84** (1990) 641.
5) H. Nakata *et al.*, Nucl. Phys. A **625** (1997) 521.
6) M. Hirsch *et al.*, At. Data Nucl. Data Tables **53** (1993) 165.
7) J. Guo *et al.*, Z. Phys. A **335** (1996) 111.

2.7 APPLICATION OF THE METHOD OF MULTIDIMENSIONAL SPECTRUM TO ANALYTICAL CHEMISTRY

Y. HATSUKAWA, T. HAYAKAWA, Y. TOH, N. SHINOHARA, M. OHSHIMA

Nuclear scientists have achieved many successful results in the nuclear structural studies by using multidimensional spectrum, because of its high sensitivity to gamma rays with small intensities. In this study, application method of multidimensional spectrum for analytical chemistry was developed. Two reference igneous rock (JP-1, JB-1a) samples issued by the Geological Survey of Japan (GSJ) were irradiated at a research reactor, and gamma rays from produced radioisotopes via neutron capture reactions were measured using an array of 12 germanium detectors with BGO Compton suppressors, GEMINI. Simultaneously 27 elements were observed with no chemical separation. Even Eu contained in JP-1 with abundance of 4 ppm was detected (see in Fig.1). Although there are no previous data for contents of bromine in the JP-1 and JB-1a samples, bromine in the both samples was detected in this study (see in Fig.2).

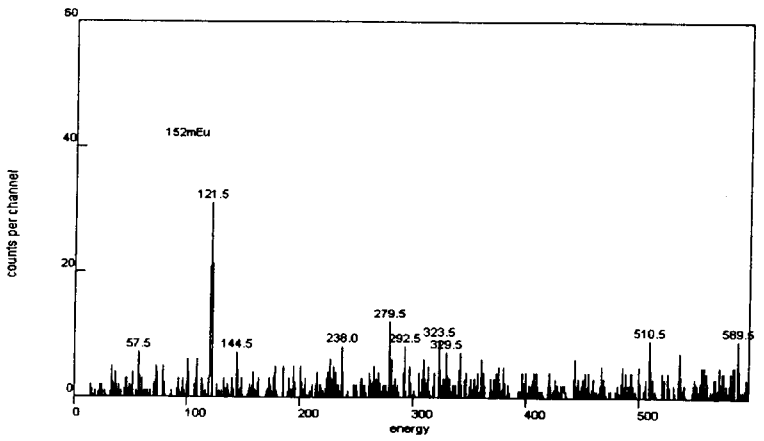

Fig.1 A gated spectrum coincident with 842 keV γ-ray from the JP-1 sample.
The 841.6 keV-121.5 keV γ-ray sequence from ^{152m}Eu (9.3 h) was found.

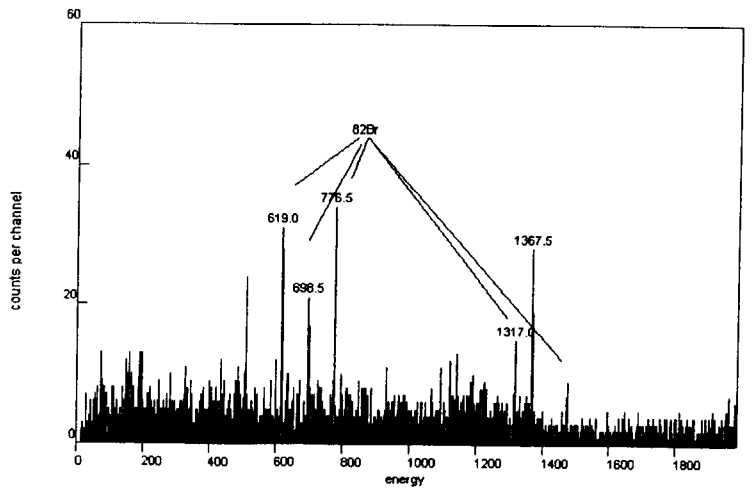

Fig.2 A gated spectrum coincident with 554 keV γ-ray from the JB-1a sample.
The 554.3 keV-1317.0 keV-776.5 keV and 554.3 keV-619.0 keV-698.5 keV-776.5 keV γ-ray sequences from ^{82}Br (35.3 h) were found.

2.8 THREE-NUCLEON CLUSTER STRUCTURE IN THE A=19 MIRROR NUCLEI; ^{19}F AND ^{19}Ne

A. YAMAZAKI[1], T. NAKAGAWA[1] , K. KUMAGAI[1] , M. HIRAI[1] , T. SUEHIRO[2], S. KATO[3], H. ISHIYAMA[4], Y. SUGIYAMA, and S. HAMADA

A cluster model is one of models for nuclear structure. In this model, a nucleus consists of a cluster and an inert core. The most famous cluster model is an alpha cluster model. A large number of experimental data have shown the evidence for exsisting of the alpha cluster structure in light nuclei. Recently, It has been shown that the alpha cluster structure also exists in some fp-shell nuclei [1, 2].

As an analogy of the alpha cluster model, a three-nucleon cluster model can be considered. In order to explore a three-nucleon cluster structure, many three-nucleon transfer reactions have been done. However, an evidence for the existence of a three-nucleon cluster structure has not been obtained yet, because of a lack of the spin-parity information about possible candidates of highly-exited cluster states even in light nuclei.

On the other hand, it is well known that multi-nucleon cluster states are selectively populated through a multi-nucleon transfer reaction and also that mirror reactions on a self-conjugate target selectively excite mirror states in residual mirror nuclei. In this study, the (^{6}Li,^{3}He) and (^{6}Li,t) mirror reactions on ^{16}O were executed to obtain information about highly-excited states in the A=19 mirror nuclei; ^{19}F and ^{19}Ne.

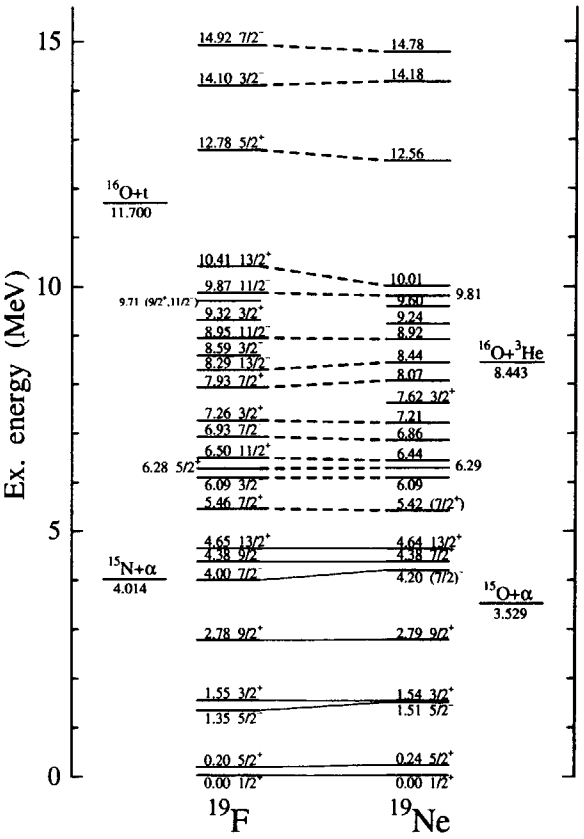

Fig. 1: Energy levels observed in the present experiment. The excited states connected by the solid lines are known as mirror states, those by the dashed lines are mirror states assigned in this study.

The experiment was carried out using a 63-MeV ^{6}Li^{3+} beam from the JAERI Tandem Van de Graaff accelerator. Natural oxygen gas enclosed in a cylindrical cell was used as the ^{16}O target. Gas pressure was 100 Torr. The emitted triton and ^{3}He particles were momentum-analyzed with the JAERI magnetic spectrograph ENMA, and were detected by a single wire proportional counter and a thin plastic scintillator placed behind the counter. Particle identification was made using a ΔE-E method. Overall energy resolution of the emitted particles was about 150 keV for both the (^{6}Li,^{3}He) and (^{6}Li,t) reactions.

[1]Department of Physics, Tohoku University.
[2]Tohoku Institute of Technology.
[3]Department of Physics, Yamagata University.
[4]National Laboratory for High Energy Physics, Tanashi branch.

From this experiment, about 20 states were observed in a high excitation energy region up to 16 MeV for each nucleus and their angular distributions were measured for c.m. angle $10° \sim 80°$ with steps of $3° \sim 6°$. Angular distributions of the mirror states are so similar that mirror relations in the both residual nuclei can be assigned from the comparison of the angular distributions.

Figure 1 shows the energy levels observed in the present experiment and also the mirror relations between ^{19}F and ^{19}Ne. The relations in the excitation energy region above 5 MeV are assigned in the present study. From this relations we have obtained new spin-parity information about many highly-excited states in ^{19}Ne.

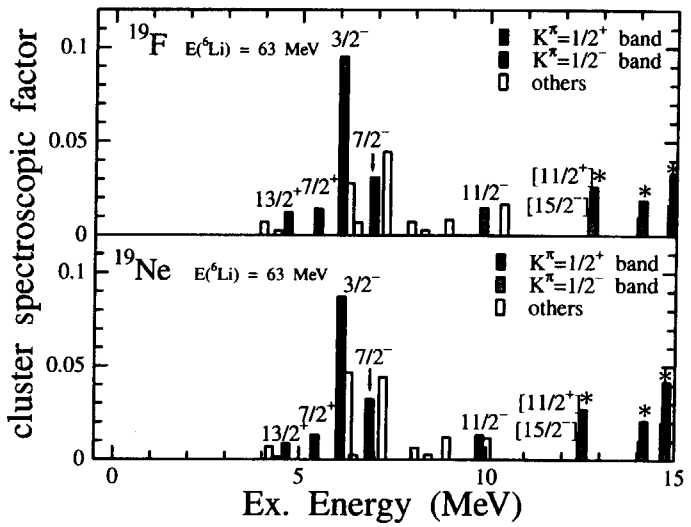

Fig. 2: Cluster spectroscopic factors for each state of the A=19 nuclei. Black bars represent the members of the $K^\pi = 1/2^+$ band and hatched bars represent the candidates for the members of the $K^\pi = 1/2^-$ band. Asterisk marks indicate the states which are assumed as high spin members of the $K^\pi = 1/2^\pm$ bands ($11/2^+$ for black bars and $15/2^-$ for hatched bars).

Spectroscopic information was obtained with a finite-range DWBA analysis. Figure 2 shows three-nucleon cluster spectroscopic factors for each state of the A=19 nuclei. In the present experiment, three prominent states are populated above the excitation energy of 12 MeV in each A=19 nucleus. So far they have been assinged to be low-spin states (lower than J=4) in compilations [3]. However, calculated angular distributions for these states do not reproduce the experimental results which are almost structureless and the extracted spectroscopic factors are too large for the low-spin states. If these states are assumed to be high-spin states, calculated angular distributions well reproduce the experimental ones. In addition, spectroscopic factors (asterisked in Fig. 2) are as large as those for the members of the $K^\pi = 1/2^\pm$ bands which have fairly large spectroscopic factors. As the result, these states above 12 MeV can be candidates for the high-spin members of the $K^\pi = 1/2^\pm$ bands. The existence of the $K^\pi = 1/2^\pm$ bands is a good evidence for the three-nucleon cluster structure. Therefore, the present study has suggested that a possibility of the existence of the three-nucleon cluster structure in ^{19}F and ^{19}Ne has been shown in the present study.

References

[1] T. Yamaya, S. Oh-ami, M. Fujiwara, T. Itahashi, K. Katori, M. Tosaki, S. Kato, S. Hatori, and S. Ohkubo, Phys. Rev. **C42**(1990)1935.

[2] T. Yamaya, M. Saitoh, M. Fujiwara, T. Itahashi, K. Katori, T. Suehiro, S. Kato, S. Hatori, and S. Ohkubo, Nucl. Phys. **A573**(1994)154.

[3] D. R. Tilley, H. R. Weller, C. M. Cheves, and R. M. Chasteler, Nucl. Phys. **A595**(1995)1.

2.9 $(\nu g_{9/2}^{-2})_{8^+}$ ISOMERS IN $^{82}Se_{48}$ AND $^{80}Ge_{48}$ POPULATED BY DEEP-INELASTIC COLLISIONS

A. MAKISHIMA[1], M. ASAI, T. ISHII, I. HOSSAIN[2], M. OGAWA[2], S. ICHIKAWA and M.ISHII

New 8^+ isomers in ^{82}Se and ^{80}Ge and their decays were studied by the deep-inelastic collisions (DIC's) of 9 MeV/nucleon ^{82}Se projectiles with ^{198}Pt, using an isomer-scope[1]. The 374 and 1410 keV γ rays were found to be coincident with the known 1080($4^+ \rightarrow 2^+$) and 655($2^+ \rightarrow 0^+$) keV γ rays in ^{82}Se[2]. A $\gamma\gamma$-coincidence sum spectrum for these transitions is shown in Fig. 1. A ^{80}Ge isomer was found by sorting out γ rays in coincidence with the known 1084($4^+ \rightarrow 2^+$) and 659($2^+ \rightarrow 0^+$) keV γ rays[2,3]. The 467 and 1236 keV γ rays were coincident with these γ rays.

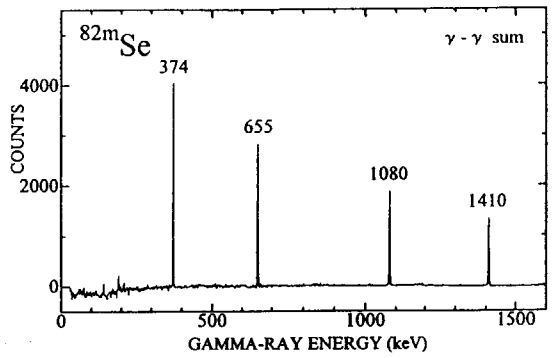

Fig. 1. A $\gamma\gamma$ coincidence sum spectrum of γ rays from the new ^{82}Se isomer.

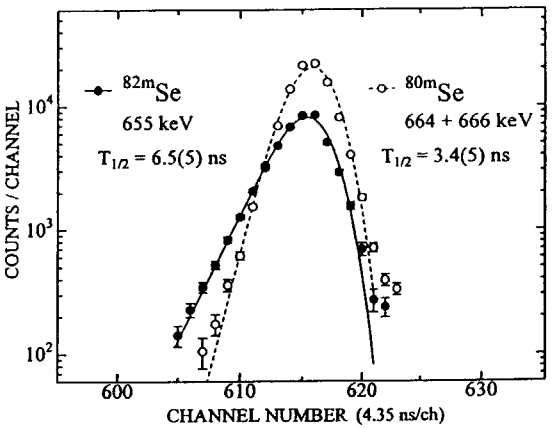

Fig. 2. The time spectrum of γ rays from ^{82m}Se and ^{80m}Se. These were obtained from $t_{\gamma\text{-PLF}}$ coincidence data.

Figure 2 shows the $t_{\gamma\text{-PLF}}$ time spectrum for the 655 keV γ ray in ^{82}Se. The adopted value of $T_{1/2}$ is 6.6(4) ns for the isomer in ^{82}Se. Because of the poor statistics for ^{80m}Ge, a lower bound of the lifetime was estimated from the γ-ray yields. In the isomer-scope, projecti-like fragments take a flight of about 1.7 ns before they reach the Si detector. In the present experiment, the γ-ray yield ratios of the N=48 isotones $^{84m}Kr(T_{1/2}=1.84\mu s)$, ^{82m}Se and ^{80m}Ge were measured to be 1 : 1.6(1) : 0.07(1). To estimate the lower bound of the lifetime, we took a conservative assumption that the ^{80m}Ge yield was at most the same as ^{84m}Kr. This assumption gives an attenuation in flight, $\exp(-1.7/\tau)>0.07$, resulting in $T_{1/2}>0.4$ ns.

The decay schemes of ^{82m}Se and ^{80m}Ge are shown in Fig. 3 together with those of the known 8^+ isomers in the N=48 isotones[2,4]. The new 374 and 1410 keV γ rays in ^{82}Se, and the 467 and 1236 keV γ rays in ^{80}Ge[3], were assigned to the $8^+ \rightarrow 6^+$ and $6^+ \rightarrow 4^+$ transitions, assuming the stretched E2 coupling scheme for the yrast states. This assumption is based on the property that DIC's bring large angular momenta to the fragment nuclei.

[1]Department of Liberal Arts and Sciences, National Defense Medical College
[2]Research Laboratory for Nuclear Reactors, Tokyo Institute of Technology

The lifetime data also support the above assignments; the 374 and 467 keV γ rays are isomeric E2 transitions.

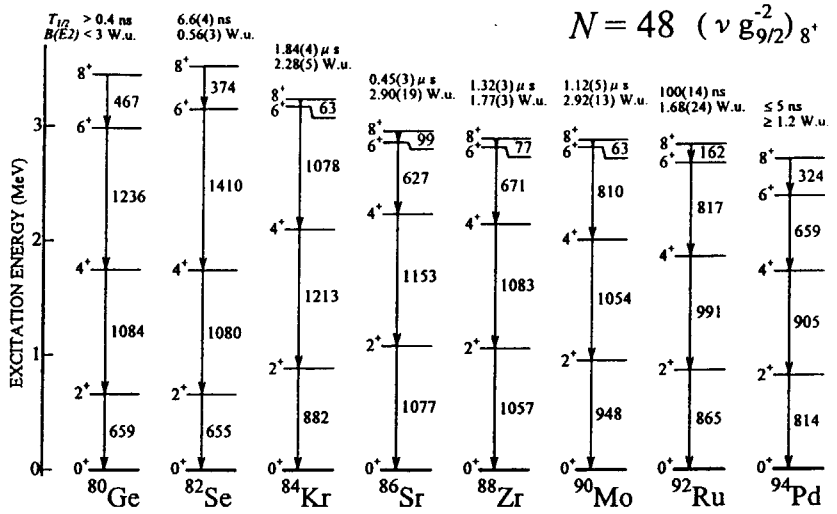

Fig. 3. Decay schemes of the 8^+ isomers in the N=48 isotones from ^{80}Ge to ^{94}Pd. Transition energies are given in units of keV. B(E2;$8^+ \rightarrow 6^+$) values are also shown.

As shown in Fig. 3, ^{86}Sr, ^{88}Zr, ^{90}Mo and ^{92}Ru have 8^+ states at almost the same excitation energy; in ^{94}Pd[4], the 8^+ and 6^+ states are excited at somewhat lower energies. They show a trend that the excitation energies of the 2^+ and 4^+ states decrease monotonically as the atomic number increases. Compared with these nuclei, ^{84}Kr has a large energy gap of over 1 MeV between the 6^+ and 4^+ states. In ^{82}Se and ^{80}Ge, the 8^+ states are excited at higher energies, the 6^+ states lying about 0.4 MeV below them. The energy gap between the 6^+ and 4^+ levels further increases while the 2^+ and 4^+ levels lie lower in energy than in ^{84}Kr. The energy spectra of the N=48 isotones with Z < 38 differ significantly from those with Z ≥ 38. This difference probably originates from the orbital occupied by valence protons; in the former nuclei the valence protons mainly occupy the fp orbitals while in the latter they occupy the $g_{9/2}$ orbital.

The B(E2) values for the $8^+ \rightarrow 6^+$ transitions in the N=48 isotones[2,4] are also given in Fig. 3. These values are not far from the Weisskopf estimates and seem not to be systematic with the atomic number. For ^{82m}Se, however, the B(E2) value of 0.56(3) W.u. is significantly smaller than those in heavier isotones. This fact suggests that the configuration of the 8^+ state is different from that of the 6^+ state in ^{82}Se; the former state mainly comprises the $(\nu g_{9/2}{}^{-2})_{8^+}$ component while in the latter state, other components mix largely with $(\nu g_{9/2}{}^{-2})_{6^+}$. This interpretation is in good accord with the energy spectrum in ^{82}Se.

References

1)T. Ishii *et al.*, Nucl. Instrum. Methods Phys. Res. A**395**, 210(1997).
2)R.B. Firestone and V.S. Shirley, Table of Isotopes, 8th. ed. (John Wiley & Sons, New York, 1996).
3)P. Hoff and B. Fogelberg, Nucl. Phys. A**368**, 210(1981).
4)M. Gorska *et al.*, Z. Phys. A**353**, 233(1995).

2.10 IN-BEAM γ-RAY STUDY OF ^{79,80}Kr

M. SUGAWARA[1], H. KUSAKARI[2], S. MITARAI[3], M. OSHIMA, T. HAYAKAWA,
Y. HATSUKAWA, J.KATAKURA, H.IIMURA

We made an in-beam spectroscopic study on ^{79,80}Kr through the reaction of ^{50}Ti(^{37}Cl,pαxn) to elucidate the M1 band structures in A≈80 region. A stack of two 0.5 mg/cm^2 ^{50}Ti foils was bombarded with a 150MeV ^{37}Cl beam. Gamma-rays from the reaction products were measured by the GEMINI array[1] consisting of 11 BGO anti-Compton spectrometers in conjunction with a Si ball[2] made up of 21 detector segments. Approximately 1.6×10^8 two- or higher fold γγ events were collected and sorted into an individual E_γ-E_γ matrix tagged with the number of protons and α particles detected in the Si ball.

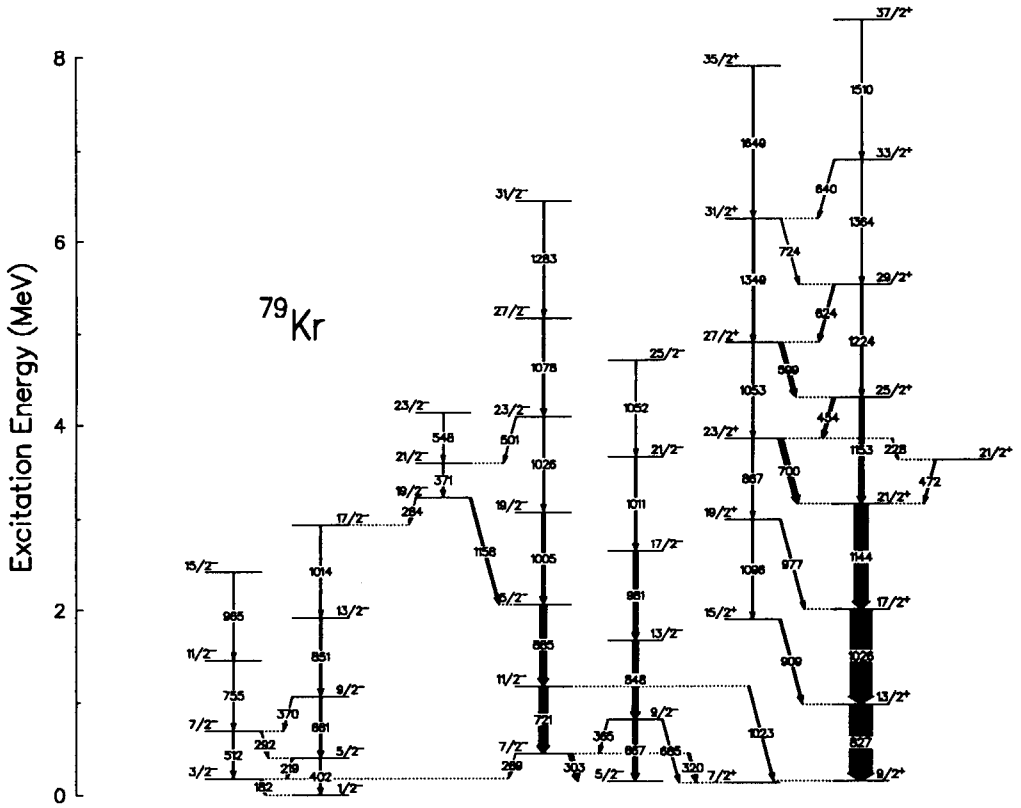

Fig. 1 The level scheme of ^{79}Kr

[1]Chiba Institute of Technology
[2]Faculty of Education, Chiba University
[3]Faculty of Science, Kyushu University

We constructed the level schemes of ^{79}Kr and ^{80}Kr as shown in Fig.1 and Fig.2 respectively using the 1p1α matrix. In ^{79}Kr, the rotational band based on the $(\nu g_{9/2}^{-1})$ configuration was extended to the $37/2^+$ state. In this band, the cascade M1 transitions became prominent after the rotational alignment of $(\pi g_{9/2}^{2})$. Unfortunately, any dipole band could not be observed in ^{80}Kr, however, we could observe the forking of the ground state rotational band caused by the rotational alignment of $(\pi g_{9/2}^{2})$ or $(\nu g_{9/2}^{-2})$. Moreover the negative parity band, which was observed to rather high spin state in ^{78}Kr was extended to the 19^- state.

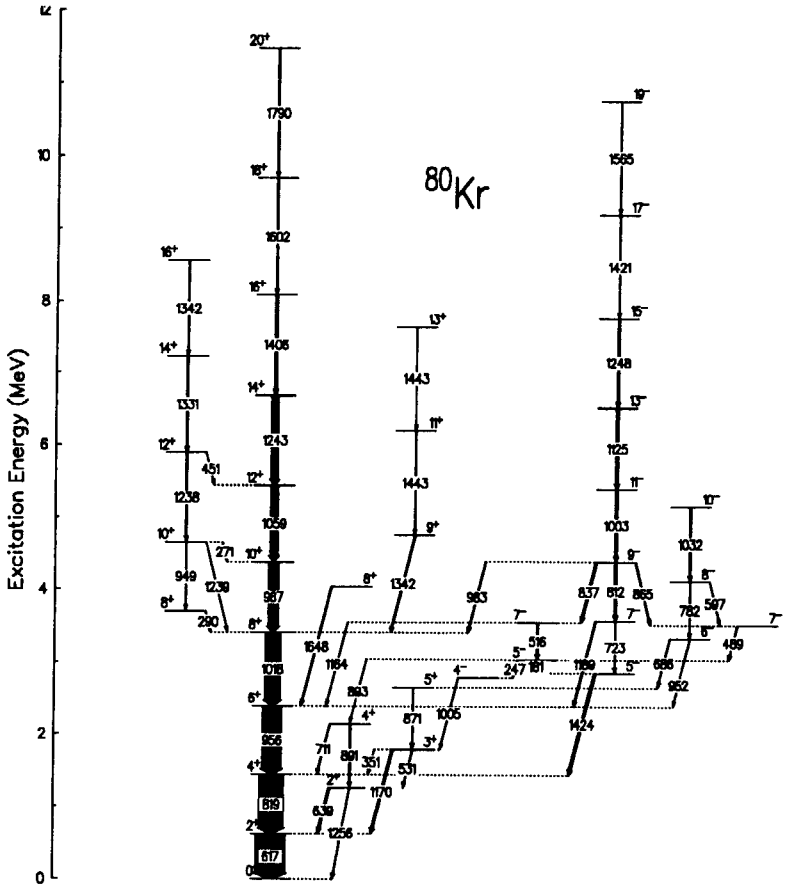

Fig.2 The level scheme of ^{80}Kr

Reference
1) K. Furuno et al., Nucl. Inst. & Method in Phys. Rese. A421(1999)211
2) T. Kuroyanagi et al., Nucl. Inst. & Method in Phys. Rese. A316(1992)289

2.11 HIGH-SPIN STATES IN ^{180}Os

T. SHIZUMA[1] , T. JUMATSU[1], K. UCHIYAMA[1,2] , K. SATO[1], K. YAMADA[1],
Y. SASAKI, H. ISHIYAMA[1], T. KOMATSUBARA[1], K. FURUNO[1],
M. SUGAWARA[3] , M. OSHIMA, T. HAYAKAWA, Y. HATSUKAWA,
J. KATAKURA, H. IIMURA and M. MATSUDA

Nuclei around the mass number $A = 180$ region can accumulate spins by collective rotation and/or orientation of individual angular momenta into the nuclear symmetry axis. The latter is called as deformation alignment. Since the projection of the total spin onto the symmetry axis (K) is approximately conserved, an additional selection rule is imposed for transitions between states with different K values (K selection rule). As a result, high-K states are usually observed as isomers with long half-lives. These isomers are often referred to as K isomers. Studies of high-K isomers are one of the current topics on nuclear structure physics [1, 2].

In the previous work [3], two high-K isomers with $I,K \geq 20$, $T_{1/2} = 12$ ns and $I,K > 16$, $T_{1/2} = 41$ ns were found in ^{180}Os. However, no detailed decay scheme of these isomers was reported. The present experiment was intended for revealing them, and investigating decay properties of the isomers.

High-spin states of ^{180}Os have been populated by the ^{170}Er(^{16}O,6n) reaction at a beam energy $E_b = 103$ MeV. The target consisted of a 2 mg/cm^2 metallic foil of ^{170}Er (95.88 % enrichment) with a 10 mg/cm^2 lead backing. Emitted γ rays were measured by the **GEMINI** spectrometer [4] consisting of 12 Compton-suppressed Ge detectors. These were positioned at 32° (2 detectors), 58° (2), 90° (4), 122° (2) and 148° (2) with respect to the beam direction. Detection of two or more γ rays was required for trigger condition. The resolving time of the trigger system was set to 200 ns, allowing us to observe delayed transition from isomers with half-life ranging from $\sim$ 10 to $\sim$ 100 nano seconds. A total of 400 million events were stored onto magnetic tapes. Figure 1 shows a γ-ray energy spectrum obtained in the present experiment. Preliminary inspection of the data has indicated a dominant population of ^{180}Os (6n exit channel) compared to ^{181}Os (5n), with all lines identified being consistent with the previous work [5]. Further analysis of delayed coincidence γ rays is in progress.

[1] Tandem Accelerator Center, University of Tsukuba
[2] RIKEN
[3] Chiba Institute of Technology

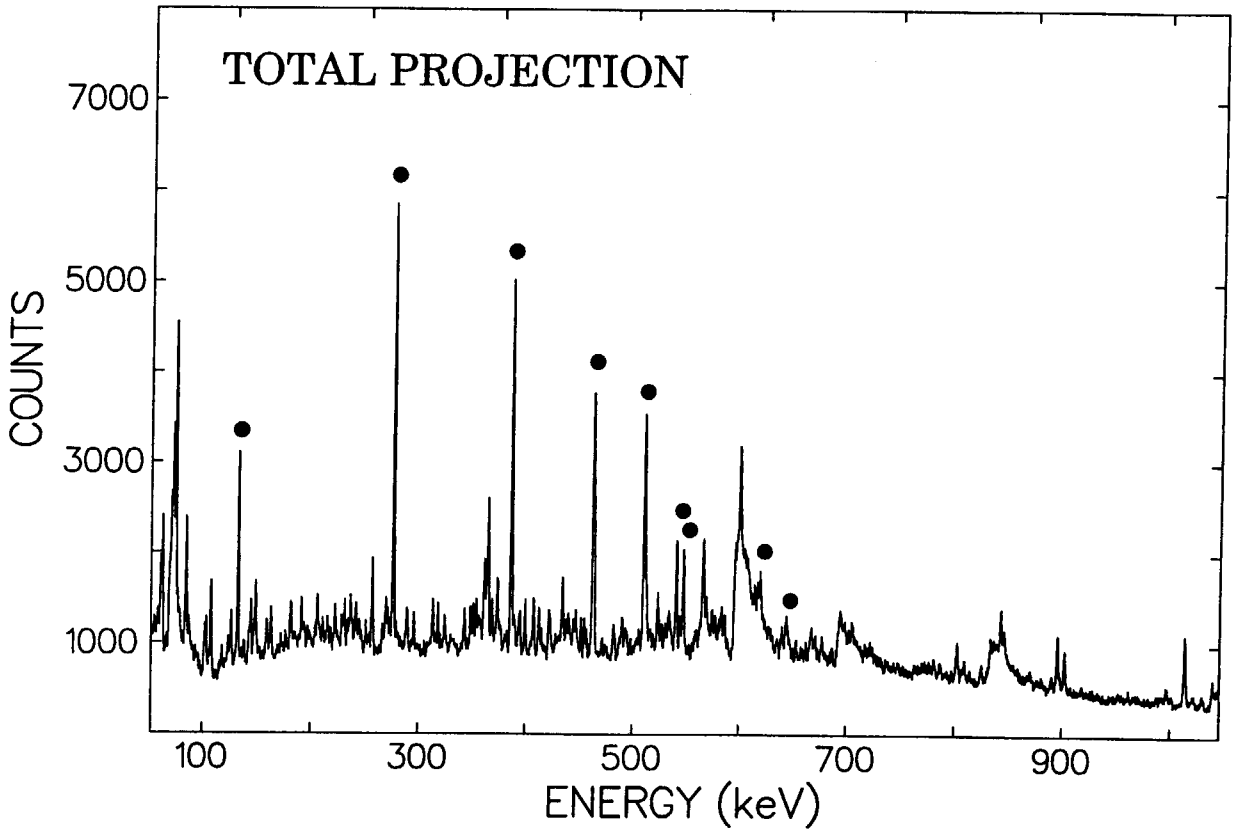

Fig. 1. Total projection of γ-ray spectra obtained in the ^{170}Er(^{16}O,xn) reaction at E_b = 103 MeV. Assigned peaks are marked by filled circles.

References

[1] K. Narimatsu et al., Nucl. Phys. **A601** (1996) 69

[2] T. Shizuma et al., Nucl. Phys. **A626** (1997) 760

[3] Ts. Venkova et al., Z. Phys. **A344** (1993) 417

[4] K. Furuno et al., Nucl. Instr. and Meth. **A421** (1999) 211

[5] R.M. Lieder et al., Nucl. Phys. **A476** (1988) 545

3. Nuclear Reactions

This is a blank page.

3.1 ENERGY DEPENDENCE OF THE TWO-NEUTRON TRANSFER REACTION IN THE NI+NI SYSTEM AROUND THE COULOMB BARRIER

Y.SUGIYAMA, S.HAMADA and A.YAMAZAKI[1]

The strong enhancement of pair-transfer between the ground states of superfluid nuclei was predicted in a heavy-ion collision due to the coherent nature of the superfluid states [1]. Weiss estimated the pair-nucleon transfer cross section based on a semi-classical description and concluded that the enhancement depended on an incident energy[2]. He predicted the possibility of the strong enhancement of pair-transfer, which was called as nuclear Josephson effect, just below the Coulomb barrier.

So far we measured two-neutron transfer reactions leading to the ground states for the ^{58}Ni+^{60}Ni , ^{62}Ni+^{64}Ni ,^{58}Ni+^{64}Ni abd ^{64}Ni+^{64}Ni systems at energies above the Coulomb barrier(V_{CB}=100MeV) [3,4]. The pair-transfer cross section was observed to increase as the number of valence neutron. The ^{64}Ni+^{64}Ni system had the larger pair -transfer cross section than the one predicted by the BCS wave function of the ground state.

In order to get more insight into the nuclear Josephson effect, we measured two-neutron transfer cross sections for the ^{58}Ni+^{64}Ni and ^{64}Ni+^{64}Ni systems at a sub-barrier energy of E_{cm}=95MeV by using the JAERI tandem accelerator and the heavy-ion magnetic spectrograph "ENMA"[5]. The spectrograph has a characteristic feature that the kinematic energy broadening is well compensated, so that a high energy resolution is achieved. Angular distributions of ^{58}Ni(^{64}N,^{62}Ni$_{g.s.}$)^{60}Ni$_{g.s.}$ and ^{64}Ni(^{64}N,^{62}Ni$_{g.s.}$)^{66}Ni$_{g.s.}$ at E_{cm}=95MeV are shown in Fig.1. In the figure the data measured at above-barrier energies are shown as well.

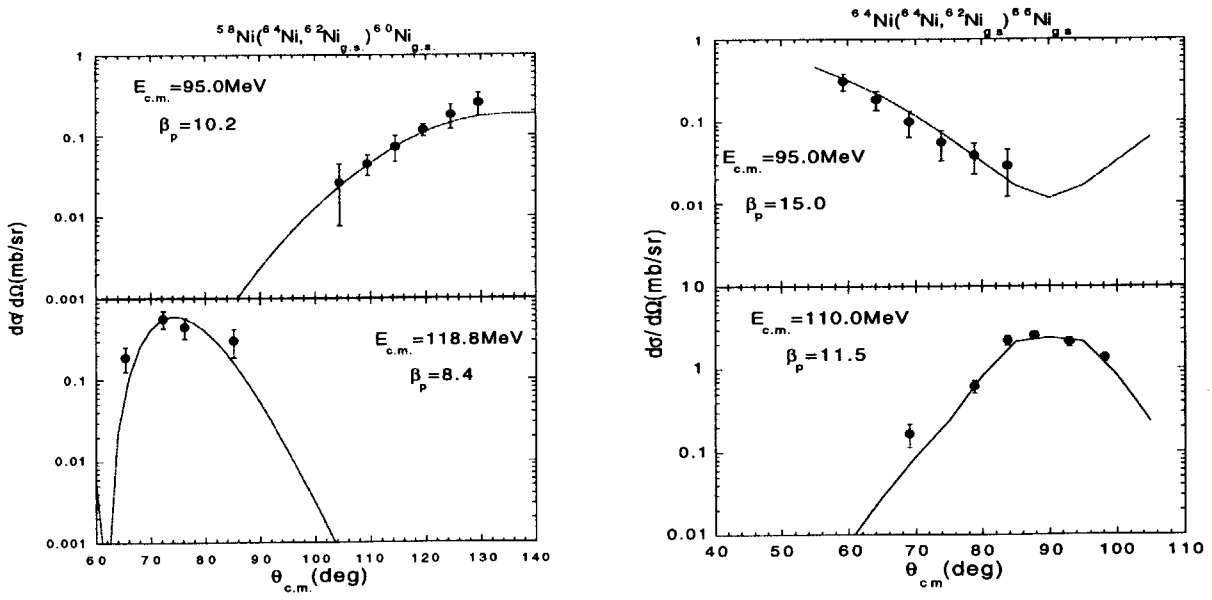

Fig.1 Angular distributions of ^{58}Ni(^{64}Ni,^{62}Ni$_{g.s.}$)^{60}Ni$_{g.s.}$ (left) and ^{64}Ni(^{64}Ni,^{62}Ni$_{g.s.}$)^{66}Ni$_{g.s.}$(right) reactions measured at two energies below and above the Coulomb barrier(V_{CB}=100MeV). Solid lines are the results of the DWBA calculations.

[1]Physics Department, Tohoku University

Elastic scattering data measured at the same time were analyzed by the coupled-channels calculation including the first 2^+ and 3^- states of target and projectile nuclei. We obtained the optical potential parameter by fitting the data.

The two-neutron transfer amplitude was calculated by using the macroscopic pair-transfer form factor of $F(r)=(\beta_p R/3A)(dU/dr)$, where β_p is the pair-deformation parameter which measures the collective strength of the pair modes[6]. R, A and U are the nuclear radius, mass number and the optical potential, respectively. For the case of superfluid systems, a large pair-transfer cross section is predicted by the BCS approximation in which the pair-deformation parameter β_p is expressed as $\beta_p=2\Delta/G$, where Δ and G are the gap parameter and the pairing strength, respectively[7]. For the Ni+Ni system ,the pair-deformation parameter is estimated as β_p~9.5 with the approximated values of $\Delta=12/A^{1/2}$ (MeV) and G=20/A (MeV). The experimental data were analyzed by DWBA calculations with the computer code Ptolemy where β_p was adjusted to fit the data. The calculated results are shown by solid lines in Fig.1. The obtained pair-deformation parameter β_p increases just below the Coulomb barrier for both systems like as the prediction by Weiss[2] . Especially the $^{64}Ni+^{64}Ni$ system had the pair-neutron transfer cross section of $\beta_p=15.0$ at $E_{c.m.}=95.0$MeV larger than the one predicted for the g.s. BCS wave function. This result can suggest a possible existence of the nuclear Josephson effect in the $^{64}Ni+^{64}Ni$ system just below the Coulomb barrier.

References

1)V.I.Gol'danskii and A.I.Lapkin, Th. Eksp.Theor. Fiz.53(1967)1032.
2) H.Weiss, Phy. Rev. C19 (1979) 834.
3)Y.Sugiyama et al., Phys. Rev. C55(1997)R5.
4)Y.Sugiyama et al., J. Phys. G. 23 (1997)1393.
5)Y.Sugiyama et al., Nucl. Instrum. Methods Phys. Res.A281(1989)512.
6)C.H.Dasso and G.Pollarolo, Phys. Lett. 155B(1985)223.
7)D.R.Bes, P.Lotti, E.Maglione and A.Vitturi, Phys. Lett. 169B(1986)5.

3.2 NUCLEON INTERACTION AND COLLECTIVE STRUCTURE OF ^{12}C BY THE SOFT-ROTATOR MODEL

S. CHIBA, O. IWAMOTO and E. Sh. SUKHOVITSKIJ[1]

The ^{12}C nucleus has attracted a good deal of attention from both the basic and applications points of view. On the fundamental side, the collective nature of ^{12}C has been offering very good tests for nuclear structure and reaction theories. Until now, however, no consistent attempt has been given to describe the low-lying collective level structure and nucleon scattering data in a unified framework. The purpose of this work is to give a consistent description of the collective nuclear structure and nucleon scattering properties of ^{12}C in the framework of the soft-rotator model. As the details of the measurement and theoretical analysis are described in our publications[1-4], only the typical results and discussions are given below.

The neutron elastic and inelastic scattering angular distribution data were measured at 28.2 MeV at JAERI tandem accelerator to strengthen the data-base on neutron-carbon interactions. Then, the soft-rotator model was applied to analyze the collective nuclear level structure of ^{12}C. The experimental level scheme is compared with the prediction of the soft-rotator model in Fig. 1. Rotational bands are not prominent in the case of ^{12}C. Nevertheless we could assign the first excited level of the ground state rotational band, 2^+ (4.44 MeV), and 3^+ (20.56 MeV) to be a level of $K \fallingdotseq 2$ band with a good accuracy. The experimentally measured 0^+ (7.65 MeV) level in our scheme appears to be a band head of K=0, $n_{\beta 2}$=1 band, with predicted energy of 7.72 MeV. The 4^+ ground state rotational band level is suggested to be at 13.7 MeV, while the experimental energy is 14.08 MeV. A level with spin 2^+, K=0 and $n_{\beta 2}$=1 is predicted by our model with energy 11.94 MeV which can be attributed to one of the experimentally measured levels with energies 16.11 and 15.4 MeV having no spin assignment, as we see no other assignment possibility. It is seen that our model permits the description of the experimentally measured levels of positive parity up to 20 MeV, except those 1^+, which are not considered.

The intrinsic wave function obtained in the above analysis was used to calculate the coupling potentials in the coupled-channels theory, which yielded the neutron total cross section and neutron and proton scattering cross sections via the direct reaction mechanism. Figure 2 shows the elastic scattering angular distributions for neutrons and protons. It is evident that the experimental scattering data are described fairly well by the present model. Similar good description was obtained for the inelastic scattering. The poor description for a couple of lowest energy data can be easily understood because the compound resonance structure influences neutron interaction data up to approximately 22 MeV and the proton scattering data up to 25 MeV.

References

1) S. Chiba, O. Iwamoto, Y. Yamanouti, M. Sugimoto, M. Mizumoto, K. Hasegawa, E.S. Sukhovitskij, Y.V. Porodzinskij and Y. Watanabe, Nucl. Phys. **A624**(1997)305.
2) E.S. Sukhovitskij, S. Chiba, O. Iwamoto and Y.V. Porodzinskij, Nucl. Phys. **A640**(1998)147.
3) E.S. Sukhovitskij, Y.V. Porodzinskij, O. Iwamoto, S. Chiba and K. Shibata, "Programs OPTMAN and SHEMMAN VERSION 5(1998) ", JAERI-Data/Code 98-019 (1998).
4) E.S. Sukhovitskij, S. Chiba and O. Iwamoto, Nucl. Phys. **A646**(1999)19.

[1] Radiation Physics and Chemistry Problems Institute, 220109, Minsk-Sosny, Belarus

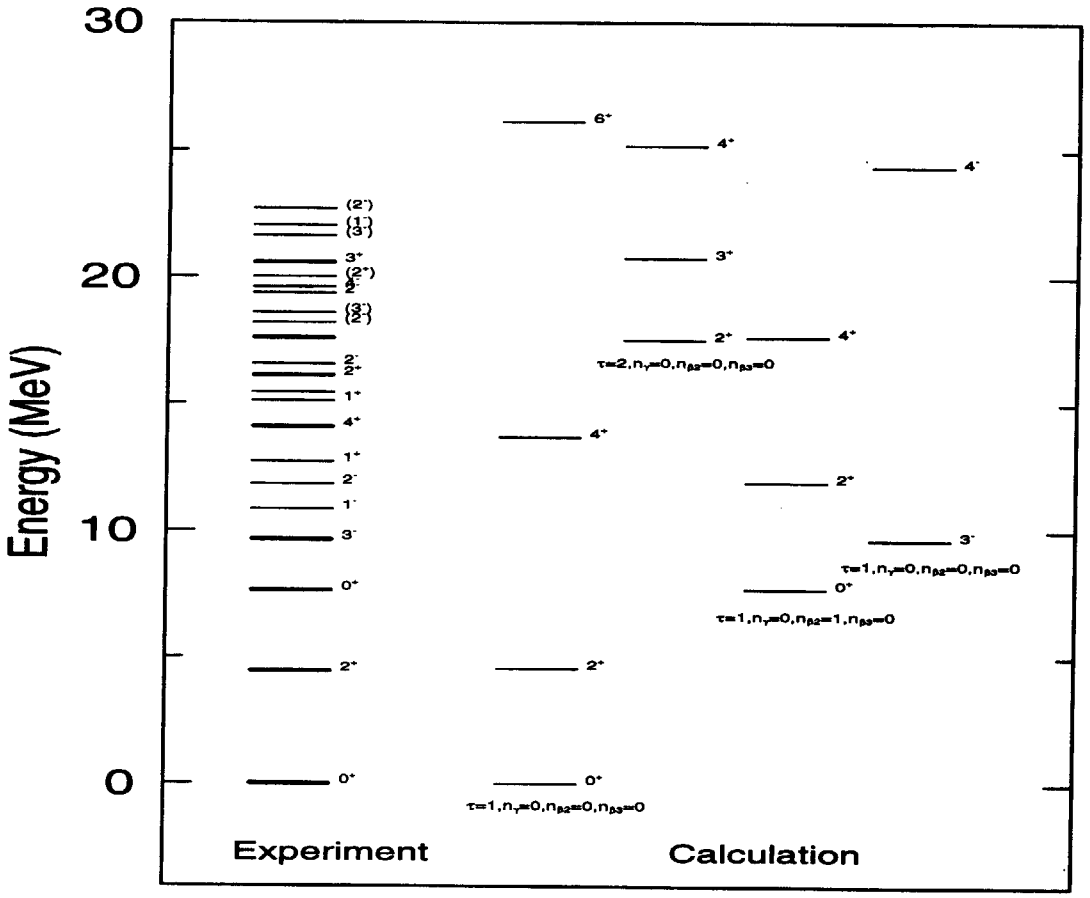

Fig. 1 Comparison of experimental and calculated level schemes. Thick lines show experimental levels described by the soft-rotator model.

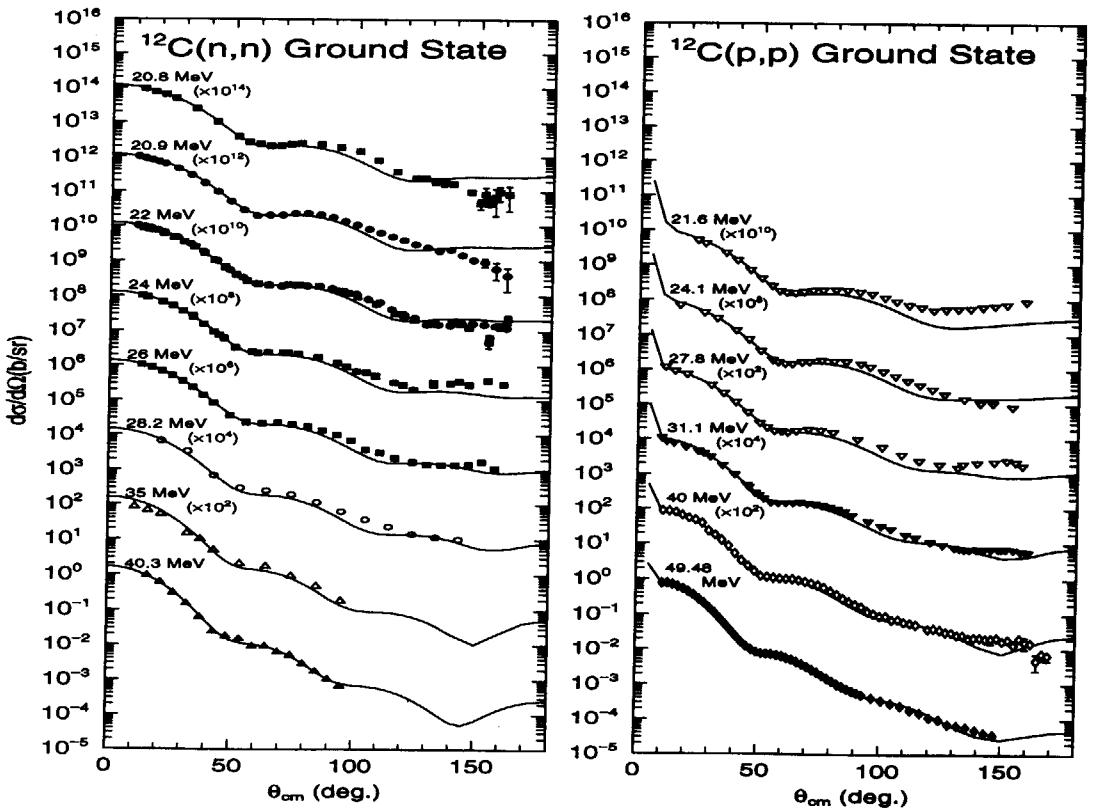

Fig. 2 Comparison of experimental and calculated angular distributions for elastically scattered nucleons from ^{12}C. Left : neutron scattering, right : proton scattering. Solid line : Present calculation, symbols : experimental data.

3.3 SUB-BARRIER FUSION OF DEFORMED NUCLEI IN THE REACTIONS OF ^{60}Ni+^{154}Sm and ^{32}S+^{182}W

S. MITSUOKA, H. IKEZOE, K. NISHIO, J. LU

As a new approach to the superheavy-element production, the gentle fusion [1] and the hugging fusion [2] between deformed nuclei have been theoretically proposed. It is predicted that the fusion cross section to form the compound nucleus may be significantly large when two well deformed nuclei take the most compact touching configuration. In order to investigate this prediction experimentally, we have measured the fusion cross section in the ^{60}Ni+^{154}Sm reaction near the Coulomb barrier, where the ^{154}Sm target is well deformed (β_2=0.32). In such reaction between the heavy ions, it is considered that the extra-push phenomenon becomes much important to the compound-nucleus formation in the sub-barrier region. To get the direct evidence that the heavy-ion projectile really fuses with the deformed target in the entrance channel, the fusion-evaporation residues (ER) were measured in the ^{60}Ni+^{154}Sm reaction and also in the ^{32}S+^{182}W reaction, where the ^{182}W target is also well deformed (β_2=0.28). In both the reactions, the same compound nucleus ^{214}Th was formed. Since the ^{32}S+^{182}W reaction with the light projectile is expected to need no extra-extra push energy, this reaction system was used as a reference to know the fusion-evaporation process from the compound nucleus ^{214}Th in the exit channel.

^{60}Ni and ^{32}S beams from the JAERI tandem accelerator were used to bombard 350 μg/cm^2 thick ^{154}Sm target (oxide, 98.6% enriched) and 400 μg/cm^2 thick ^{182}W target (metal, 94.5% enriched), respectively. The ER separated in flight from the primary beam by the JAERI-RMS [3] were passed through two thin-foil timing detectors and then implanted into a double-sided position sensitive detector. The kinetic energy, the detecting time and two-dimensional positions of both the implanted ER and the subsequent α-decay particles were measured. The identification of the detected ER was achieved by the correlation analysis of the α-decay events. Since the α-decay properties of some two isotopes (e.g. ^{212}Th and ^{211}Th, ^{211}Ac and ^{210}Ac, and so on) are very similar each other until they reach their granddaughter nuclei, the definite identification between them were not achieved.

The measured ER's excitation function in the ^{32}S+^{182}W reaction is shown in Fig. 1. The data were compared with statistical model calculation (the solid lines) using the code HIVAP [4], where the level density parameters at the ground state deformation and the saddle point deformation were varied with excitation energies with assuming the ratio of these parameters to be 1.0. The fission barrier was assumed to be the substruction of the shell correction energy from the liquid drop fission barrier. The later barrier height, which generally tends to be large, was reduced by half so as to reproduce the absolute ER's cross section. In this experiment, in order to obtain the absolute total fusion cross section, the fission fragments were measured by using two gas ionization detectors [5]. The fusion-fission cross section was compared with a couple-channel calculation using the code CCDEF [6], where the target deformation and the coupling effects of the inelastic excitations were taken into account for both the projectile and the target. Since the good agreement between the data and the calculated results was obtained, the above parameters used for the ^{32}S+^{182}W system were also used in the calculation for the ^{60}Ni+^{154}Sm system.

Figure 2 shows the measured ER's cross section in the ^{60}Ni+^{154}Sm reaction together with the calculated results (the solid lines). It is remarkable that no ER was observed at E_{cm} = 175 and 182 MeV in the contrast with the calculations for the ER corresponding to the 2n, α and αp channels. The upper limits of the cross section at each E_{cm} were determined as 1-event counting yield as shown in Table 1. In addition, the ER cross sections corresponding to the 3n, p2n, αp, αn and α2n channels were considerably smaller than those of the calculated results at the low energy region of E_{cm} = 180 ~ 200 MeV. In the CCDEF calculation, the Coulomb barrier height depends on the colliding angle θ of ^{60}Ni projectile with respect to the orientation of the symmetric axis of the deformed ^{154}Sm target. When the projectile collides at the tip of the ^{154}Sm (θ = 0°), the barrier height becomes the lowest value of 172 MeV, while the maximum is 198 MeV at the side collision (θ = 90°). Since the barrier distribution becomes slightly wide due to the inelastic coupling to the projectile and the target, the ER yields at E_{cm} ~ 180 MeV mainly come from the near tip collisions, and from the side collision at E_{cm} ~ 200 MeV. The fact that no ER was observed at E_{cm} = 175 and 182 MeV suggests that the fusion probability is significantly small at the near tip collision. And it is considered that the complete fusion occurs at the side collisions, since the data at the higher energy than E_{cm} ~ 200 MeV are well reproduced.

In order to confirm this, we calculated the ER's cross section by assuming the extra-extra push energy E_{xx} of 20 MeV at the barrier top in the tip collision and no E_{xx} at the side collision, that is E_{xx} = 20(1-θ/90°). The fact that the calculated results (the dashed lines in Fig. 2) agree with the data supports that the E_{xx} around 20 MeV is needed in the tip collision and nearly zero E_{xx} in the side collision. This suggest that the compact touching configuration leads to form the compound nucleus more easily than an elongated configuration.

References

1) W. Nörenberg, Proc. Int. Workshop on Heavy-Ion Fusion, Padva, Italy (1994).
2) A. Iwamoto et al., Nucl. Instrum. and Methods A596, 329 (1996).
3) H. Ikezoe et al., Nucl. Instrum. and Methods A376, 420 (1996).
4) W. Reisdorf and M. Schädel, Z. Phys. A343, 47 (1992).
5) K. Nishio et al., JAERI Tandem & V.D.G Annual Report 1998.
6) J. Fernandez et al., Comp. Phys. Comm. 54, 409 (1989).

Table.1 Upper limit of the ER cross sections in the ^{60}Ni+^{154}Sm reaction.

E_{CM} (MeV)	$\overline{\sigma}$ (mb)	E_{CM} (MeV)	$\overline{\sigma}$ (mb)
175	1.5×10^{-6}	200	2.5×10^{-6}
182	2.4×10^{-6}	203	1.5×10^{-6}
184	2.6×10^{-6}	209	1.3×10^{-5}
188	4.3×10^{-6}	214	7.3×10^{-6}
194	9.6×10^{-6}		

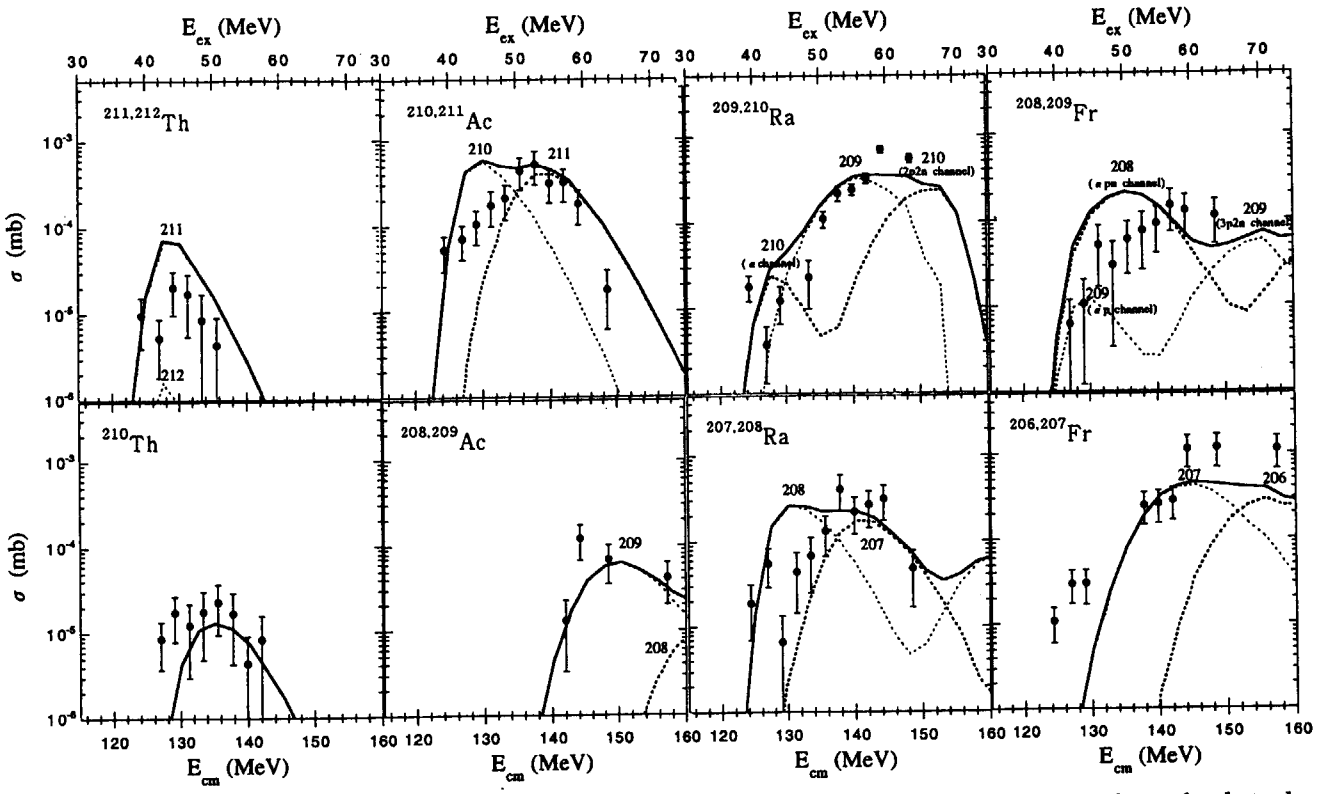

Fig.1 Measured ER cross sections in the $^{32}S+^{182}W$ reaction. The solid lines are the calculated results of HIVAP. The dotted lines show the components of each ER mass.

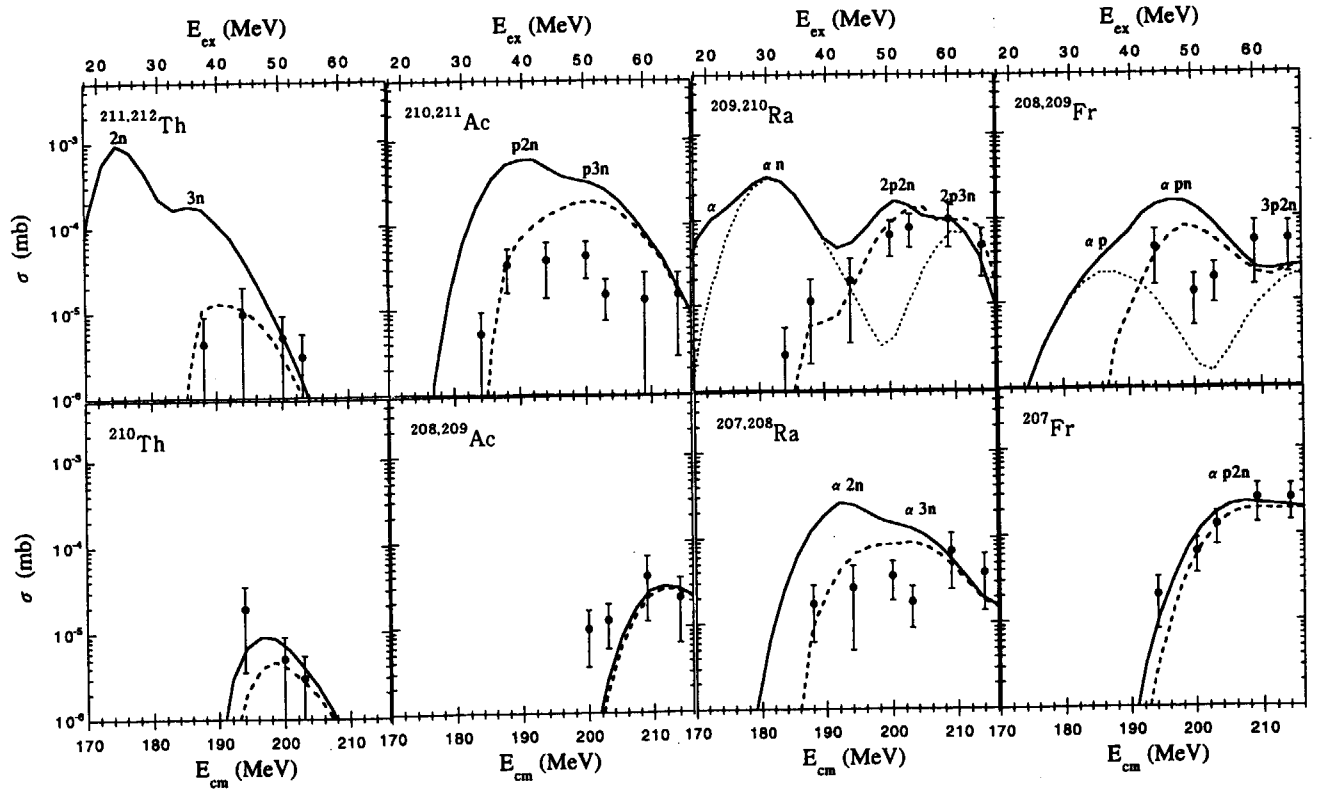

Fig.2 Measured ER cross sections in the $^{60}Ni+^{154}Sm$ reaction. The solid and dashed lines are the calculated results of HIVAP without and with the extra-extra push energy, respectively. The dotted lines show the components of some ER channels.

3.4 Measurement of fusion cross section for $^{32}S + ^{182}W$

K. NISHIO, J.LU [1], H. IKEZOE and S. MITSUOKA

Heavy-ion fusion cross sections at bombarding energies near the Coulomb barrier show a large enhancement relative to the predictions of the one-dimensional barrier penetration model. A coupled channel model has been widely used to explain this enhancement [1]. We have determined the fusion cross section for $^{32}S + ^{182}W$ (compound nucleus ^{214}Th), by measuring the fission cross section. The experimental results were compared with the coupled channels calculation using the code CCDEF [2].

In order to measure the fission cross section, we have developed a position sensitive ΔE-E ionization chamber. The structure of the ionization chamber is shown in Fig.1. It consists of the position sensitive detector (PSD) and the ionization chamber, which are mounted in the stainless steel container. The container has the entrance window of 2.0 μm Mylar film. The PSD has an active area of 34.0 mm length × 2.5 mm width. The ionization chamber is located in front of the PSD to pick up the energy loss signal of reaction products. It consists of three electrodes (anode (A), grid(G) and cathode (C)) having trapezoid-like shape. The ionization chamber is operated with 20 ± 1 Torr isobutane under gas flow condition. The voltage applied to the grid and the anode is 60 V and 180 V, respectively, and the cathode is grounded.

Fusion cross section for the $^{32}S + ^{182}W$ reaction was measured by using the ^{32}S beam (145 ~ 200MeV) supplied by the JAERI-tandem accelerator. The target of 180 μg/cm^2 thickness was made by sputtering the enriched material of ^{182}W isotope on a 30 μg/cm^2 carbon foil. We used two ΔE-E ionization chambers, which covered the laboratory angles of φ_{LAB}= 60°~90° and φ_{LAB}= 120°~150°. The fission fragments were clearly distinguished from other reaction products in the ΔE-E spectrum. The position signal of the PSD was used to determine φ_{LAB} of the fission fragments. The angular distribution of fission fragments in the center-of-mass system was obtained by applying the laboratory to center-of-mass Jacobian to the cross section obtained in the laboratory system. In this process, the symmetric mass division was assumed and the total kinetic energy was estimated from the Viola systematics [3]. We thus determined the fusion cross section for each bombarding energy by integrating the fission angular distribution over angle.

The measured fusion cross sections for $^{32}S + ^{182}W$ are shown in Fig.2 by solid circles as a function of c.m. energy E_{cm}. In this figure data cited from ref.[4] is also shown by open circles. The dotted curve is the prediction by the one-dimensional barrier penetration model. This model cannot reproduce the experimental data below E_{cm}=142 MeV. The long dashed curve in Fig.2 is the calculated results which takes into account the effects of static quadrupole (β_2=0.272) and hexadecapole (β_4=–0.106) deformations for the target [5]. The fusion barrier height for the $^{32}S + ^{182}W$ system varies with the colliding angle of the projectile with respect to the symmetric axis of the target, leading to the enhancement of the fusion cross section at the sub-barrier energy. However the calculation considering only the static deformation of the target cannot reproduce the experimental fusion cross sections for the energy below the Bass barrier (137 MeV). We considered the inelastic channel as the additional couplings. The solid curve show the results including couplings to the quadrupole (2^+) and and ocyupole (3^-) vibrational states in ^{32}S. The deformation parameters (excitation energies) used in this calculation

1 Institute of Modern Physics, Chinese Academy of Sciences, 730000 Lanzhou, China

are β_2=0.312 (2.23MeV) [6] and β_3=0.485 (5.006MeV) [7]. We also considered the octupole vibrational state in ^{182}W with β_3=0.050 (1.37MeV) [7]. The calculated fusion cross section reproduce the experimental data quite well. The couplings of the inelastic channels as well as the static deformation of the target extends the barrier distribution to about E_{cm}=123 MeV, which give rise to the large fusion enhancement at the sub-barrier energy region.

References

[1] W. Reisdorf, J. Phys.G **20** (1994) 1297.
[2] J. Fernandez-Niello *et al.*, Comput. Phys. Commun. **54**, (1989) 409.
[3] V.E. Viola *et al.*, Phys. Rev. C **31** (1985) 1550.
[4] J.G. Keller *et al.*, Phys. Rev C **36** (1987) 1364.
[5] I.Y. Lee *et al.*, Phys. Rev. C **12** (1975) 1483.
[6] S. Raman *et al.*, At. Data and Nucl. Data Tables **36** (1987) 1.
[7] R.H. Spear, At. Data and Nucl Data tables **42** (1989) 55.

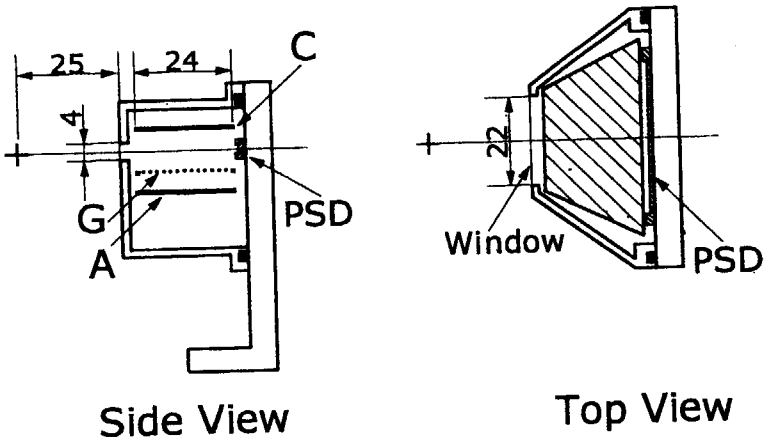

Fig.1 Design of the position sensitive ΔE-E ionization chamber. The dimension is indicated by mm unit.

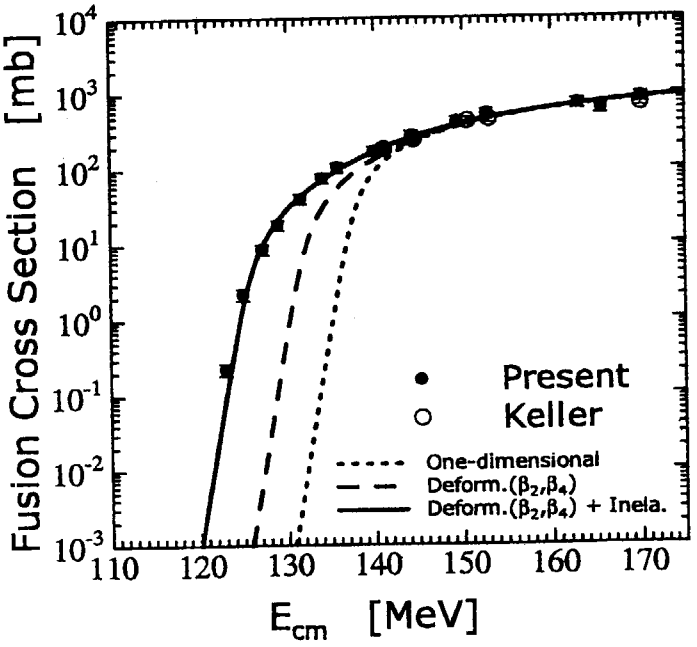

Fig.2 Fusion cross section for ^{32}S + ^{182}W.

3.5 Preequilibrium fission following fusion of $^{32}S + ^{182}W$

K. NISHIO, H. IKEZOE, S. MITSUOKA and J.LU[1]

In recent years there has been much interest in the failure of the transition state model (TSM) of fission fragment angular distributions in sub-barrier fusion reactions involving actinide target. Two of the popular models that attempt to explain the anomalously high anisotropies [$A=W(180°)/W(90°)$] of fission fragments are the preequilibrium K-state model [1] and the orientation-dependent quasi-fission model [2]. In order to investigate this phenomena, we have measured the fission fragment angular distribution for the $^{32}S + ^{182}W$ reaction. As the colliding nuclei are not fissile, the present reaction exclude the transfer fission, which is peculiar to the system involving an actinide nucleus. The anisotropy for $^{32}S + ^{182}W$ showed the anomalous enhancement relative to the prediction of TSM below the sub-barrier energy. This work suggested that fission took places before the K-degree of freedom was equilibrated for $^{32}S + ^{182}W$.

A beams of ^{32}S was used to irradiate the ^{182}W target whose thickness was 180 μg/cm^2. Two position sensitive ΔE-E ionization chambers [3] were used to measure the fission fragment angular distribution. Figure 1 shows examples of the measured fission fragment angular distributions for $^{32}S + ^{182}W$. The data points are fitted with

$$W(\theta) = a \sum_{I=0}^{\infty} (2I+1) T(I) \frac{\sum_{K=-I}^{I} \frac{1}{2}(2I+1) \left| d^{I}_{0,K}(\theta) \right|^2 \exp(-K^2 / 2K_0^2)}{\sum_{K=-I}^{I} \exp(-K^2 / 2K_0^2)},$$

which involves a summation over spin I and its projection K on the symmetry axis of the fissioning system. The variance K_0^2 and a are the adjustable free parameters. In this formula, $d^{I}_{0,K}$ stands for the symmetric top wave function. We have calculated the transmission coefficient $T(I)$ for the partial wave I by using the code CCDEF [4]. In this calculation the static target deformation and couplings to inelastic channels of the projectile and target nuclei were incorporated. The results of fitting the data with this formula are shown in Fig.1 by solid curves. The dashed curves are the estimated error limits. The variance K_0^2 determined in this analysis is shown in Fig.2(a) as a function of mean square spin $\langle I^2 \rangle$. Figure 2(b) shows the anisotropy A plotted as a function of center-of-mass energy normalized to the Bass barrier, E_{cm}/V_b (V_b=137MeV) . Data cited from ref.[5] are also shown.

The TSM calculation was made to demonstrate the variance K_0^2 and the anisotropy, and the results are shown by the dashed curves in Fig.2. This model cannot explain the sharp decrease of the K_0^2 observed at the energy below the Bass barrier and underestimates the anisotropy. The results of the calculation based on the preequilibrium fission model [1] are shown by solid curves. This model reproduces the K_0^2 as well as the anisotropy. The quasifission below the Coulomb barrier is not observed from the measurement of evaporation residue cross section for $^{32}S + ^{182}W$ [6], thus the quasifission is not the reason for the anomalous anisotropy or the variance K_0^2.

1 Institute of Modern Physics, Chinese Academy of Sciences, 730000 Lanzhou, China

References

[1] Z.Liu *et al*, Phys. Rev. C **54** (1996) 761.
[2] D.J.Hinde *et al.*, Phys. Rev. Lett. 74 (1995) 1295.
[3] K. Nishio *et al.*, JAERI Tandem & V.D.G Annual Report 1998.
[4] J. Fernandez-Niello *et al.*, Comput. Phys. Commun. **54**, (1989) 409.
[5] J.G. Keller *et al.*, Phys. Rev C **36** (1987) 1364.
[6] S. Mitsuoka *et al.*, JAERI Tandem & V.D.G Annual Report 1998.

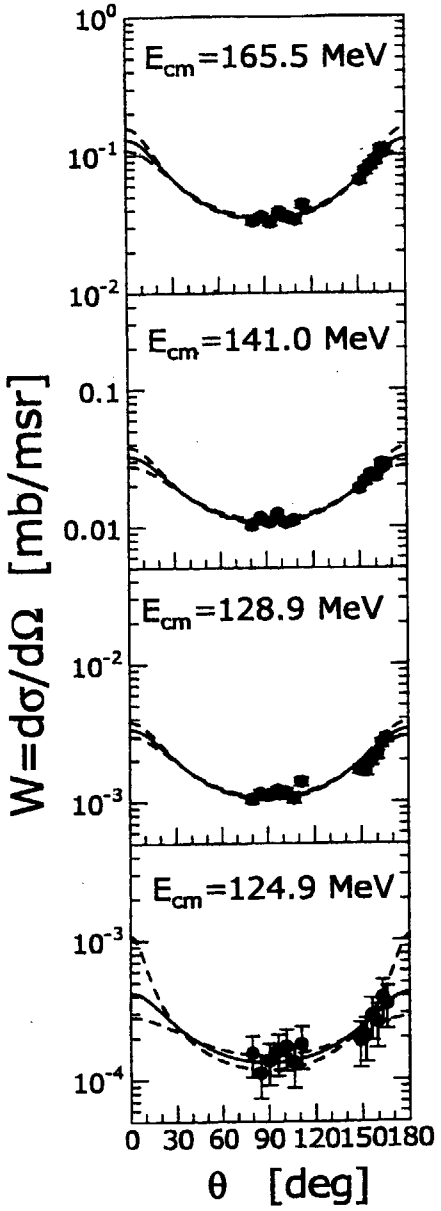

Fig.1 Fission Fragment angular distribution for ^{32}S + ^{182}W.

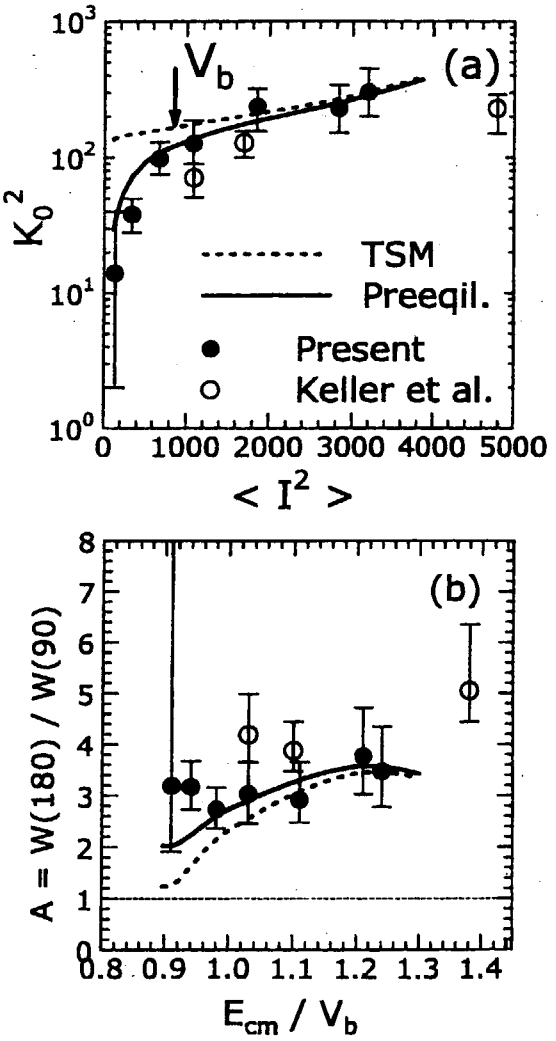

Fig.2 (a) Variance K_0^2 as a function $\langle I^2 \rangle$.
(b) Anisotropy A=W(180°)/W(90°)

3.6 MEASUREMENTS OF FUSION AND EVAPORATION RESIDUE CROSS SECTIONS FOR $^{28}Si+^{198}Pt$

K. NISHIO, H. IKEZOE and S. MITSUOKA

When proton numbers of a projectile (Z_p) and target nuclei (Z_t) increase to beyond the Z_pZ_t value of 1800, the reaction system does not fuse together below the kinetic energy corresponding to the fusion-barrier [1]. We have indicated in the ^{60}Ni + ^{154}Sm system (Z_pZ_t =1736; compound nucleus ^{214}Th), by measuring the cross sections of the evaporation resudues, that the minimum kinetic energy needed to fuse the sytem is about 20 MeV higher than the calculated fusion-barrier when the projectile collides with the tip of the deformed ^{154}Sm nucleus [2]. On the other hand, the extra energy is not needed to fuse the system when the projectile collides with the side of ^{154}Sm. As the Z_pZ_t value for the ^{76}Ge + ^{150}Nd is large (Z_pZ_t =1920; compound nucleus ^{226}U) compared to the ^{60}Ni + ^{154}Sm system, the additional energy is predicted to be larger than 20 MeV. In order to investigate such entrance channel effects on the fusion mechanism, it is important to understand the deexitation process (exit channel) of ^{226}U. This was performed by measuring the fission- and evaporation residue cross sections for the ^{28}Si + ^{198}Pt system, which forms the same compound nucleus ^{226}U.

A beams of ^{28}Si was used to bombard the ^{198}Pt target whose thickness was 460 $\mu g/cm^2$. In this study, two kinds of experiments were made. The first one was to measure the fission cross section. The fission fragments were detected with an ΔE-E ionization chamber [3]. We have measured the evaporation residue cross sections as the second experiment. The evaporation residues emitted to the beam direction were separated in flight from the beams by the recoil mass separator (JAERI-RMS [4]) and focused to a focal plane detector. The evaporation residues were identified by measuring the energy and life-time of their α-decay.

The fission cross sections measured in this work are shown by open circles with error bars. The thick curve is the calculated fusion cross section based on the coupled channels model [5]. In this calculation, the deformations of ^{28}Si and ^{198}Pt are included. The couplings to the vibrational levels of both nuclei are also considered. The calculation nicely reproduces the experimental data. On the other hand, the one-dimensional barrier penetration model (thick dotted curve) underpredict the data at the energy below the Coulomb barrier. The experimental results of the evaporation residue cross sections are shown by solid circles in (a)-(f). Thin curves are the results from a statistical model calculation. In this calculation, the fusion cross section (thick solid curve) calculated by the coupled channels model was adapted. The parameters describing the evaporation process are taken from the results we have obtained in the previous study of $^{32}S+^{182}W$ [2]. For the channels in (a)-(d), the experimental data agree well with the calculations. The calculations for the proton emission channels ((e) and (f)) are underestimated. The present data indicates that the projectile and target completely fuse together at energies below the fusion barrier in the ^{28}Si + ^{198}Pt system.

References

[1] H. Gäggeler, *et al.*, Z. Phys. A, **316** (1984) 291.
[2] S. Mitsuoka *et al.*, JAERI Tandem & V.D.G Annual Report 1998.
[3] K. Nishio *et al.*, JAERI Tandem & V.D.G Annual Report 1998.
[4] H. Ikezoe *et al.*, Nucl. Instr. Meth. **A376** (1996) 420.
[5] J. Fernandez-Niello *et al.*, Comput. Phys. Commun. **54**, (1989) 409.

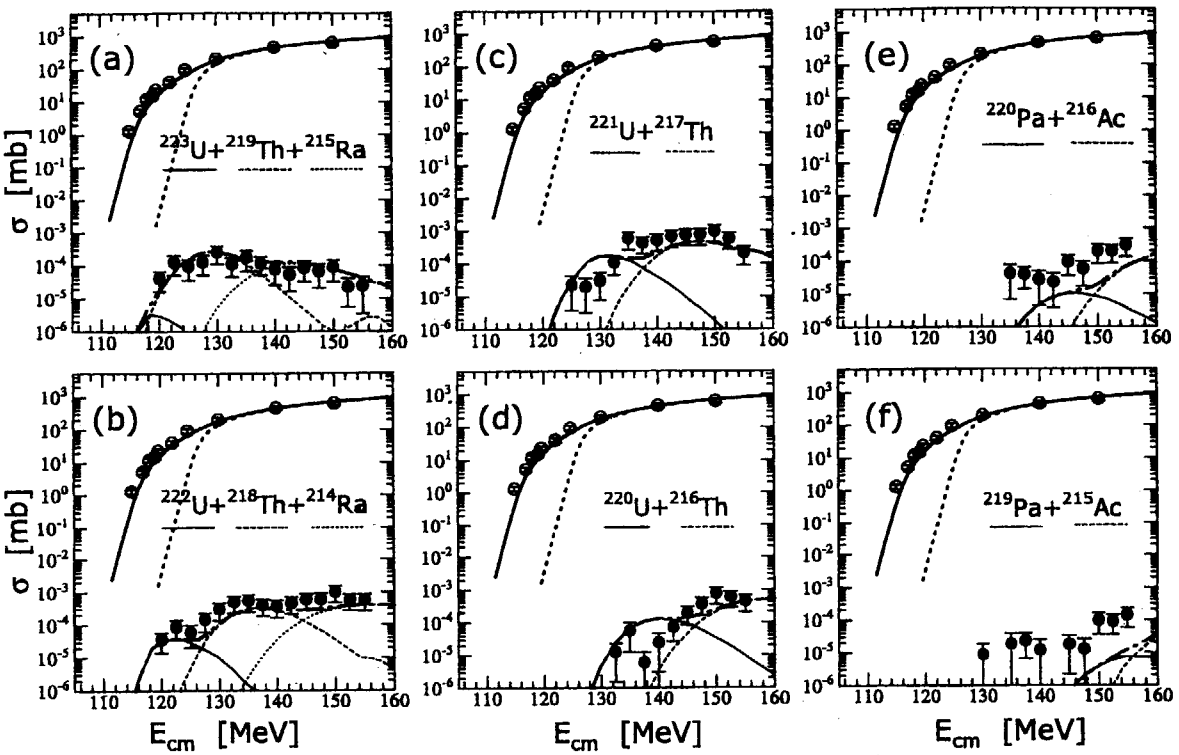

Figure Evaporation residue cross sections for ^{28}Si + ^{198}Pt.

3.7 SOURCE PREPARATION FOR γ-RAY EMISSION PROBABILITY MEASUREMENT OF PROTON-RICH NUCLEI

H. MIYAHARA[1], N. MARNADA[2], N. UEDA[2], K. IKEDA[2], N. HAYASHI[2], M. SAKAMA, H. HABA, I. NISHINAKA, K. TSUKADA, Y. NAGAME and S. ICHIKAWA

Gamma-ray emission probability is one of the important decay parameter of radionuclides and many researchers are paying efforts to improve the certainty of it. It has been improving for neutron-rich nuclides, but the certainty for proton-rich nuclides is insufficient. Production of pure neutron-rich nuclides is easy in nuclear reactor. However, production of pure proton-rich nuclides is difficult by accelerator. We plan to measure γ-ray emission probability of ^{66}Ga and ^{147}Eu which decay by electron capture or β^+-particle emission by using a 4πβ–γ coincidence system[1].

The radioactive sources of ^{66}Ga were produced by 13 MeV proton irradiation of enriched ^{66}Zn (enrichment : 99.29%) and those of ^{56}Co for efficiency calibration of an HPGe detector were similarly produced by the ^{56}Fe(p,n) reaction (^{56}Fe enrichment : 99.87%). The γ-ray spectra of both nuclei showed no significant presence of impurity. On the other hand, making ^{147}Eu by ^{147}Sm(p,n) reaction produced large amount of ^{146}Eu by the ^{147}Sm(p,2n) reaction (^{147}Sm enrichment : 98.34%). This impurity shows small effect for γ-ray intensity measurement but affects seriously for disintegration rate measurement. Then excitation functions for both reactions were investigated for determination of good source preparation condition.

A 0.1 μg cm^{-2} of ^{147}Sm was electrodeposited on Al foil with thickness of 1.65 μg cm^{-2} and twenty foils were stacked for target. This target was irradiated by 5.1×10^{16} protons with energy of 18 MeV in the JAERI tandem accelerator facility. After irradiation, each foil was measured by a γ-ray spectrometer and production amounts of ^{146}Eu and ^{147}Eu were determined. The energy loss in each foil was estimated and each excitation function obtained is plotted in Fig. 1. The theoretical one calculated by the ALICE code [2] is shown in the same figure. The calculated values are relatively larger than the experimental results, but the shape agrees with each other. Considering these results, it became clear that 10 MeV proton irradiation for enriched ^{147}Sm is best for preparation of ^{147}Eu.

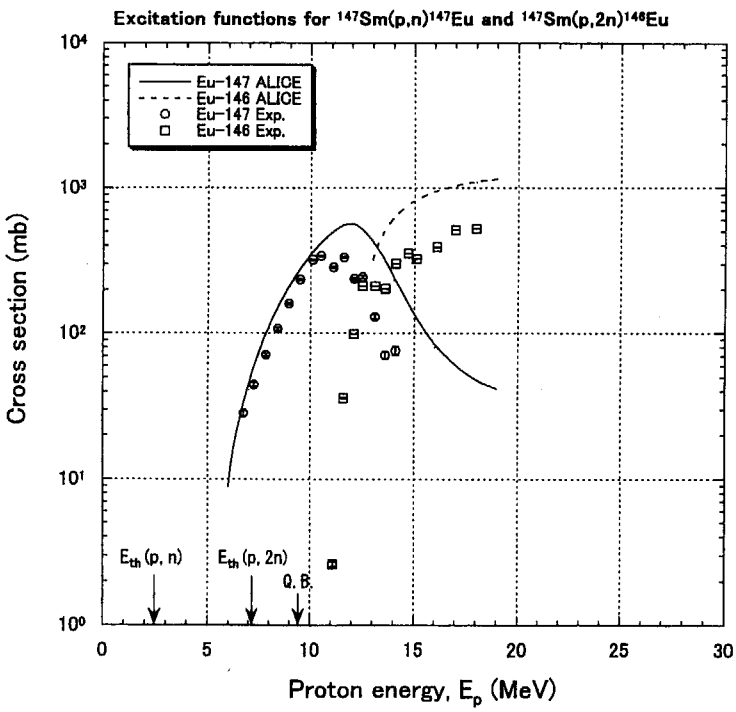

Fig.1. Measured excitation functions of ^{147}Sm(p,n)^{147}Eu and ^{147}Sm(p,2n)^{146}Eu, and those calculated by the ALICE code.

References

1) H. Miyahara et al., Nucl. Instrum. Methods A353 (1994) 229.
2) M. Blann and H. K. Vonach, Phys. Rev. C 28 (1983) 1475.

[1]Department of Radiological Technology, School of Health Sciences, Nagoya University
[2]Department of Nuclear Engineering, Graduate School of Engineering, Nagoya University

3.8 DEFORMATION DEGREES OF SCISSIONING NUCLEI

Y.L. ZHAO[1], I. NISHINAKA, Y. NAGAME, M. TANIKAWA[2], K. TSUKADA, S. ICHIKAWA, S. MITSUOKA, H. IKEZOE, Y. OURA[1], K. SUEKI[1], and H. NAKAHARA[1]

A dramatic change of fission properties has been reported [1,2] for very heavy nuclei such as Fm isotopes. Fission of a very heavy nucleus results in very sharp mass-yield curve with a large kinetic energy release which deviates from the prediction of the existing TKE systematics [3]. Such observations lead to a widely accepted opinion that as the atomic nucleus becomes very heavy fission properties suddenly change and hence become unpredictable as the number of neutron and proton of fissioning nuclide varies. In this work, the fission process of an atomic nucleus is studied via a new viewpoint of deformation degrees of scissioning nuclei. It is found that the extent of the deformation of scissioning nuclei shows continueous and gradual change from preactinides through actinides and up to the begining of transactinide with no sudden change.

The fission of ^{233}Pa, ^{239}Np, ^{245}Am and ^{249}Bk were investigated using the ^{232}Th, ^{238}U, ^{244}Pu and ^{248}Cm targets with the proton beams supplied from the JAERI tandem accelerator. The proton energies were 14.7 MeV for thorium and uranium, and 15.0 MeV for plutonium and curium. The fission products were detected by a double velocity time-of-flight (TOF) system consisting of 3 microchannel plate detectors (MCPDs) and 1 two-dimensional position sensitive parallel plate avalanche counter (PPAC), using the TOSCA [4] (Time Of Flight Scattering Chamber for Actinide Fission) apparatus. The experimental method is similar to the one described in Ref.[4].

In order to allow an estimation of the degree of deformation at scission for different combinations of A_1 and A_2 fragment pairs, and for different fissioning nucleus A_f, a shape elongation β is defined. For a detail description of this β quantity which is a measure of how much the scissioning nucleus deviates from the two touching spheres, the reader may refer to Ref.[5].

The shape elongation of the scissioning nucleus undergoing mass-symmetric deformation (β_{sym}) is given in Fig. 1 *versus* the mass of the fissioning nucleus, A_f. In this figure, the values evaluated from our TKE data are shown by filled triangles whereas those estimated from TKE data in literature are depicted by solid circles for fission at the excitation energies below 30 MeV. Based on the value of the β_{sym}, two types of the shape elongation for the mass-symmetric deformation path are seen. The first is for nuclei in the region from preactinide up to the actinide with $A_f \sim 245$, where the β_{sym} values are nearly constant. The second is for nuclei in the region around $A_f = 260$, where the constant β_{sym} is again observed but with much smaller values than that of the first one. This difference provides a direct evidence for the correctness of the speculation that the properties of the symmetric fission in the low-energy fission of the light and heavy actinides are different [1]. In between the first and the second β_{sym} types, a transition area ($A_f = 245 \sim 255$) exists. The value of β_{sym} gradually decreases as A_f becomes heavier. The deformation properties smoothly vary between the two types with no sudden change. In Fig. 1 the shape elongations for high energy fission (the excitation energies of compound nuclei higher than 65 MeV) are also studied and shown by open circles. For all of high-energy fission, the β_{sym} values are constant, and unlike those for the low-energy fission, the β_{sym} values for high-energy ones in the region of $A_f > 245$ are not lowered.

[1]Graduate School of Science, Tokyo Metropolitan University
[2]Department of Chemistry, University of Tokyo

In Fig. 2, nuclei which can fission asymmetrically are also investigated and the β_{asym} for a typical asymmetric mass division leading to the fragment mass A_l=140 are plotted as a function of the mass of the fissioning nucleus, A_f, for not only the fission systems of the present work (solid triangles) but also for other systems in literature. This fragment mass of 140 nearly represents the peak mass of the heavier fragment in the asymmetric fission. The final shape elongation of the scissioning nucleus undergoing the asymmetric deformation is independent of the mass of the fissioning nucleus. Any atomic nucleus undergoing the mass-asymmetric deformation reachs a similar value of the deformation at scission. The origin of the mass-asymmetry is probably related with the effects of nuclear shells on the nuclear deformation towards fission. But the fact that the observed constancy of the deformation among a large number of different scissioning nuclei is a new property of an atomic nucleus, which needs to be explained by theory.

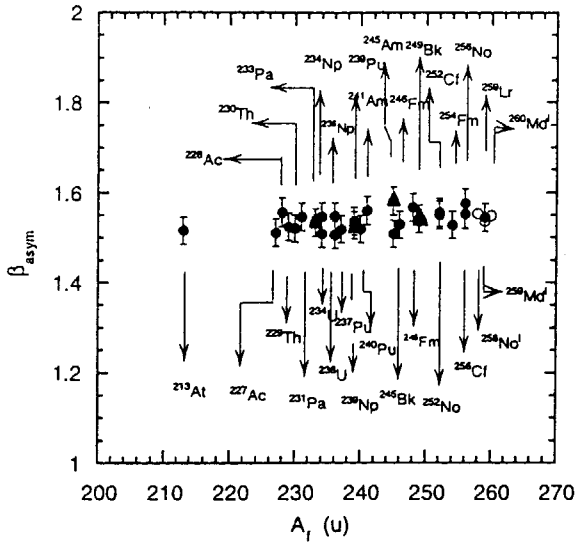

FIG.1, Shape elongations of scissioning nuclei that undergo the mass-symmetric deformation in the fission process, *versus* A_f. Solid circles are for nuclei at low excitation energies (E_X<30MeV), while open circles are those at high excitation energies (E_X>65MeV).

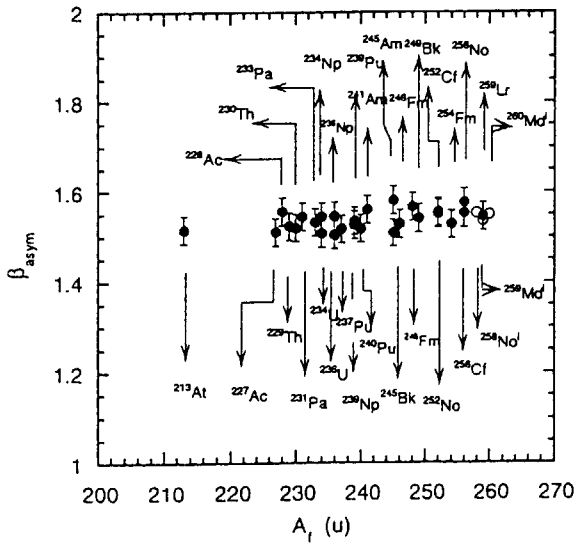

FIG.2, Shape elongations of scissioning nuclei undergoing the mass-asymmetric deformation in the fission process, *versus* A_f. Solid circles are for nuclei which experienced the ordinary mass-asymmetric deformation process influenced by the structural shells of the nucleus and open circles for nuclei which result in the low-TKE component in the bimodal fission of heavy nuclei.

References

1) D.C. Hoffman, *et. al*, Phys. Rev. C **21** (1980) 972;
2) D.C. Hoffman, *et. al*, Radiochim. Acta. **70/71** (1995) 135.
3) V.E. Viola, *et. al*, Phys. Rev. C **31** (1985) 1550.
4) Y. Nagame, *et. al*, Phys. Lett. B**387** (1996) 26.
5) Y.L. Zhao, *et. al*, Phys. Rev. Lett. **82** (1999) 3408.

4. Nuclear Theory

This is a blank page.

4.1 SYSTEMATIC STUDIES OF FISSION SADDLE-POINT SHAPES

A. IWAMOTO and P. MÖLLER [1]

We calculate the nuclear potential-energy as a function of shape in the three-quadratic-surface parameterization in a macroscopic-microscopic model, based on the finite-range liquid-drop model and the folded-Yukawa single-particle model [1]. It is particularly important to include some model enhancements that allow the potential energy to be properly calculated as the nuclear shape evolves from *one* single ground-state configuration to *two* touching fission-fragment shapes [2]. A minimum of 5 shape-degrees of freedom are required to generate realistic fission saddle-point shapes over a large region of nuclei: elongation, neck radius, left emerging-fragment deformation(ε_{f1}), right emerging-fragment deformation(ε_{f2}), and mass asymmetry(M_H/M_L).

Once the potential energy has been calculated, a non-trivial problem is the determination of the saddle-point energies and shapes. An ingenious method that avoids all the difficulties that would occur in identifying saddle points in an approach based on numerical differentiation was recently proposed in Ref. [3]. In this approach one imagines that a potential minimum is gradually filled with water. The level at which the water in the minimum flows over the local confining walls across a saddle region and spills over into an adjoining minimum or valley and makes the grid points there "wet" determines the saddle-point height.

One should observe that calculations, purporting to be multi-dimensional, that show potential energies versus one or two deformation parameters where the energy has been minimized with respect to additional shape degrees of freedom do not correctly reflect the structure of the full multidimensional space which we have considered here for the first time. Saddle-point energies obtained in calculations based on "minimizations" may be either too high or too low, and the shape obtained can be expected to be incorrect. A simple two-dimensional illustration of this difficulty, based on a macroscopic energy is discussed in Ref. [4]. Higher-dimensional surfaces with microscopic effects included, as in this work, are even more complex.

We find here, for the first time, in a properly executed high-dimensional calculation, that fragment shapes such as a spherical fragment with $A \approx 132$ connected to a smaller deformed fragment establish their identity already at certain saddle-point configurations, cf. Fig. 1 for ^{232}Th. Well established nascent fragment shapes are seen clearly at the outer saddle point. For ^{258}Fm we find a saddle-point configuration that correlates well with the high TKE of the fission fragments for this nucleus. For ^{256}Fm we find a quite different saddle-point shape for which no neck has yet developed. Systematic studies of the relation between saddle-point

[1]Theoretical Division, Los Alamos National Laboratory

shapes and final-fragment TKE and mass distributions are in progress.

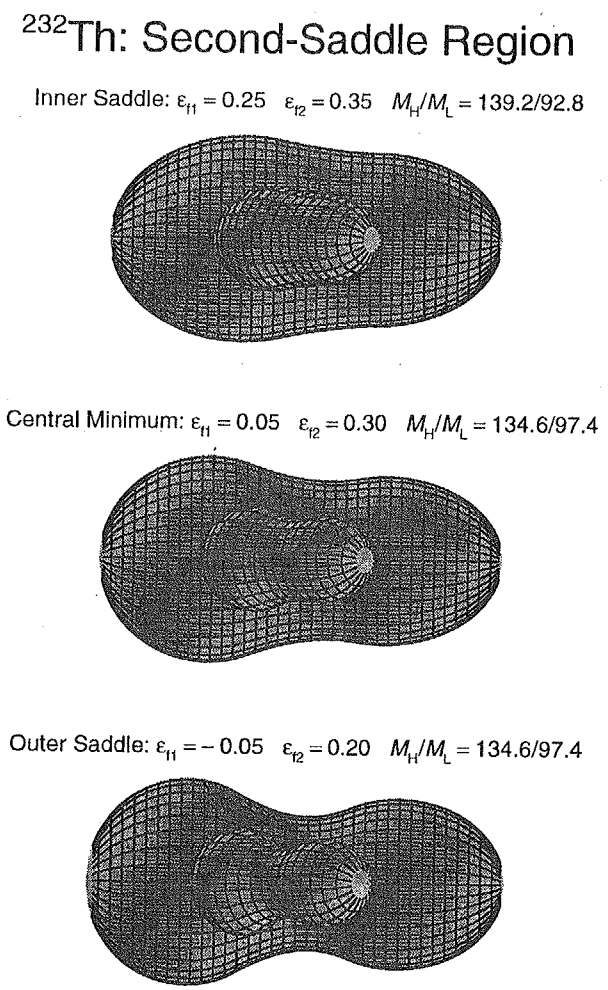

Fig.1. Calculated extremum shapes for ^{232}Th in the second-saddle region. Only at the outer saddle point do the final fragment shapes become established. The shapes presented are viewed from two angles, the large shape from θ=90°, ϕ=0° and the small shape "floating" in front from θ=50° , ϕ=0°.

References

1) P. Möller, J. R. Nix, W. D. Myers, and W. J. Swiatecki, Atomic Data Nucl. Data Tables **59** (1995) 185.

2) P. Möller, J. R. Nix, and W. J. Swiatecki, Nucl. Phys. **A492** (1989) 349.

3) A. Mamdouh, J. M. Pearson, M. Rayet, and F. Tondeur, Nucl. Phys. **A644** (1998) 389.

4) W. D. Myers and W. J. Swiatecki, Nucl. Phys. **A601** (1996) 141.

5. Atomic Physics, Solid State Physics and Radiation Effects in Materials

This is a blank page.

5.1 EJECTED ELECTRON SPECTRA FROM HIGH ENERGY HIGHLY CHARGED OXYGEN IONS IN COLLISIONS WITH HELIUM ATOMS

S.KITAZAWA, M.SATAKA, H.TAWARA[1], M.IMAI[2], H.SHIBATA[3], K.KOMAKI[4], K. KAWATSURA[5], Y.KANAI[6] and T.AZUMA[7]

We have studied collision processes of fast highly charged ions with gas or foil targets using ejected electron spectroscopy observed at zero degrees at Japan Atomic Energy Research Institute (JAERI) Tokai[1]. Slow highly charged ions with gas targets experiments have also been performed[2,3]. In this work, spectra of ejected electron at zero degrees are measured for O^{q+} + He and carbon foils (q=3,4,5).

The experiment has been performed using several MeV/u O^{q+} ions provided from the Tandem accelerator. The Auger electrons produced in the target gas cell and carbon foils measured at zero degrees relative to the incident beam direction[4,5]. In measurements of the Auger transition spectrum of oxygen ions, the energy resolution was set at 0.25 eV.

Figure 1 shows electron spectra measured for 36 MeV O^{3+} + He collisions. The vertical axis is ejected electron energy in emitter frame. The richness of peaks are due to O^{3+} projectile have five electrons. For 45MeV O^{4+} + He and carbon foil collisions, Coster-Kronig transition were observed only on He target, but not on carbon foil target. Figure 2 shows electron spectra measured for 45 MeV O^{4+} + He collisions. The peaks are mainly from Coster-Kronig transition $1s^22pnl$ -> $1s^22s$. For 54MeV O^{5+} + He and carbon foil collisions, peaks of K-Auger were observed but Coster-Kronig were not observed.

[1]Depertment of Physics, Kansas State University, Manhattan KS 66506, USA
[2]Department of Nuclear Engineering, Kyoto Univ., Kyoto 606-8501, Japan
[3]Research Center for Nuclear Sciences and Technology, University of Tokyo, Ibaraki 319-1106, Japan
[4]Institute of Physics, Graduate School of Arts and Sciences, University of Tokyo, Meguro, Tokyo 153-8902, Japan
[5]Depertment of Chemistry and Materials Technology, Kyoto Institute of Technology, Kyoto 606-8585, Japan
[6]The Institute of Physical and Chemical Research (RIKEN), Saitama 351-0198, Japan
[7]Institute of Applied Physics, University of Tsukuba, Ibaraki 305-8573, Japan

References

1. K. Kawatsura et al., Nucl. Instrum. Methods B 48(1990) 103.
2. S. Kitazawa et al., J.Phys.B 31 (1998) 3233.
3. N. Nakamura et al., J. Phys.B 27 (1994) L785.
4. K. Kawatsura et al., J. Electron Spectrosc. Relat. Phenom. 88-91 (1998) 83.
5. K. Kawatsura et al., J. Electron Spectrosc. Relat. Phenom. 88-91 (1998) 87.

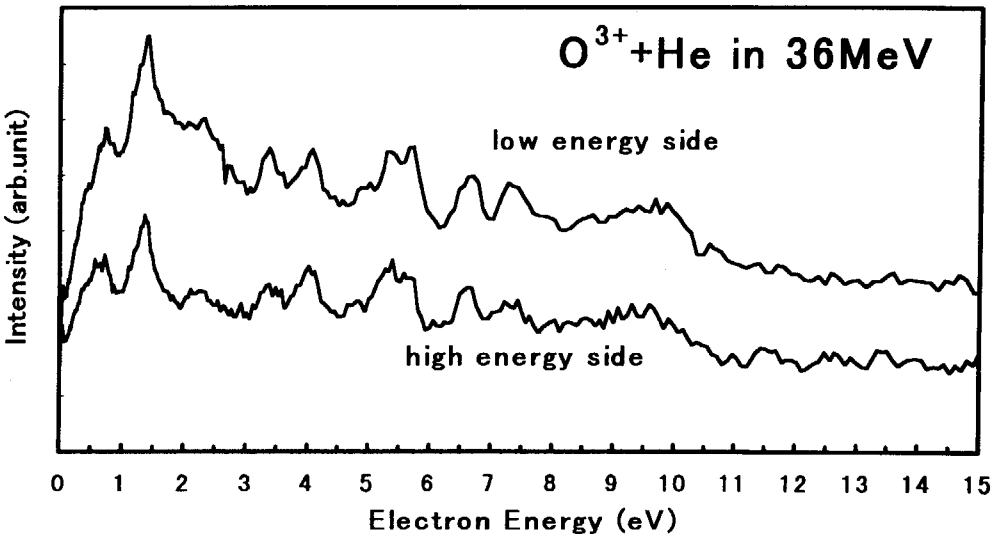

Figure 1 Ejected electron spectra from 36MeV O^{3+} + He collision

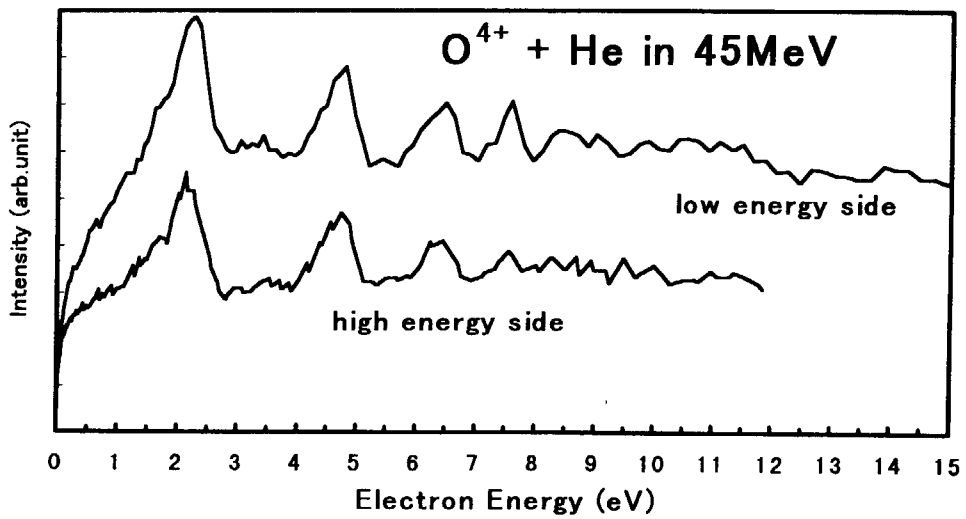

Figure 2 Ejected electron spectra from 45MeV O^{4+} + He collision

5.2 HIGH-RESOLUTION ZERO-DEGREE ELECTRON SPECTROSCOPY (V)

K. KAWATSURA[1], M. SATAKA, S. KITAZAWA, M. IMAI[2], K. KOMAKI[3], Y. YAMAZAKI[3,4], H. TAWARA[5], H. SHIBATA[6], T. AZUMA[7] and Y. KANAI[4]

Recently, we have applied the method of zero-degree electron spectroscopy to projectile Auger and Coster-Kronig (C-K) electrons reducing the kinematic broadening effects [1-4]. The broadening effects cancel in first order at zero-degree observation angle of the emitted electrons. Thus, high resolution study is possible for projectile energies from several keV to several hundreds of MeV. It is another advantages that low energy lines which are difficult to detect, may be shifted to an energy range which is readily accessible to the electron spectrometer.

Dynamic properties of the collision processes inside a solid have been one of the major interests in ion-solid interactions. Zero-degree electron spectroscopy is an excellent tool to study these phenomena by measuring Auger, C-K and secondary electrons emitted from the projectile and/or electrons captured or lost to the continuum. Concerning C-K electrons from Rydberg states in high energy projectiles, it has been shown that a weak and an intense series of C-K electrons are observed as for a gas and a solid target, respectively [1,2,4-10], although they cannot survive inside the solid, which indicates that Rydberg states are formed upon or near the exciting surface of the solid target. The models for producing such high Rydberg electrons and subsequent enhancement of high angular momentum have been proposed [4,11]. These measurements are also useful as a test for an important subject for highly charged ion-atom collisions of forming doubly excited states via correlated or uncorrelated electron excitation [2,12-14]. In the present work, we measured zero-degree electron spectra with high resolution for 2 MeV/u sulfur projectiles though a carbon foil target to investigate static and dynamic properties of the highly charged fast ions inside a solid.

The experiments to measure emitted electrons in high-energy ion-atom collisions at zero-degree were performed using the tandem-type electrostatic spectrometer inside the high vacuum scattering chamber at the H-2 line of the JAERI tandem facility of Tokai. The experimental setup used in these measurements has been described previously [1,2].

[1]Department of Nuclear Engineering, Kyoto University.
[2]Department of Chemistry and Materials Technology, Kyoto Institute of Technology.
[3]Graduate School of Arts and Sciences, University of Tokyo.
[4]The Institute of Physical and Chemical Research (RIKEN)
[5]National Institute for Fusion Sciences.
[6]Research Center for Nuclear Sciences and Technology, University of Tokyo.
[7]Institute of Applied Physics, University of Tsukuba.

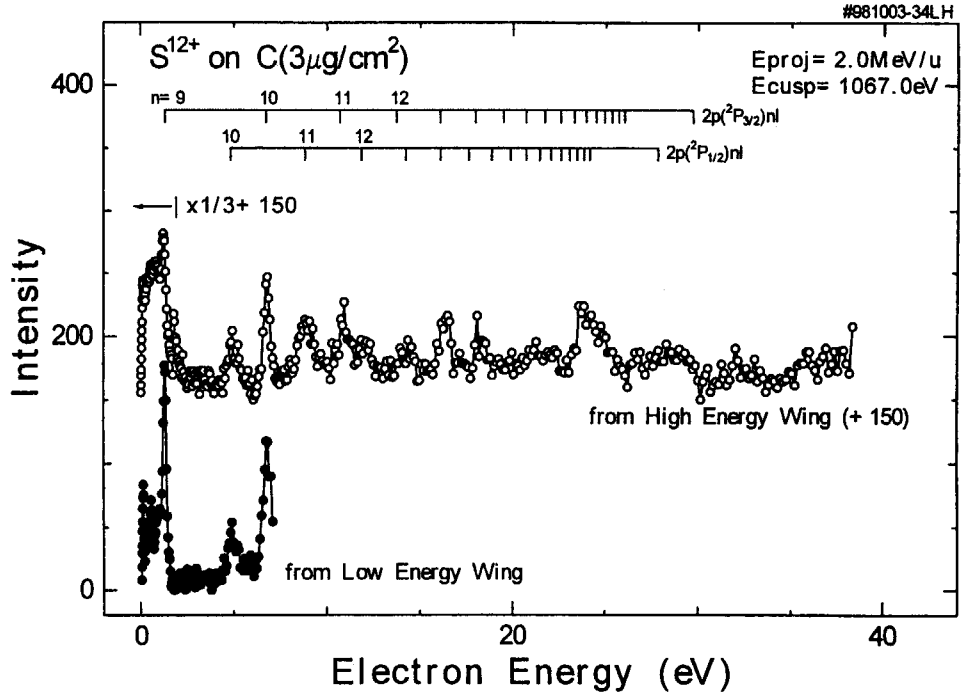

Fig. 1. Electron energy spectrum ejected at 0° in collisions of 2 MeV/u S^{12+} on a C-foil target. The data are transformed into the projectile rest frame.

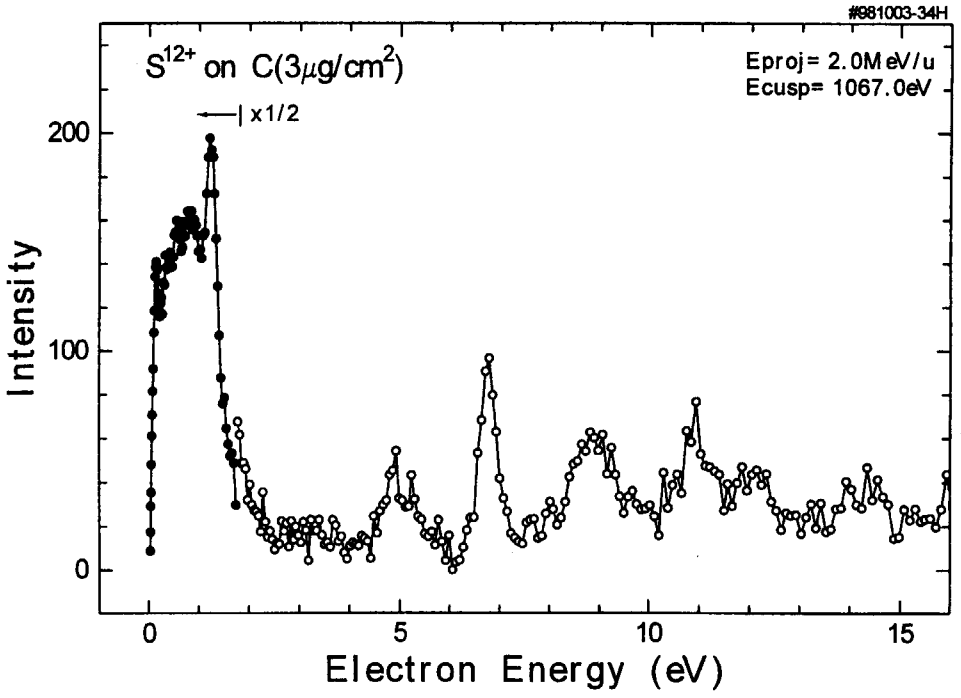

Fig. 2. Part of electron energy spectrum ejected at 0° in collisions of 2 MeV/u S^{12+} on a C-foil target. The data are transformed into the projectile rest frame.

Figures 1 and 2 show electron spectra ejected at zero degree from 2 MeV/u S^{12+} + C. The data are transformed into the projectile rest frame. In both spectra, Coster-Kronig electrons from the autoionizing Rydberg states of 2 MeV/u sulfur projectile excited through a thin carbon foil (3.0 $\mu g/cm^2$) are observed. The most prominent lines came from S^{12+} $1s^22p(^2P^0_{1/2})nl$ - $1s^22sl'$ and $1s^22p(^2P^0_{3/2})nl$ - $1s^22sl'$ transitions, where the n appears from 9 to 20. For S ion impact, electron spectra form S^{6+} and S^{13+} projectiles incident on a thin C-foil target were also measured. The detailed analysis for the these experimental results will be given [15].

References

1) K. Kawatsura *et al.*, Nucl. Instr. Meth. Phys. Res. **B48** (1990) 103.
2) K. Kawatsura *et al.*, Nucl. Instr. Meth. Phys. Res. **B53** (1991) 421.
3) M. Sataka *et al.*, Phys. Rev. **A44** (1991) 7290.
4) M. Imai *et al.*, Nucl. Instr. Meth. Phys. Res. **B67** (1992) 142.
5) N. Stolterfoht, Phys. Rep. **146** (1987) 315.
6) Y. Yamazaki, Nucl. Instr. Meth. Phys. Res. **B96** (1995) 517.
7) Y. Yamazaki *et al.*, Phys. Rev. Lett. **61** (1988) 2913.
8) K. Kawatsura *et al.*, Nucl. Instr. Meth. Phys. Res. **B124** (1997) 381.
9) M. Imai *et al.*, Phys. Scr. **T73** (1997) 93.
10) K. Kawatsura *et al.*, Phys. Scr. **T73** (1997) 235.
11) J. Burgdorfer and C. Bottcher, Phys. Rev. Lett. **61** (1988) 2917.
12) D. Schneider *et al.*, Nucl. Instr. Meth. Phys. Res. **B24/25** (1987) 173.
13) N. Stolterfoht, J. Electron Spectrosc. Relat. Phenom. **67** (1994) 309.
14) B. Sulik *et al.*, Phys. Rev. **A52** (1995) 387.
15) K. Kawatsura *et al.*, in preparation.

5.3 EMISSION OF SECONDARY IONS FROM CONDUCTIVE MATERIALS BOMBARDED WITH HEAVY IONS

T. SEKIOKA[1], M. TERASAWA[1], M. SATAKA and S. KITAZAWA

Recently, the electronic sputtering in conductive materials has been attracting great interest. Several experiments have been performed to investigate the incident charge state dependence of the secondary ion yield from conductive materials irradiated with low energy highly charged ions (HCI) [1-3], and the incident charge state dependence of the charge equilibration time of low energy HCI through thin carbon foils [4]. The results of the experiments suggest importance of the electronic excitation effect in the interaction between low energy HCI and the conductive solid targets.

We have studied the secondary ions mass spectra from thin conductive solid targets irradiated with heavy ion beams from the JAERI tandem accelerator at an energy regions where the electronic stopping power is dominant. It is interesting to study the electronic sputtering in the conductive materials in a different way from the experiment using low energy HCI. Very fast neutralization occurs when a low energy HCI collides with a conductive material, so that the electronic excitation energy is deposited in a small region of the solid surface. On the contrary, when a high energy heavy ion penetrates a solid target, the electronic excitation energy is deposited along the ion track. It is also important to study the fundamental process of the extended defects production in a solid irradiated with high energy heavy ions.

The C-foil of 30μg/cm^2 thickness, Cu and Au foil targets of 1000Å thickness evaporated on C-foils of 10μg/cm^2 were irradiated with high energy heavy ions beam from the tandem accelerator. The secondary ions ejected from the front surface of the target were collected by a time of flight (TOF) mass spectrometer by applying an acceleration voltage of –500V and detected by an electron multiplier. Secondary electrons from the back side of the target were detected by another electron multiplier and this signal was used as a start signal of the TOF. The projectiles were 80 and 100 MeV I ions, 100, 120 and 200 MeV Au^{12+} ions and 300 and 320 MeV Au^{25+} ions.

Figure 1 shows the yield of the secondary ions of C^+, Cu^+ and Au^+ from C, Cu and Au target respectively, normalized by the counts of secondary electron signal as a function of the electronic stopping power. The values of the electronic stopping power are obtained from Ziegler's table by TRIM. The solid line in the figure represents the slope of $(dE/dx)^2$. As can be seen in the figure, the secondary ion yield increases remarkably above an electronic stopping power of 2keV/Å, and can be approximately fitted by $(dE/dx)^2$.

The strong dependence of the secondary ion yield from conductive materials on the electronic stopping power suggests that even in the conductive materials, the electronic excitation effects play an important role in the secondary ion sputtering. The $(dE/dx)^2$ dependence of the secondary ion yield suggests that the Coulomb repulsion between ionized target atoms in the high electronic excitation region is the main mechanism of the electronic sputtering.

To confirm these experimental results, it is important to study the secondary ions mass spectroscopy in a wide range of electronic stopping power with various combinations of projectiles and conductive targets. In order to improve the resolution of the mass spectroscopy, we are planning to develop a magnetic spectrometer, which is also useful to measure the secondary ions from bulk solid targets.

---

[1] Faculty of Engineering, Himeji Institute of Technology

References
1) M.Terasawa, T.Sekioka, T.Mitamura, S.Winecki, M.P.Stöckli and C.L.Cocke, Physica Scripta, **T73**, 326 (1997)
2) Robert W.Schmieder and Robert J.Bastasz, Nucl. Instrum. Methods **B43**, 318 (1989)
3) T.Schenkel, M.A.Briece, A.V.Barnes, A.V.Hamza, H.Schmidt-Böcking, K.Bethge and D.H.Schneider, Phys. Rev. Lett., **78**, 2481 (1997)
4) M.Hattass, T.Schenkel, A.V.Hamza, A.V.Barnes, M.W.Newman, J.W.McDonald, T.R.Niedermayr, G.A.Machicoane and D.H.Schneider, Phys. Rev. Lett., **82**, 4795 (1999)

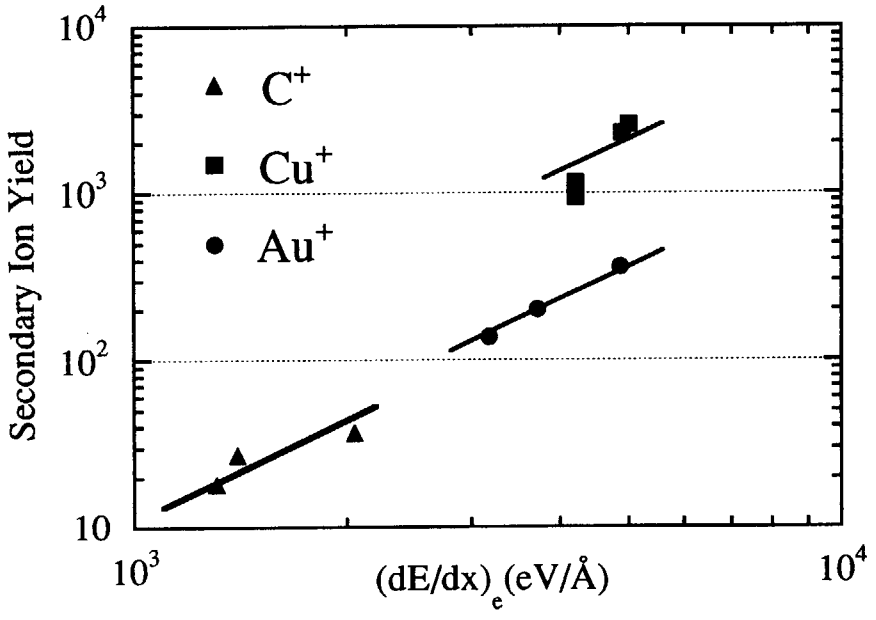

Fig. 1. The yield of the secondary ions of C^+, Cu^+ and Au^+ normalized by the counts of secondary electrons signal as a function of the electronic stopping power. The values of the electronic stopping power are obtained by Ziegler's table (TRIM). The solid line represents the slope of $(dE/dx)^2$.

5.4 THE EFFECT OF SPLAYED COLUMNAR DEFECTS ON TRANSPORT CHARACTERISTICS IN $YBa_2Cu_3O_y$ THIN FILM

N. ISHIKAWA, T. SUEYOSHI[1], A. IWASE, Y. CHIMI, T. FUJIYOSHI[1], K. MIYAHARA[1], and T. KISS[2]

It is well-known that columnar defects produced by swift heavy-ion irradiation enhance the pinning of vortices in the mixed state of oxide superconductors. Recently it has been reported that the pinning properties can be further improved by dispersing the orientation of columnar defects, namely splayed columnar[1-3]. The remarkable feature of the splayed columnar defects is that although the pinning has been considered as the strongest when columnar defects are aligned with magnetic field direction, tilting the orientation of columnar defects from the field direction further enhance pinning. Therefore, the angle difference between orientation of magnetic field and that of columnar defects may be an important parameter to understand the effect of splayed columnar defects. In this study, the effect of columnar defects aligned parallel to +15° (or to −15°) off the c-axis and that of splayed columnar defects on pinning properties has been analyzed and compared.

A c-axis oriented $YBa_2Cu_3O_y$ (YBCO) epitaxial thin film was prepared by a laser ablation technique. The zero-resistivity critical temperature T_{c0} was 90.0K. The film was irradiated with 200MeV ^{197}Au ions from a tandem accelerator at JAERI(Japan Atomic Energy Research Institute)-Tokai. Planar splayed columnar defects were produced in the film by irradiating ions (B_Φ=0.5T) from the angle +15° off the c-axis and successively irradiating the same amount of ions (B_Φ=0.5T) from the angle −15° off the c-axis. These two sets of irradiations produced splayed columnar defects (B_Φ=1T) which define a splay plane containing c-axis. The irradiation temperature was about 80K. The *in-situ* measurements of transport critical current density J_c as a function of magnetic field direction with respect to c-axis θ was performed at T_{meas}=83K applying B=1T without warming the sample above 83K. The transport current was always applied in the direction perpendicular to the magnetic field direction, c-axis, and the splay plane. In this experiment, low-temperature irradiations and *in-situ* measurements of J_c without warming the sample were performed because irradiation experiments using multiple samples inevitably causes scattering of data, and because irradiations and measurements at low temperature rule out the possibility of thermal annihilation of irradiation defects. Figure 1 shows θ -dependence of J_c at 83K under magnetic field before irradiation , after irradiation from +15° , and after successive irradiation from −15° . After the first irradiation from +15° a shoulder appeared around θ =+15° .

---

[1]Department of Electrical and Computer Engineering, Kumamoto University.

[2]Graduate School of Information Science and Electrical Engineering, Kyushu University.

After the successive irradiation from -15° a symmetric peak for J_c appeared around θ =0° instead of two shoulders at ±15° . The height of peaks at θ =±90° , indicating the intrinsic pinning, decreased due to irradiations, because of the decrease in T_c accompanied by the increase in $t=T_{meas}/T_c$. The irradiation-induced change in $J_c(\theta)$ can be attributed to two competing effects; the effect due to the interaction between defects and vortices and the effect due to decrease in T_c. Since our focus is only on the former effect, the latter effect should be excluded. This can be done by normalizing $J_c(\theta)$ by J_c (θ =±90°). The increment of normalized J_c (θ) due to the first irradiation from +15° shows a maximum near θ =15° , and the irradiation from −15° would have the same effect but having the maximum near θ =-15° . However, we find that a mere sum of these effects cannot describe the effect of splayed columnar defects, showing that splayed configuration of columnar defects creates an extra effect. When θ =0° , the effect of splayed defects is larger by 24 % than the sum of the effects of respective columnar defects from +15° and −15° .

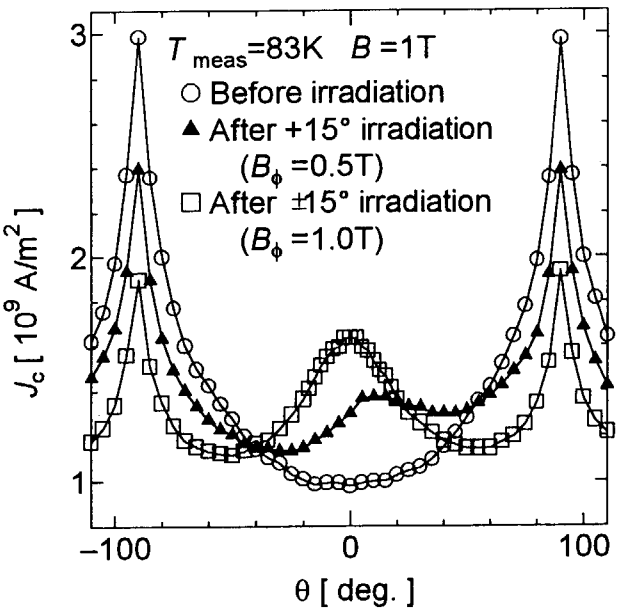

Fig.1. θ -dependence of J_c under magnetic field at 83K before irradiation , after +15° irradiation, and after successive −15° irradiation.

References

1) L. Krusin-Elbaum et al., Phys. Rev. Lett. 76 (1996)2563.

2) W. K. Kwok et al., Phys. Rev. Lett. 80 (1998) 600.

3) T. Hwa et al., Phys. Rev. Lett. 71 (1993) 3545.

5.5 INTRODUCTION OF COLUMNAR DEFECTS IN Bi-2212 SINGLE CRYSTALS BY HIGH-ENERGY HEAVY-ION IRRADIATION

K.OGIKUBO[1], T.TERAI[1], S.OKAYASU and K.HOJO

Particle-beam irradiation is one of the most hopeful methods to introduce strong pinning centers into High-T_c superconductors. We have been studying magnetic property change of Bi-2212 ($Bi_2Sr_2CaCu_2O_{8+x}$) single crystal due to irradiation with several kinds of particles such as light and heavy ions, neutrons and electrons. In order to realize a particle-beam irradiation technique as a method for J_c enhancement, many different conditions such as the kind, the energy and the fluence of particles should be examined. In particular, high-energy heavy-ions are expected to produce columnar defects, which give a very large pinning force for the vortices parallel to the defects. In this report, we show experimental results on the enhancement in the critical current density J_c of Bi-2212 single crystals irradiated with several kinds of high-energy heavy-ion beam.

The Bi-2212 single crystal specimens were prepared by the floating-zone method. Their size was 2mm×2mm×0.1mm. The specimens were irradiated with a heavy-ion beam (200MeV Au^{13+}, 180MeV Cu^{11+} or 150MeV Xe^{10+}) parallel to the c-axis with a tandem accelerator at Japan Atomic Energy Research Institute. The fluences were from 1×10^{10} to 5×10^{11} cm^{-2}. Magnetization curves of the specimens were measured with a vibrating sample magnetometer at 20, 40 and 60K as a function of applied magnetic field up to 7T parallel to the c-axis. The critical current density J_c in the a-b plane of the specimen was derived from the magnetization hysteresis curve using the modified Bean's model[1]. Each J_c value is normalized by the average penetration depth of the incident ions.

The critical current density J_c increased due to irradiation all over the range of fluence and magnetic field regardless of ion species. The fluence dependence of J_c at typical conditions of magnetic field and temperature is shown in Fig.1. J_c took a maximum value around the fluence of $5\times10^{10}cm^{-2}$ and decreased at higher fluence for 200MeV Au irradiation. On the other hand, J_c increased monotonically with the fluence for 150MeV Xe and 180MeV Cu irradiation.

To elucidate the reason of the different behavior of J_c between Au irradiation and Xe and Cu irradiation, the electronic stopping power (S_e) of each incident ion species in Bi-2212 was calculated using Trim (Srim96) code. The depth profile of the electronic stopping power is shown in Fig.2. The values of S_e near the target surface for 200MeV Au, 150MeV Xe and 180MeV Cu irradiation are 29.5, 23.0 and 13.5 keV/nm, respectively. It is reported that the diameter of columnar defects increases monotonically with S_e of the incident ion in heavy-ion irradiated High-T_c superconductors[2]. Therefore, the diameter of columnar defects would decrease in the order of Au, Xe and Cu. According to TEM observation on 230MeV Au[3] and 180MeV Fe[4] irradiated Bi-2212 single crystals, which are similar ion species to 200MeV Au and 180MeV Cu in our study, respectively, the diameters of

[1]Department of Quantum Engineering and Systems Science, The University of Tokyo.

the columnar defects for Au and Fe irradiation at 1μm in depth are 13.5 nm and 3 nm, respectively.

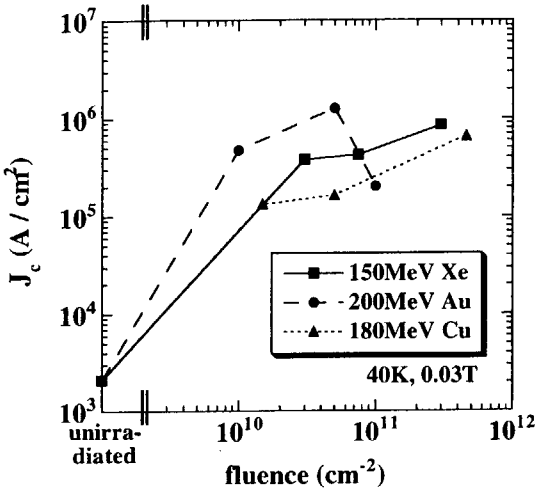

Fig.1 Fluence dependence of J_c

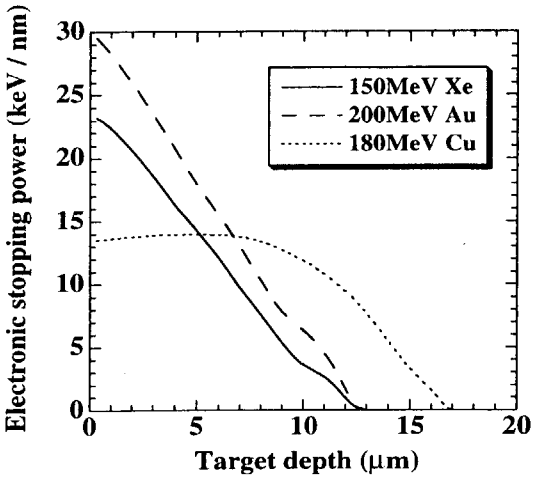

Fig.2 Electronic stopping power of incident ions in Bi-2212

In Fig.1, J_c in Au irradiation increased with fluence due to the increase of the number of columnar defects. The decrease of J_c at the fluence of 1×10^{11} cm^{-2} in Au irradiation is considered to be attributed to the overlapping of columnar defects. At this fluence, the ratio of the defect area to the specimen area is estimated to be 0.143 ($=(13.5\times10^{-7}$[cm]$/2)^2\pi\times\ 1\times10^{11}$[cm^{-2}]). It is considered that the enough amount of defect overlapping area which deteriorates the superconductivity of the specimen is formed in this condition. On the other hand, the increase of J_c with the fluence up to 5×10^{11} cm^{-2} in Cu irradiation suggests that the columnar defects do not overlap even at such a higher fluence, because they have relatively smaller diameter and the ratio of the defect area to the specimen area is 0.035 even at the fluence of 5×10^{11} cm^{-2}. In the case of Xe irradiation, which produce the columnar defects having a middle diameter between the case of Au irradiation and the case of Cu irradiation, J_c increased monotonically with the fluence up to 3×10^{11} cm^{-2}. This fluence dependence of J_c is similar to the case of Cu irradiation. This result suggests that the amount of defect overlapping area is not so much as the case of Au irradiation and the ratio of the defect area to the specimen area is similar to that in Cu irradiation in the fluence range less than 3×10^{11} cm^{-2}. Judging from these results, the degree of defect overlapping is an important parameter for J_c change. In order to elucidate this point, light-ion irradiation at higher fluences is being planned.

References

[1] E.M. Gyorgy *et al.*, *Appl. Phys. Lett.* **55** (1989) 283.
[2] Y. Zhu *et al.*, *Phys. Rev.* **B 48** (1993) 6436.
[3] D.X. Huang *et al.*, *Phys. Rev.* **B 57** (1998) 13907.
[4] Y. Sasaki *et al.*, *The 10th Symposium of High T_c Superconductors, JAERI-Review* **99-009** (1999) 49.

5.6 NOVEL ASYMMETRIC CRITICAL STATE IN $YBa_2Cu_3O_{7-\delta}$ WITH COLUMNAR DEFECTS

K. ITAKA[1], M. YASUGAKI[1], T. SHIBAUCHI[1], T. TAMEGAI[1], and S. OKAYASU

Heavy-ion irradiation is one of the most promising technique to enhance J_c in high temperature superconductor and introduce columnar defects (CDs) in the sample. However, the enhancement of the pinning potential has strongly field and angular dependence. The relation between this result and the irradiation is not clear yet. In this paper, we report that the field dependency of the critical state field profile is very large and geometrically asymmetric in YBCO with CDs. This phenomenon is explained by our model that a large in-plane magnetization is generated when the vortices are trapped in CDs.

We used rectangular-shaped twinned single crystals along the a and the b axis [1]. The critical temperature of the pristine sample is around 91 K. The crystal was irradiated with 600 MeV iodine ions at an influence $\Phi_t = 5 \times 10^{10}\mathrm{cm}^{-2}$ tilted 10° from the c axis. The matching field (B_Φ) is determined by the field where the number of vortices along CDs is equal to that of CDs and in our sample $B_\Phi = 1\mathrm{T}$
Figure 1 shows M-H curve and the critical field profile. We found peaks around $1/3B_\phi$ on $M-H$ curve similar to BSCCO system [2]. We observed critical field profile with the discontinuous line (d-

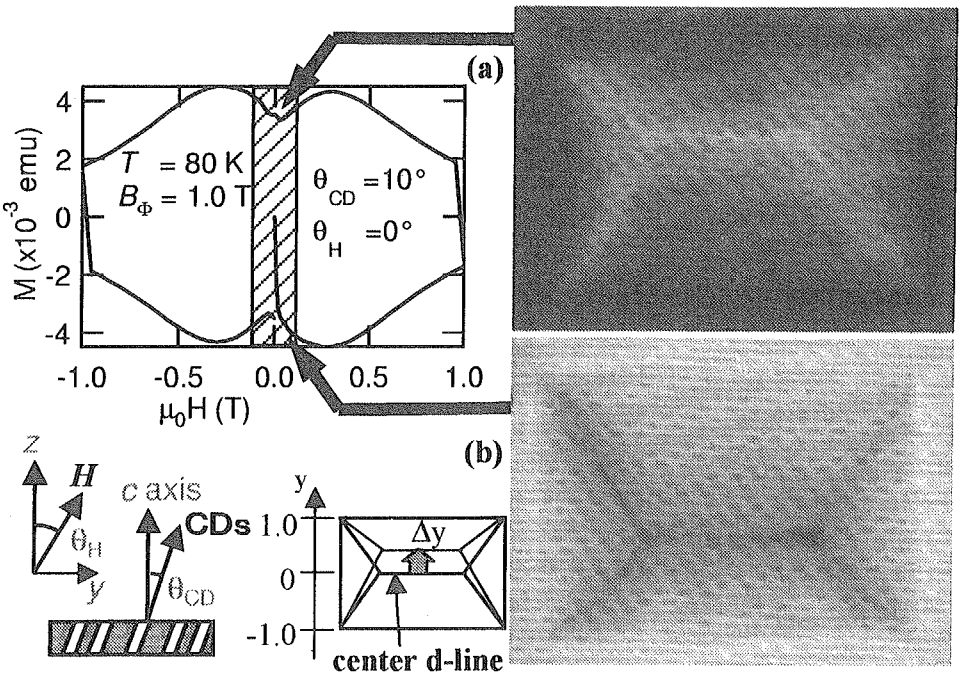

Figure 1: M-H curve at T=80K and the typical critical state field profile when the field sweeps up (b) and down (a). We observed the profile in hatched area. θ_H and θ_{CD} show the angle from the c axis towards y axis. Δy is determined by the shift of the center d-line.

[1]Department of Applied Physics, The University of Tokyo

line) using magneto-optical technique on the hatched field range. This profile drastically changed to asymmetrical rooftop shape by sweeping the applied field. When the field is decreasing (a), center d-line shifted to the other side edge, whereas when the field is increasing, or case (b), center d-line shifted to the one side edge. The direction of the shift is parallel to the tilted CDs. The y axis is determined by this direction. To make the shift of the center d-line clear, Fig. 2 (a) shows the filed dependency of the shift Δy. If the magnetization is the same direction to the applied field, the shift is negative, while if it is not the same, the shift is positive. When the field-sweep direction changed, the current center d-line disappeared and the new center d-line is generated at the opposite side. We could not consider that these behavior are caused by twin boundaries, because twin boundary randomly run along [110] direction and the symmetry of twin boundaries is different from that of d-line motion.

Previously, it was reported that the asymmetric field profile was observed in YBCO with CDs at $T = 60$K and they discussed that this behavior was caused from the difference of pinning potential between the top and the bottom surfaces [3]. To check the surface effect, we turned over the sample and observed the field profile again. However, the shift direction is independent on the surface quality. Accordingly, it is too difficult for their model to explain our results.

We propose a new model for the explanation of these behaviors as follows. When the field increase in the sample with CDs, the vortices are arranged along CDs. Then in-plane magnetization is generated only when the misalignment between the field and CDs exist. The new current in the top surface of the sample flows by in-plane magnetization. The sum of the new current and the normal circular current caused by the c-axis magnetization can not exceed the critical current. The field profile ,thus, is redistributed and we observed the asymmetric field profile. We can estimate that the ratio of the current density from in-plane magnetization and the c axis magnetization (J^y/J^z) is 0.4 at $T = 80$K and $H = 0.12$T.

In conclusion, we observed a novel asymmetric behavior of the field profile, which depends on the field sweep direction and the misalignment of the field from the c axis. We interpret this asymmetry as caused by the in-plane magnetization, which is originated from the alignment of vortices to the CDs. The field dependence of the correlation length of vortices along CDs may result in the enhanced pinning with increasing field around the magnetization peak.

References

1) F. Hortzberg and C. Feild, Eur. J. Solid State Inorg. Chem. **27**, 107 (1990).
2) N. Chikumoto *et al.*, Phys. Rev. B **57**, 14507 (1998).
3) T. Schuster *et al.*, Phys. Rev. B **51**, 16358 (1995).

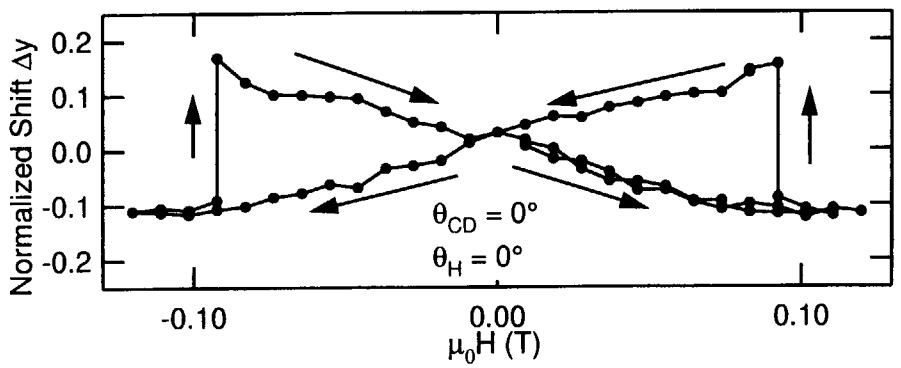

Figure 2: The hysteresis curve for Δy in the field sweep at $T = 80$K $\theta_H = 0°$, $\theta_{CD} = 10°$

5.7 JOSEPHSON PLASMA RESONANCE IN HEAVY ION IRRADIATED $Bi_2Sr_2CaCu_2O_{8+\delta}$ SINGLE CRYSTALS

I. KAKEYA[1], R. NAKAMURA[1], K. KADOWAKI[1],
S. OKAYASU, M. SATAKA, Y. KAZUMATA

Josephson plasma resonance (JPR) is a powerful tool to sense the interlayer coupling of adjacent CuO_2 superconducting layers quantitatively [1]. Several authors measured JPR in $Bi_2Sr_2CaCu_2O_{8+\delta}$ (BSCCO) with columnar defects (CD) and discussed two vortex states divided by characteristic magnetic fields depending upon those irradiation doses B_ϕ [2]. We present here experimental results of JPR in BSCCO with several doses of CD, and give a phenomenological picture which may represent the interlayer coupling quantitatively and universally.

We measured JPR for four single crystals with different doses of B_ϕ = 0.2, 0.5, 1, 2 T. Single crystals were grown by the traveling solvent floating zone method and irradiation of I^{28+} ion was performed by a tandem accelerator at Japan Atomic Energy Research Institute (JAERI). For microwave measurements, we employed a cavity perturbation method with a cavity resonator at the rectangular TE_{102} mode (resonant frequency: 34 GHz). The resonance curves were obtained by sweeping external magnetic field generated by a split-pair superconducting magnet, and rotated at the center of it by a high precision goniometer.

The observed resonance shows considerable dependence upon temperature and irradiation doses. The plots of the resonance field as a function of the external field angle at several temperatures in samples of B_ϕ =0.2 and 1 T are represented in Fig. 1. The global features are summarized that the drastic rise near $\theta = 0$ (H $\parallel$ ab) observed in pristine samples is less significant at lower temperature in sample with denser dose. Temperature dependence of the resonance field for H $\parallel$ c is shown in Fig. 2. The resonance field at a given temperature is largely enhanced as the irradiation dose increases. The temperature dependence shows takeoff below $T^* \simeq 80$ K, which is almost independent of CD doses. It is noted that the resonance field near the ab plane below T^* shows two minima and one sharp dip. These anomalous behavior near ab plane will be described elsewhere. The results lead to the qualitative understanding that the interlayer coupling of BSCCO is drastically enhanced by introducing CD below T^*.

In order to describe such a change of interlayer coupling at T^* quantitatively, we apply a general scaling function to the angular dependence of the resonance field, that is,

$$H_{\rm res}(\theta) = \frac{H_{\rm res}(90^\circ)}{\sqrt{\sin^2\theta + \gamma_{\rm eff}^{-2}\cos^2\theta}}. \qquad (1)$$

Here, $H_{\rm res}(\theta)$ represents the resonance field at arbitrary angle θ, and $\gamma_{\rm eff}$ is a temperature dependent effective anisotropy parameter, which renormalizes the effects of the vortex states in wider temperature region. The agreement between the experimental results and Eq. (1) is excellent except in the vicinity of $\theta = 0$ as shown in Fig. 1.

$\gamma_{\rm eff}$ for all samples are plotted as a function of temperature in Fig. 2 (open symbols). It is clear that $\gamma_{\rm eff}$ value has little temperature dependence below T^*, whereas it sharply increases above T^* and approaches the value for pristine sample. The behavior of $\gamma_{\rm eff}$ suggests that the

[1]Institute of Materials Science, University of Tsukuba.

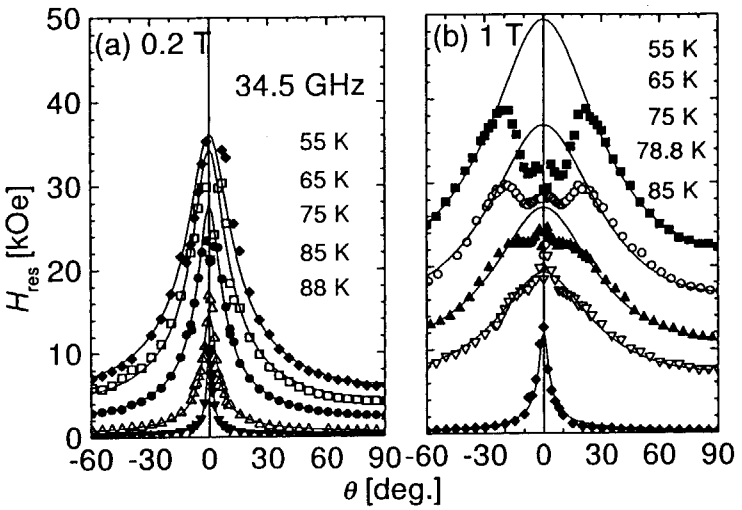

Figure 1: Angular dependence of the resonance field $H_{\rm res}$ in samples of B_ϕ = (a) 0.2 and (b) 1 T. Solid lines are given by Eq. (1) with $\gamma_{\rm eff}$ being a unique fitting parameter.

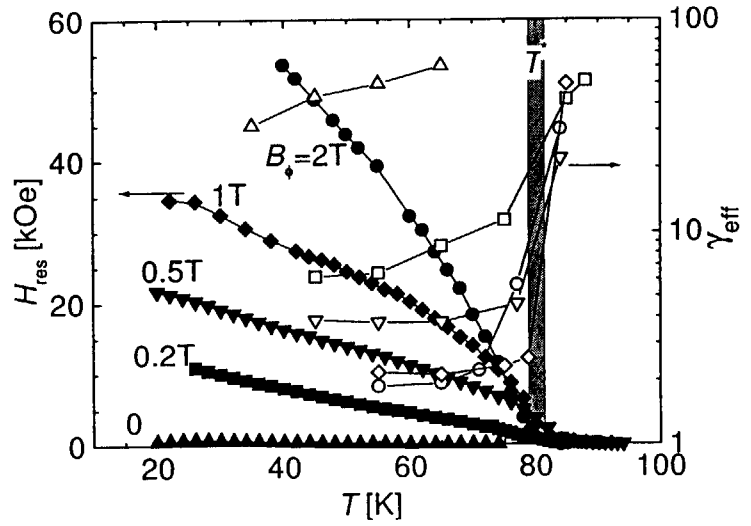

Figure 2: Temperature dependence of the resonance field (solid) and the effective anisotropy parameter $\gamma_{\rm eff}$ (open) for all samples. The same shape of symbols means the result obtained in the identical sample. Hatched area indicates the threshold temperature T^*, and the solid lines are drawn for the eyes.

interlayer vortex-vortex correlation grows rapidly in the irradiated samples with decreasing temperatures and it develops fully at T^* below which the anisotropy of the vortex state essentially no longer changes. This behavior can be interpreted by a picture that the pancake vortex are confined into CD below T^* and they are excited thermally to the almost freely movable state above T^*, which is independent of irradiation doses. This means that the confinement of the vortex into CD is governed by the nature of the single particle excitation.

In conclusion, we succeeded in setting a quantitative description of interlayer coupling in the vortex liquid state by JPR in irradiated BSCCO single crystals.

This wark has been supported by Core Research for Evolutional Science and Technology, Japan Science Technology Cooperation.

References

[1] O. K. C. Tsui *et al.*, Phys. Rev. Lett., **73**, 724 (1994). L. N. Bulaevskii, M. P. Maley, and M. Tachiki, *ibid.*, **74**, 801 (1995); Y. Matsuda *et al.*, *ibid.*, **75**, 4512 (1995).

[2] T. Hanaguri *et al.*, Phys. Rev. Lett., **78**, 3177 (1997); M. Kosugi *et al.*, *ibid.*, **79**, 3763 (1997).

5.8 INFLUENCE OF ION VELOCITY ON DAMAGE EFFICIENCY IN THE $Bi_2Sr_2CaCu_2O_X$ SINGLE CRYSTAL IRRADIATED WITH Au IONS

D.X. HUANG[1], Y. SASAKI[1], Y. IKUHARA[2]

Based on the high resolution TEM (HREM) observations of the columnar defect along the ion path, we developed a method to study the influence of ion velocity on ion irradiation damage. By investigation the dependence of damage efficiency on the ion velocity, we can minimize the influence of the different ion effective change on the ion irradiation damage. The application on the Au irradiated $Bi_2Sr_2CaCu_2O_x$ system shows that there is a critical velocity vc $\sim$ 0.057c (c; the velocity of light) at which the damage efficiency is maximum. From this observation, the irradiation damage process is divided into two stages. In high ion velocity region the irradiation damage is ion velocity controlled and in the low ion velocity region the irradiation damage is the energy-density threshold controlled. The peak of damage efficiency corresponds to the turning point between two stages.

A $Bi_2Sr_2CaCu_2O_x$ single crystal formed by flowting-zoon method was irradiated with 230-MeV Au ions at room temperature along <001> direction. The incident Au ions were produced in a Tandem accelerator at Japan Atomic Energy Research Institute. TEM images were taken along the ion penetration path using Topcon EM-002B (200kV). The damage cross section A in each penetration depth region was measured by the HREM images. Supposing that the damaged area is a regular cylinder, the relation $A=\pi(D/2)^2$, where the D is a diameter of the radiation defect. We can calculate the value of stopping power dE/dx using EDEP-1 code. Consequently, the damage efficiency ε can be obtained through the relation $\varepsilon = A/(dE/dx)$ [1].

A series of HREM images for the irradiation-induced columnar defects have been taken continuously along the ion penetration path [2]. Figure 1 shows four pieces of typical image picked out from them. From this figure, we can see that the diameter of the damaged amorphous cylinder gradually decreases from 13.5nm to 3 nm when the penetration depth of the incident Au ion in the target changes from 1 μm to 7.5 μ

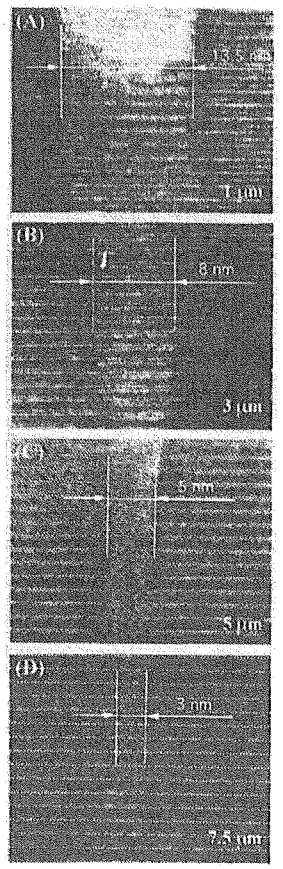

Fig. 1 HREM images respectively taken at penetration depths along the ion path

1. Japan Fine Ceramics Center, 2. Department of Material Science, Tokyo University

nm when the penetration depth of the incident Au ion in the target changes from 1 μ m to 7.5 μ m. All the measured data, calculated data, and two previously data for the same ion-target irradiation system have been summarized and shown in table 1.

Target	Ion	Energy (MeV)	Energy (MeV/amu)	dE/dx (keV/nm)	D (nm)	A (nm^2)	Relative velocity v/c	ε (nm^3/keV)	Ref.
Bi-2212	Au	2640	13.4	38.5	7.1	39.59	0.169	1.03	3
	Au	300	1.52	31.5	16	201.06	0.057	6.38	4
	Au	200	1.02	28.8	13	132.73	0.047	4.61	
	Au	172	0.87	27.2	10	78.54	0.043	2.89	
	Au	120	0.61	23.8	7	38.48	0.036	1.62	
	Au	98	0.5	21.9	6	28.27	0.032	1.29	
	Au	77	0.39	19.8	4.8	18.1	0.029	0.91	
	Au	59	0.3	17.3	3.6	10.18	0.025	0.59	
	Au	50	0.25	15.9	2.8	6.16	0.023	0.39	

Table 1. Experimental data measured by the HREM method in Au-irradiated $Bi_2Sr_2CaCu_2O_x$ single crystals.

Figure 2 shows a curve of damage efficiency versus ion velocity in electron stopping power region by using the measured data in this study and combining with two previous data [3, 4] in the same ion-target irradiation system. As shown by this curve, in the high-velocity region, the damage efficiency increases with decreases of ion velocity along the ion penetration path. When the ion velocity decreases to some value around 0.057c, the damage efficiency reaches a maximum value. There is a peak of damage efficiency on the ε -v curve in the low-velocity region. The damage-efficiency peak on the measured ε -v curve indicates the existence of a turning point in the irradiation-damage process.

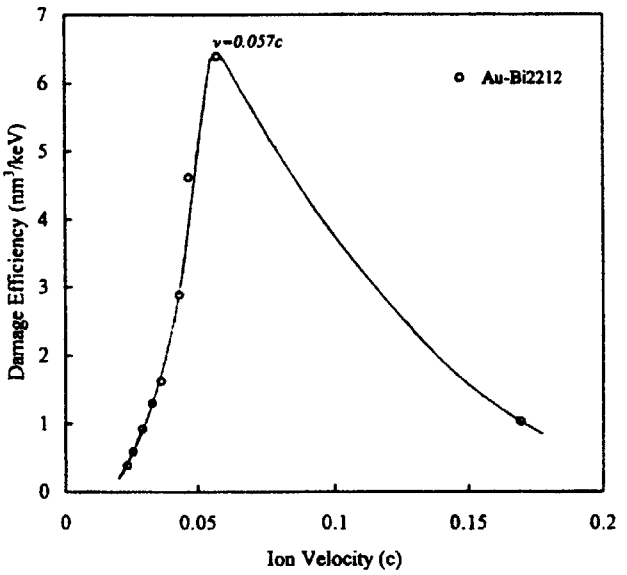

Fig. 2 Dependence of damage efficiency on ion velocity in single ion-target irradiation system.

Reference

[1] D.X. Huang. Y. Sasaki, S. Okayasu. T. Aruga, K. Hojou and Y. Ikuhara, Phys. Rev. **B 57**, 13907 (1998)

[2] D.X. Huang. Y. Sasaki and Y. Ikuhara, Phys. Rev. **B 59**, 3862 (1999)

[3] M. Toulemonde, S. Bouffard and F. Studer, Nucl. Instrum. Nethods Phys. Res. B91,108(1994)

[4] A. Meftah, F. Brisard, J.M. Costantini, M. Hage-Ali, J.P. Stoquert, F. Studer and M. Toulemonde, Phys. Rev. **B 48**, 920(1993)

5.9 STRUCTURE OF DEFECTS INDUCED BY HIGH-ENERGY HEAVY IONS IN HIGH-T_c SUPERCONDUCTOR

M. SASASE, S. OKAYASU, H. KURATA and K. HOJOU

High energy heavy ions dissipate most of their energies though electronic excitation rather than though nuclear collisions. Through the electronic excitation process, ions produce beam tracks in some insulators and semiconductors[1]. In particular for high-T_c superconductors, heavy ions with energy above several hundreds MeV create amorphous region along their linear tracks. In some conditions of irradiation, the enhancement of the J_c is observed since these tracks (columnar defects) act as strong pinning centers for flux lines[2]. Therefore, it is important to clarify the size, distribution, and structures of columnar defects and mechanisms of columnar defect formation. We have investigated columnar defects produced with energetic ions of Au ions using transmission electron microscopy (TEM) equipped with electron energy-loss spectroscopy (EELS).
$Bi_2Sr_2CaCu_2O_x$(Bi-2212) samples were irradiated with Au ions (60 ~ 300 MeV) with the fluence of 2.0×10^{10} ions/cm^2 at the room temperature using a tandem accelerator at JAERI. The TEM observations were performed on the irradiated samples. In order to estimate the contribution of energy loss process to the defect formation in the present conditions of irradiation, we calculated the energy loss (electronic and nuclear) in the Bi-2212 sample for each incident ion energy using the TRIM code[3].
Fig. 1 shows TEM image of the Bi-2212 irradiated with 240 MeV Au ions. This lattice image was observed in the [001] direction of columnar defects. The observed defects show an average diameter of 12.5 nm. The observed diameters from other conditions versus electronic energy loss (dE/dx)e were shown in Fig. 2. It is understood that the size of the defects depended on the energies deposited into the target. The correlations between the size of the defects and the deposited energy by incident ions have been applied to the time dependent line source model (TDLSM)[4] of thermal spike, in order to evaluate the experimental results for the defects produced in the Bi-2212. From the calculation of temperature distribution around the ion track using the TDLSM, it was found that about 1/3 of the energy deposited into the electronic excitation by an ion contributes effectively to thermal spike resulting in track formation in Bi-2212.

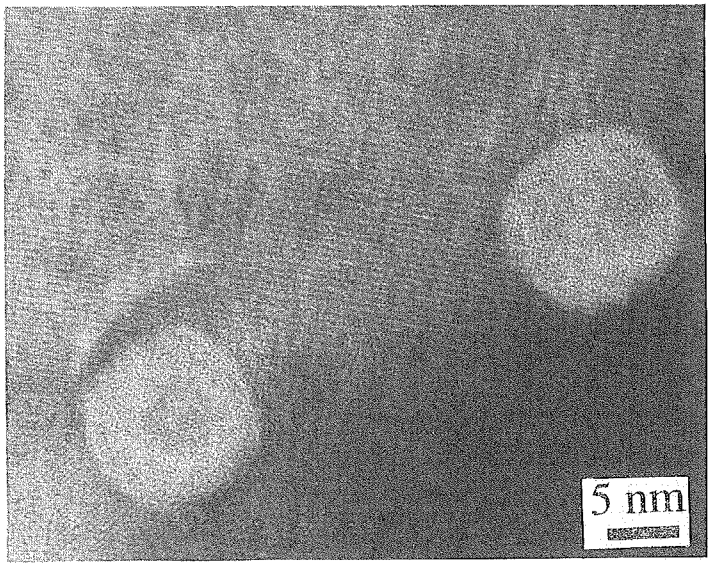

Fig. 1 TEM image of columnar defects observed along [001] direction.

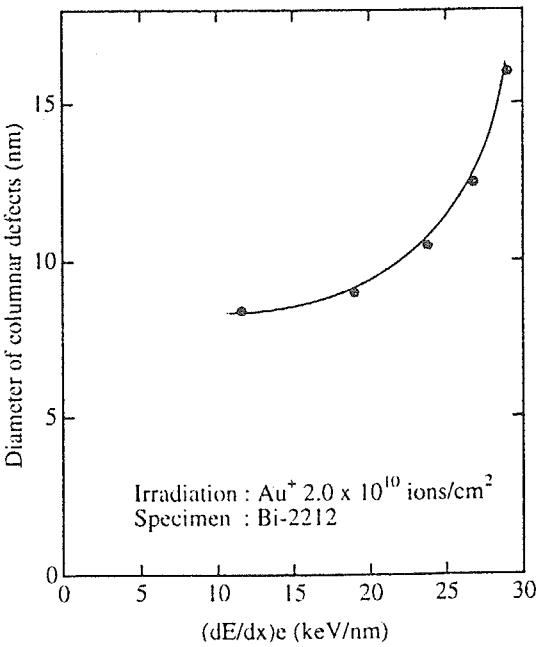

Fig. 2 Diameter of columnar defects versus dE/dx in Bi-2212.

REFERENCES

[1] M. Toulemonde, S. Bouffard and F. Studer, Nucl. Instrum. Methods, B91(1994) 108.
[2] L. Cival, A. D. Marwick, T. K. Worthington, M. A. Kirk, J. R. Thompson, L. Krusin-Elbaum, Y. Sun, J. R. Clem and F. Holtzberg, Phys. Rev. Lett., 67(1991) 648.
[3] J. F. Ziegler : Handbook of Stopping Cross Section for Energetic Ions in All Elements (Pergamon Press, New York, 1980).
[4] K. Izui, J. Phys. Soc. Jpn., 20(1965) 915.

5.10 SUPERCONDUCTIVITY AND WEAK LOCALIZATION IN MULTI-LAYERED Ge/Nb FILMS

K.MIMA[1],K.NARA[1],K.NAKADA[1],H.KAJITA[1],S.OKAYASU and Y.OCHIAI[1]

1. INTRODUCTION

In most low-dimensional superconducting films, frequently, a superconductivity fluctuation (SF) behavior is observed in the low temperature magneto-resistance (MR) near the transition. Also, it has been studied on the physical properties of artificial superconducting multi-layer systems which offer an ideal stage to investigate the dimensional crossover effects, since it is easy to control the degree of disorder, and the strength of coupling, just by varying the layer thickness[1]. Such dimensional crossover effects have previously been clearly observed in the physical properties of a variety of multi-layer systems. In particular, much theoretical and experimental interest has focused on the relation between the system dimensionality and the upper critical magnetic field, H_{c2},[2] since H_{c2} reflects the dimensionality of the superconductivity and is also sensitive to the quality of layering. In recent studies of the susceptibility of Si/Nb multi-layered films, similar to the samples studied in this report, a dimensional crossover was clearly observed in the fluctuation-induced diamagnetism[3]. In addition to studies of the magnetic properties, the correction to the electrical conductivity, due to weak localization (WL), has also been shown to exhibit layering effects in Si/Nb multi-layer systems.[1,4]

2.MAGNETORESISTANCE THEORY

We have determined the inelastic scattering time τ_ϕ using a combination of Aslamazov-Larkin (AL) [5] and Maki-Thompson (MT) [6,7] superconducting fluctuation theories based on weak localization (WL) effect for 2D. Theoretical MR, $\Delta\sigma$[8,9], is given by

$$\Delta\sigma = \sigma_{AL}+\sigma_{MT} \qquad (1)$$

where $\Delta\sigma = \sigma(H,T)-\sigma(0,T)$. These quantum correction terms are calculated due to the symmetry breaking effect of the magnetic field.[6,8]The first correction term in Eq.(1), AL term, comes from pair-type fluctuation [7] and is written by

$$\sigma_{AL} = \int_0^{2\pi/d} \frac{e^2}{8\hbar\varepsilon_k}\left(\frac{\varepsilon_k}{h}\right)^2\left[\psi\left(\frac{1}{2}+\frac{\varepsilon_k}{2h}\right)-\psi\left(1+\frac{\varepsilon_k}{2h}\right)+\frac{h}{\varepsilon_k}\right]\frac{dk}{2\pi} \qquad (2)$$

where $h=(dH_{c2}/dT)^{-1}H/T_c$, $\Psi(x)$ is di-gamma function, $\varepsilon_k=\varepsilon[1+\alpha\{1-\cos(k_{//}d)\}]$, d is a thickness of the insulator layer, $\varepsilon=(T-T_c)/T_c$, and $\alpha=2\xi_{//}^2(0)/d^2\varepsilon$. Near the transition temperature ($\varepsilon<<1$), the superconducting fluctuation of AL term dominates MT term. On t[1]he other hand, the MT term arises from a normal electron type fluctuation[7,8] and is written by

$$\sigma_{MT} = \frac{e^2}{32\hbar h}\int_0^{2\pi/d} dk\,\frac{1}{B-A}\left[\psi\left(\frac{1}{2}+B\right)-\psi\left(\frac{1}{2}+A\right)\right] \qquad (3)$$

where

$$A = \frac{\varepsilon}{2h}\left[1+\alpha\{1-\cos(k_{//}d)\}\right] \qquad (4)$$

$$B = \frac{\pi h}{16hT\tau_\phi}+\frac{\alpha\varepsilon}{2h}\left[1-\cos(k_{//}d)\right] \qquad (5)$$

---

[1]Faculty of Engineering, Chiba University

Table 1. Characteristics of the films

Ge[Å]	0	20	30	50	100
Nb[Å]	500	50	50	50	50
R_0[Ω]	20	540	490	560	600
Tc[K]	2.98	2.78	2.87	2.85	2.63
λ[Å]	9.8	6.6	4.3	3.9	3.7

3.EXPERIMENTS

We have fabricated the Hall bar type samples using a Cu mask on a quartz substrate at room temperature. Ge, and Nb were successively deposited by electron beam evaporation. Each multi-layer consists 10 layers of a basic Ge/Nb unit. The thickness of the Nb layer is fixed at 50 Å and that of the Ge layer is ranged from 0 to 100Å. In these samples, the thickness of the buffer or the cover layer of Ge is more than 100Å in order to protect the Nb layer from oxidation. Both Ge and Nb layers are amorphous from X-ray measurement, since θ-2θ diffractometer scans reveal no polycrystalline texture. The low-temperature transports were measured in a ^{4}He cryostat at temperatures down to 1.8 K and in magnetic field of up to 6 T.

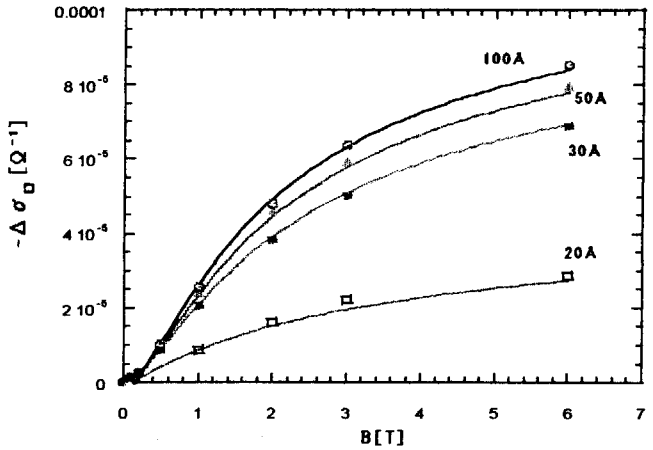

Fig.1. Magneto-conductance at T/T_c=1.4 for several different Ge layer of 20, 30, 50 and 100 Å. Solid line shows the theoretical fitting curves.

4. RESULTS AND DISCUSSIONS

We have measured and analyzed the MR using the transport parameters of the SF theories in 2D as described in Eqs.(1)-(5). In Table 1, we list the measured transport parameters of the zero field sheet resistance R_0, the transition temperature, T_c, and the mean free path λ, where T_c is defined as the midpoint of the phase transition in resistance curve. Figure 1 shows the measured MR and theoretical curve fit at several different thickness of the Ge layer using two fitting parameters of τ_φ and coherent length, $\xi_{//}$. There exists a significant good fit for all films up to 6 T or more. Negative magneto-conductance (NMC) up to 6T was observed to become gradually small as the thickness of the insulating layer decreases.

By fitting to the theories, we can determine τ_φ and $\xi_{//}$, the temperature dependence of the τ_φ as shown in Fig.2. Since τ_φ almost obeys a linear relation even in narrow temperature region, in a simple power law $\tau_\varphi \propto T^{-p}$, the value of the exponent p is considered as an unity, suggesting that strong electron-electron scattering may be present.[10]. The values of τ_φ are ranging from 10^{-12} to 10^{-11} second and is sufficiently larger than the order of the τ_φ estimated for high T_c oxide superconductors. At T/T_c =1.4, the MT term contribution is twice larger than the AL term. This indicates that the AL contribution does not ignore even at a longer τ_φ case than that of high T_c materials. Also, we can determine $\xi_{//}$ on the fitting as

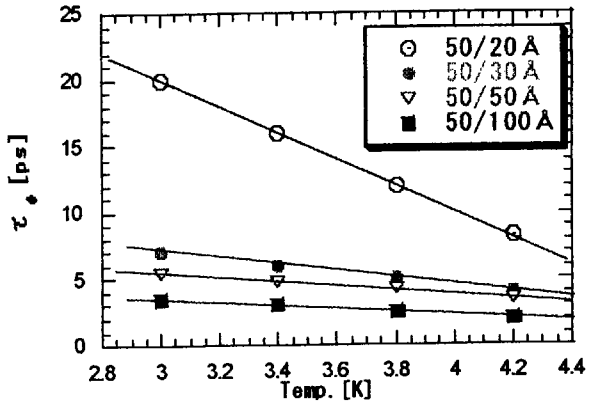

Fig.2. Temperature dependence of τ_φ for several different Ge layer of 20, 30, 50 and 100 Å. Solid line indicates a guide of eye.

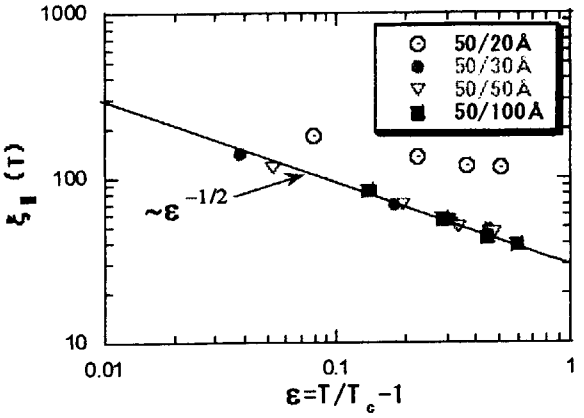

Fig.3. $\xi_{//}$ as a function of the reduced temperature ε for several different Ge layer of 20, 30, 50 and 100 Å. Solid line indicates a slope on the exponent of p=-1/2.

shown in Fig. 3 and the exponent on ε is nearly close to $-1/2$. The system can be explained by an ordinal BCS superconductivity. Never the less, at the case of Ge layer thickness of 20 Å in Figs. 2 and 3 on τ_φ and $\xi_{//}$, the behavior clearly deviates from the other thickness cases. It suggests that a quasi 3D transport can appear at the thickness less than 20 Å. Therefore, a dimensional crossover from 3D to 2D can be expected between 20 and 30 Å for the thickness of the insulator layer.

5.CONCLUSION

We have fabricated Ge/Nb superconductor-insulator multi-layers and measured their transport properties. In order to investigate the mechanism of the coupling, we have analyzed the MR using the mesoscopic parameters of WL and SF by controlling the thickness of the Ge. The MR results can be fitted to such a conductance correction up to 6 T. Although τ_φ is order of 10^{-12} or 10^{-11} second, the contribution of AL term clearly exists even at near $\varepsilon=1$. The behavior of τ_φ and $\xi_{//}$ indicates a crossover from 2D to 3D as the thickness of Ge decreases because of an increase of the coupling between conducting layers. It shows that the SF should have a relation with the coupling mechanism between superconducting layers. We ,therefore, conclude that τ_φ is a useful parameter for investigating the superconducting properties related to the coupling in these multi-layer systems. More detailed analysis is required to clarify the coupling for layering effect.

7. REFERENCES

1. T.Kitatani, J.P.Bird and Y.Ochiai, Surf.Sci. 267, 583 (1992)
2. S.T.Ruggiero, T.W.Barbee,Jr and M.R.Beasley, Phys. Rev.B, 26, 4895 (1982)
3. H.Obara, K.Uchinokura and S.Tanaka, Physica C, 157, 37 (1989)
4. S.N.Song and J.B.Ketterson, Phys. Lett., A155, 325 (1991)
5. R.Rosenbaum, Phys. Rev. B, 32,2190 (1985)
6. A.I.Larkin, JETP. Lett., 31, 219 (1980)
7. E.Abrahams, R.E.Prange and M.J.Stephen, Physica,55, 230 (1971)
8. S.Hikami, A.I.Larkin and Y.Nagaoka, Prog. Theor. Phys., 63, 707 (1980)
9. S.Hikami and A.I.Larkin, Mod. Phys. Lett. B2, 693 (1988)
10. B.L.Altshuler, A.G.Aronov and D.E.Khmelnitsky, J. Phys.C, 15, 7367 (1982)

5.11 EFFECTS OF ELECTRONIC EXCITATION ON RADIATION ANNEALING IN IRON BY ENERGETIC ION IRRADIATIONS

Y. CHIMI, A. IWASE and N. ISHIKAWA

It is of great interest that high-density electronic excitation affects atomic displacements in metals irradiated with energetic heavy ions in recent years [1, 2]. We report here the radiation effects in iron [3, 4] focussing on defect annihilation induced by irradiation, i.e. radiation annealing.

Polycrystalline iron thin films of ~200nm thick were used as specimens, which were deposited on α-Al_2O_3 single crystal substrates by rf magnetron sputtering. The electrical resistivity of the specimen was typically 10μΩ·cm at room temperature. Irradiation of the specimen with the following particles was performed at low temperature (~80K); 0.5~2.0MeV ^{1}H~^{40}Ar ions from a 2MV Van de Graaff accelerator and 84~220MeV ^{12}C~^{197}Au ions from a tandem accelerator both at JAERI-Tokai. The electrical resistance of the specimen was measured by means of a conventional four-probe method at appropriate intervals of ion fluence during each irradiation in order to observe defect accumulation behavior. After the irradiation, a defect recovery spectrum was obtained by raising the specimen temperature up to ~300K at a constant heating rate (~2K/min).

The defect annihilation cross-section, σ_r, was derived from the defect accumulation curve for each irradiation. In Fig. 1, the values of σ_r are plotted against the nuclear stopping power, S_n, which means the energy transferred from an incident particle to target atoms through elastic interactions per unit length along the ion path. For low-energy (~1MeV) ion irradiations, σ_r is nearly proportional to S_n. It means that in this case the radiation annealing is caused by the elastic interaction dominantly. On the other hand, in high-energy (~100MeV) case, the values of σ_r are much larger than those for low-energy ion irradiations at the same value of S_n. It indicates that the radiation annealing in high-energy case is enhanced by high-density electronic excitation.

Defect recovery spectra for 2.0MeV ^{40}Ar and 200MeV ^{127}I ion irradiations are shown in Fig. 2. These ions give almost the same value of PKA (Primary Knock-on Atom) median energy, $T_{1/2}$, which is characteristic of PKA energy spectrum [5]. The amount of the stage-I recovery for 200MeV ^{127}I ion irradiation, which appears mainly at ~120K in iron and corresponds to the recombination of free interstitials with vacancies, is much smaller than for 2.0MeV ^{40}Ar irradiation. It implies that electronic excitation induced by 200MeV ^{127}I irradiation annihilated free interstitials during the irradiation. The radiation annealing enhanced by high-density electronic excitation appears also as a reduction of stage-I recovery in iron.

References

1) A.Iwase and T.Iwata, Nucl. Instrum. Methods **B90**(1994)322; and references therein.
2) A.Dunlop, D.Lesueur, P.Legrand, H.Dammak and J.Dural, Nucl. Instrum. Methods **B90**(1994)330.
3) Y.Chimi, A.Iwase and N.Ishikawa, Mat. Res. Soc. Symp. Proc. **504**(1998)221.
4) Y.Chimi, A.Iwase and N.Ishikawa, J. Nucl. Mater. **271&272**(1999)236.

5) R.S.Averback, R.Benedek and K.L.Merkle, Phys. Rev. **B18**(1978)4156.

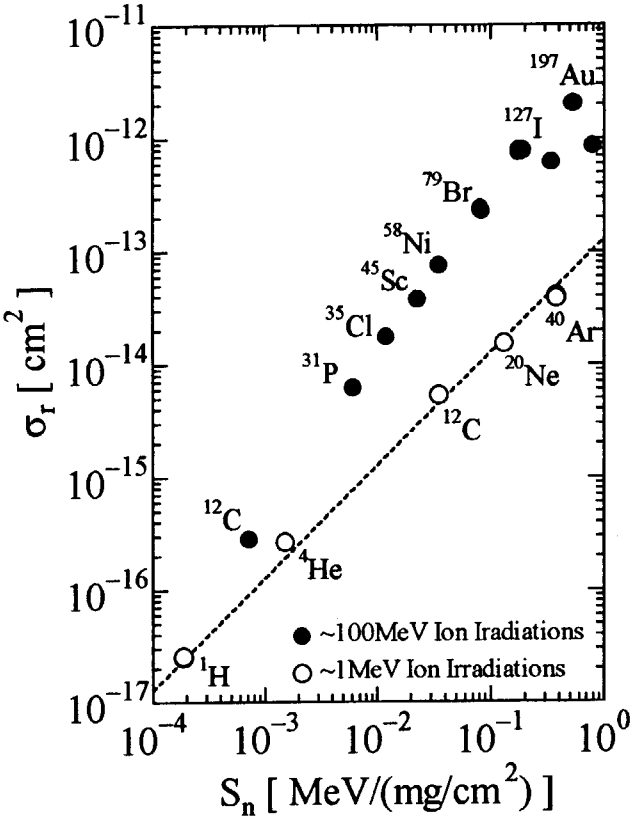

Fig. 1. Defect annihilation cross-section, σ_r, plotted against nuclear stopping power, S_n, for each irradiation.

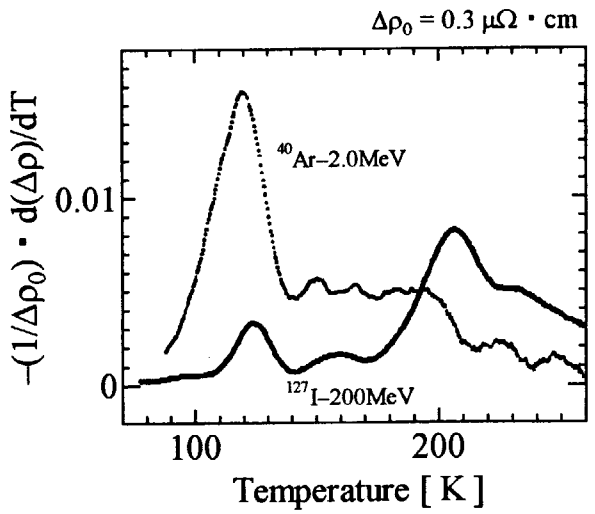

Fig. 2. Defect recovery spectra for 2.0MeV ^{40}Ar and 200MeV ^{127}I ion irradiations.

5.12 RADIATION DEFECTS IN NANOCRYSTALLINE MATERIALS

H.OHTSUKA, H.SUGAI, H.OTSU, K.HOJO, H.MAETA[1]

It is well known that near the grain boundary there exists defect free zone (denuded zone). When the size of the structural crystal is comparable to or less than the defect free zone, the defects by the irradiation would easily escape from the crystal leaving no damage in it. From this point of view, the aim of this study is to see a peculiar effect of nanocrystalline materials against radiation damage. Because the basic process of that phenomenon is diffusion of the simple defects, we consider that the temperature of the sample is an important parameter. First, we made a plan to install a experimental chamber, which is capable of heating samples up to 1000K, on a beam line from a tandem accelerator at JAERI-Tokai. We report here results of test operation of the newly provided experimental system.

Sample preparation: Developments of a device to produce nanocrystalline materials with grain sizes of about 5 to 50 nm by using the gas deposition method, especially applicable to TEM observation, is succeeded. Nanocrystalline Au, which was deposited onto a carbon film suspended by micro-grids, was irradiated with heavy ions. We found that the C-film stood against the heavy ion irradiation.

Necessary beam-time: At the planning, a question about this experiment was whether the practical beam-time (e.g. one day) is enough to produce observable defects in the nano-particles or not. After a preliminary irradiation of several hours we found a clear evidence of the defect clusters as shown in Fig.1 .

Heating: An ordinary resistive heating using W-wire is applied and 800K is attained by the electric power of 25 W. A problem was leakage of ion current through the cooling water, which brought out an error in the measurement of the ion dose. This problem, however, will easily be resolved using an insulated power supply for the chiller.

In conclusion, during this period, a system which is aimed to study an effect of nano-crystalline materials against radiation damage has been successfully provided.

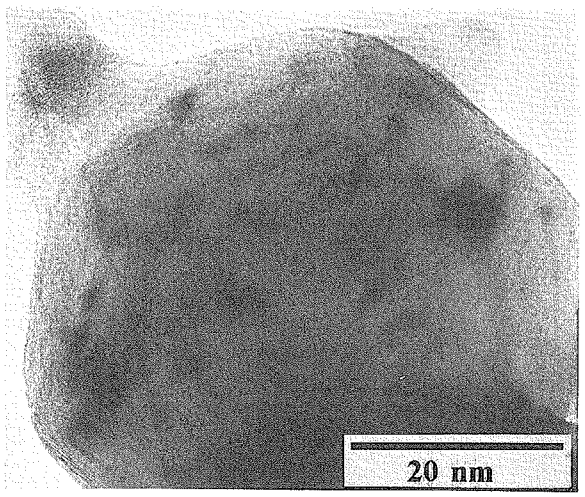

Fig. 1 A nanocrystalline-particle irradiated with iodine ions at a room temperature. Black spots in the particle are defect clusters.

[1]Facul Gen Educ, Hiroshima KG Univ.

5.13 STUDY OF IRRADIATION EMBRITTLEMENT MECHANISM WITH HIGH ENERGY IONS

K.MORITA[1)] , S. ISHINO[2)] , T. TOBITA, Y. CHIMI, N. ISHIKAWA AND A. IWASE

Pressure vessel of a nuclear reactor is a demanding component, required to have full integrity throughout the reactor lifetime with high credibility. There are various degradation modes known for the pressure vessel as neutron irradiation embrittlement, stress-corrosion cracking, fatigue and so on. Among them, the most important degradation mechanism is neutron irradiation embrittlement and in fact power reactors currently in service are equipped with surveillance test coupons, thereby confirming the integrity during the whole lifetime of the reactor. This is a corroborative approach, having its own limitations such that generic application is difficult to other reactor types or different service conditions. Large allowance to cover inherent ambiguity is imposing drawback for the demand of plant life extension. There has been a growing need to establish novel method of evaluation of degradation based on the understanding of the mechanisms of neutron irradiation embrittlement. One way to to understanding the mechanisms is establishing a modelling using a number of reliable data obtained under simplified experimental conditions. In this context, use of ion irradiation is growing rapidly for the study of embrittlement mechanisms under well controlled conditions which are difficult to obtain for neutron irradiations.

Since the damage production process by ion irradiation is different from that by neutron irradiations, it is not possible to directly compare the ion irradiation results with neutron irradiation results. However, displacement damage produced by elastic collisions is essentially the same for both cases. Moreover, ion irradiations have great advantages over neutron irradiations in that (1) the degree of activation is much lower for ion irradiation case to allow efficient post irradiation experiments mostly without using hot laboratories, (2) high damage levels are easily attainable within a short irradiation time, (3) irradiation parameters can be controlled without much difficulty. One of the biggest disadvantage is that the displacement damage is distributed non-uniformly near the specimen surface. Experimental methods to quantify the radiation damage are greatly restricted with relatively low energy ion irradiations; transmission electron microscopy and micro-indentation hardness measurements are examples of available methods. Ambiguity comes in to interpret the experimental results because damaged region is very close to the specimen surface. To overcome these difficulties, use of high energy ions has been sought for but such facilities are not readily available.

Generally accepted mechanism of irradiation embrittlement in pressure vessel steels is that radiation hardening, $\Delta \sigma_{total}$, is the sum of matrix hardening, $\Delta \sigma_{matrix}$, and the hardening due to radiation enhanced precipitates, $\Delta \sigma_{ppt}$;

$$\Delta \sigma_{total} = \Delta \sigma_{matrix} + \Delta \sigma_{ppt}$$

As for the precipitates, most extensively studied have been copper precipitates, which are known to be enhanced by neutron irradiation at the reactor operating temperature of ~300℃.

Objective of the present study is to investigate radiation embrittlement mechanisms by measuring changes in hardness in Fe-Cu model alloys by high energy heavy ion irradiations. The experimental matrices are chosen as simple as possible to obtain clear-cut information.

---

1) Course of Applied Science, Graduate School of Engineering, Tokai University, now at Japan Power Engineering and Inspection Corporation

2) Department of Nuclear Engineering, School of Engineering, Tokai University

Experimental parameters systematically varied were ion fluence, irradiation temperature and copper concentration in Fe-Cu alloys. Several high purity Fe-Cu alloys were prepared, the copper content being 0.02, 0.1, 0.6, 1.2 wt.%. Specimens were cut from large ingot into 7x7x1mm by wet polisher, mechanically polished and finally electrolytically polished just before irradiation.

Irradiations were performed using a 20MV tandem electrostatic accelerator in JAERI Tokai mostly with 200MeV Au^{13+} ions. Irradiation conditions are summarized in Table 1. In each experimental condition, four types of the alloys were irradiated simultaneously side by side to give the same irradiation conditions for them. By using an appropriate masking, irradiated and unirradiated regions were made in each of the specimens. Conventional Vickers hardness was measured for irradiated and unirradiated regions. From these results, hardness changes, ΔH_v, were derived.

Fig.1 shows ion fluence dependence of ΔH_v for irradiations at room temperature and at 250℃. For low fluence and in specimens with low Cu, copper concentration dependence is not clear. Beyond a certain fluence level, ΔH_v increases with almost identical slope. The tendency is similar to the trend curve for ΔDBTT[1]. Fig.2 shows the dependence of ΔH_v on irradiation temperature. Dependence on copper concentration is clearly observed. Probably due to copper precipitation, the hardening is most remarkable for irradiations around 250~300℃, above which the hardening decreases presumably due to coarsening of the precipitates. The data on irradiation temperature dependence of hardening by neutron irradiation is meagre. Comparing the present results with earlier neutron data[2], one finds the peak hardening temperature shifts to higher temperature side. This may be due to the difference in damage rate; about 10^{-6} dpa/s for present experiments whereas 10^{-9}~10^{-11} dpa/s for neutron irradiation case. Fig.3 shows change in hardness as a function of square root of Cu concentration. It may be seen that the hardening depends on the square root of Cu concentration above a certain threshold Cu concentration. The result is consistent with the dispersed barrier hardening model.

References

1) Radiation Embrittlement of Reactor Vessel Materials, U. S. Nuclear Regulatory Commission, Washington D. C. , May 1988 (Regulatory Guide 1.99 Rev.2)

2) L. E. Steele, IAEA Tech. Rept. Ser. No.163 (1975).

Table 1 Irradiation conditions*

Ions	200MeV Au^{13+}					
Irradiation temperature	Room temp.	200℃	250℃	300℃	350℃	400℃
Fluence	8.41×10^{10}	—	9.02×10^{10}	—	—	—
(ions/cm^2)	8.61×10^{11}	—	9.23×10^{11}	—	—	—
	5.68×10^{12}	4.98×10^{12}	6.67×10^{12}	5.08×10^{12}	5.02×10^{12}	5.19×10^{12}

* Four kinds of specimens with varied Cu concentrations were irradiated exactly under the same condition.

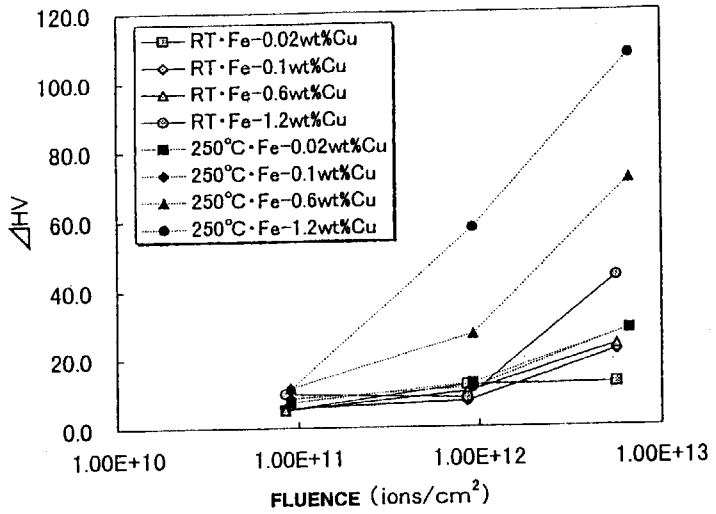

Fig. 1. FLUENCE DEPENDENCE OF IRRADIATION HARDENING

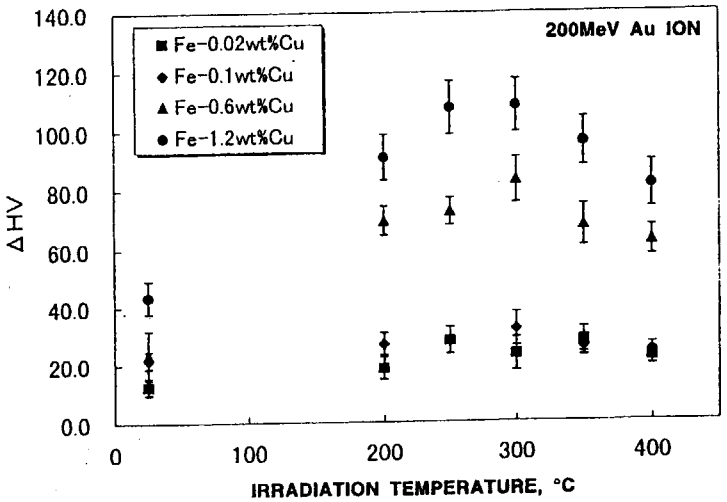

Fig.2. IRRADIATION TEMPERATURE DEPENDENCE OF HARDENING FOR SEVERAL MODEL Fe-Cu ALLOYS.

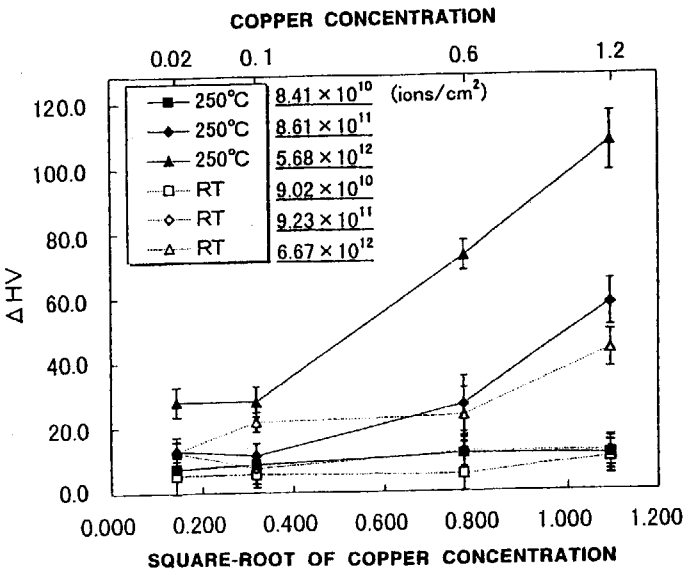

Fig. 3. DEPENDENCE OF IRRADIATION HARDENING(Δ Hv) WITH 200MeV Au IONS ON COPPER CONCENTRATION.

5.14 TOLERANCE OF SINGLE EVENT BURNOUT IN POWER MOSFETS CAUSED BY HIGH-ENERGY IONS

S.KUBOYAMA[1],T.HIRAO,T.SUZUKI[1],S.OKADA
A.MATSUMOTO[1],T.TAKAHASHI[1], T.HIROSE[2]
H.OHIRA[2],Y.NAGAI[2] and S.MATSUDA[1]

Semiconductor devices used for artificial satellites and spacecraft are affected by the radiation in space. It is well known that the incidence of high energy heavy ions into semiconductor devices causes four kinds of anomalies called single event phenomena (SEU, SEL,SEB,SEGR). Single Event Burnout (SEB) was identified as a possible catastrophic failure mode for Power MOSFETs with double-diffused MOS (DMOS) structure. Up to date, a lot of tests of SEB of Power MOSFETs have been performed, and its mechanism is getting clear. SEB is triggered when a heavy ion passed through a power MOSFET biased in the OFF state. Transient currents generated by the heavy ion turn on a parasitic bipolar transistor(BJT) inherent to the device structure. Due to a regenerative feedback mechanism, second breakdown sets in, creating a short-circuit between the source and drain which destroys the device[1]. Therefore, it is needed to increase SEB tolerance in power MOSFETs for space application.

Power MOSFET of 200V class have been developed to be used for the future artificial satellites. To determine the design parameters of Power MOSFET, we have performed irradiation tests on several types of samples. Newly, we started to study about the lifetime of carriers in Power MOSFET as one of the design parameters. It is known that the voltage drop generated by the current along the body layer cause the activation of the parasitic BJT as trigger of SEB[2]. So it can be expected to increase SEB tolerance as decreasing a amount of hole injected into parasitic BJT (decreasing the lifetime of carriers). To control the lifetime of carriers, we performed electron irradiation tests for Power MOSFET called "Life Time Control"(LTC). The lifetime of carriers is decided by electron dose and the anneal conditions. Thus, LTC samples were made by the electron irradiation and heavy ion irradiation tests of LTC samples were performed by using Energetic Particle Induced Charge Spectroscopy(EPICS) system[2]. Using EPICS system, SEB of power MOSFET was observed non-destructively.

Figure 1 shows the block diagram of EPICS used this experiment. We used the Ni ion 250MeV from the TANDEM accelerator in JAERI. Its ion beam was scattered by Au foil to control LET and fluence of ion beam. In this experiment, LET was about 27MeV/(mg/cm^2). The detail conditions are shown in Table 1.

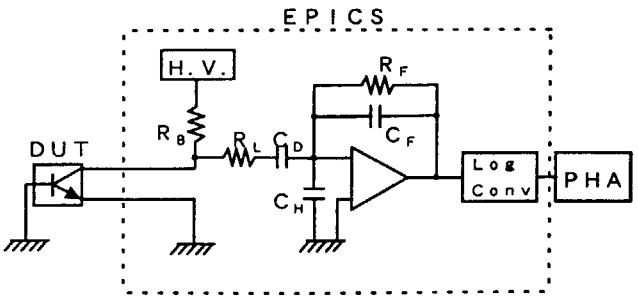

Fig.1 block diagram of EPICS

[1]Electronic and Information Technology Laboratory, Office of Research and Development, National Space Development Agency of Japan.
[2]Components Engineering Section, Engineering Dept., RYOEI TECHNICA Corporation.

Four types of LTC samples were prepared. These samples were based on 2SK3041(Power MOSFET, rated V_{DSS}=250V,V_{DSS}:Drain-Source Breakdown Voltage) which NASDA had developed previously. The characteristics of LTC samples and heavy ion irradiation test conditions are shown in Table 1. In Table 1, sample type 4 is a reference sample which LTC is not performed. In this time, anneal conditions were changed to control the lifetime of carriers under the constant electron dose. To evaluate the lifetime of carriers, Trrs(reverse recovery time) of these samples were measured as a parameter. The short Trr means the small lifetime of carriers. It is expected that the SEB tolerance increase(V_{DS} at which SEB occur increase,V_{DS}:Drain-source voltage) as Trr decrease. Heavy ion irradiation test results are shown in Fig.2.

Table 1. Characteristics of LTC samples and heavy ion test conditions

sample type	S/N	Trr [ns]	electron irradiation test condition			heavy ion test condition (Ni)	
			electron dose [Gy]	anneal condition		LET [MeV/(mg/cm^2)]	Range [μ m]
				temp.[℃]	time[min]		
1	#1	196	1.6×10^5	330	120	27.902	38.063
	#2	212				27.996	37.578
2	#3	272		357	120	27.902	38.063
	#4	272				28.143	36.848
3	#5	416		420	60	27.902	38.063
	#6	404				28.143	36.848
4*	#7	480	—	—	—	27.902	38.063
	#8	480				28.143	36.848

*No LTC(reference sample)
S/N : sample number

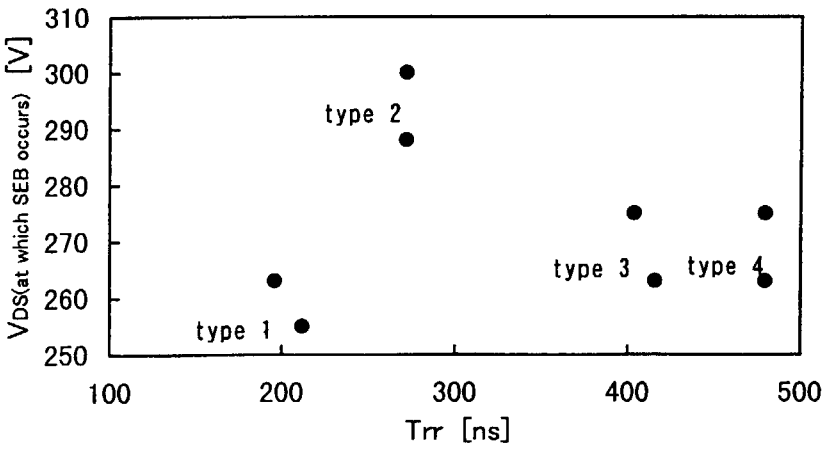

Fig.2 V_{DS}(at which SEB occurs)-Trr Characteristics

In Fig.2, SEB tolerance increased at 272ns(Trr) ,but decreased at about 200ns(Trr). It seems that there is a maximum point of SEB tolerance somewhere. It was different from our expectation. The reason was not clear yet, so we will test many types of samples to make the mechanism clear. We expect that such test results will be available to develop Power MOSFET which have high SEB tolerance.

References

1)M.Allenspach et al., IEEE Trans.Nucl.Sci., Vol.NS-43,No.6,pp.2927-2931(1996)
2) S.Kuboyama et al., IEEE. Trans.Nucl.Sci. Vol.NS-39,No.6,pp.1698-1703(1992)

This is a blank page.

6. Publication in Journal and Proceedings, and Contribution to Scientific Meetings

This is a blank page.

ACCELERATOR OPERATION AND DEVELOPMENT

Journal/Proceedings

Matsuda, M. Kobayashi, C. and Takeuchi, S.
Use of an ECR Ion Source in the High Voltage Terminal of the Tandem Accelerator at JAERI.
AIP Conference proceedings 473, "Heavy Ion Accelerator Technology, Eighth International Conference", Argonne, Illinois(Oct. 1998) pp65-73.

Takeuchi, S., Abe, S., Hanashima, S., Horie, K., Ishizaki, N., Kanda, S., Matsuda, M., Ohuchi, I., Tayama, H., Tsukihashi, Y. and Yoshida, T.
Status of the JAERI tandem Accelerator and Its Booster.
AIP Conference proceedings 473, "Heavy Ion Accelerator Technology, Eighth International Conference", Argonne, Illinois(Oct. 1998) pp152-167.

Takeuchi, S., Matsuda, M., Minehara, E., Sugimoto, M., Sawamura, M., Nagai, R., Kikuzawa, N., Nishimori, N., Ouchi, N., Kusano, J., Asaoka, N. and Mizumoto, M.
Superconducting RF Activities at JAERI
Proc. of the Eighth workshop on RF Superconductivity, Abano Terme, Italy(1997) pp233-236.

Takeuchi, S. and Matsuda, M.
First three year optional experience with the JAERI tandem-booster
Proc. of the Eighth Workshop on RF Superconductivity, Abano Terme, Italy(1997) pp237-247.

Takeuchi, S.
Study of Acceleration Across the TTF's Zero-Crossing Velocity in Independently Phased Linac.
AIP Conference proceedings 473, "Heavy Ion Accelerator Technology, Eighth International Conference", Argonne, Illinois(Oct. 1998) pp144-251.

Yoshida, T., Kanda, S., Takeuchi, S., Hanashima, S., Ohuchi, I.,
Horie, K.,Tsukihashi, Y., Abe, S., Ishizaki, N., Tayama, H. and Matsuda, M.

The Status of the JAERI Tandem Accelerator
Proc. of the 11th Workshop of the Tandem Accelerator and their Associated Technology
(Tokyo Institute of Technology, Tokyo, July 2-3, 1998)

Meetings

Takeuchi, S., Abe, S., Hanashima, S., Horie, K., Ishizaki, N., Kanda, S., Matsuda, M., Ohuchi, I., Tayama, H., Tsukihashi, Y. and Yoshida, T.
Status of the JAERI tandem Accelerator and Its Booster.
Eighth International Conference on Heavy Ion Accelerator Technology, Argonne, Illinois (Oct. 1998).

Matsuda, M. Kobayashi, C. and Takeuchi, S.
Use of an ECR Ion Source in the High Voltage Terminal of the Tandem Accelerator at JAERI.
Eighth International Conference on Heavy Ion Accelerator Technology, Argonne, Illinois (Oct. 1998).

Takeuchi, S. and Matsuda, M.
Status of the Superconducting Heavy-ion Tandem-booster Linac at JAERI.
LINAC98, Chicago(Aug. 23-28, 1998).

Takeuchi, S.
Study of Acceleration Across the TTF's Zero-Crossing Velocity in Independently Phased Linac.
Eighth International Conference on Heavy Ion Accelerator Technology,
Argonne, Illinois (Oct. 1998).

Takeuchi, S.
JAERI Tandem Accelerator System
Spring Meeting of the Atomic Energy Society of Japan, Hiroshima(March 24, 1999).

Yoshida, T., Kanda, S., Takeuchi, S., Hanashima, S., Ohuchi, I.,
Horie, K.,Tsukihashi, Y., Abe, S., Ishizaki, N., Tayama, H. and Matsuda, M.

The Status of the JAERI Tandem Accelerator
The 11th Workshop of the Tandem Accelerator and their Associated Technology
(Tokyo Institute of Technology, Tokyo, July 2-3, 1998)

Yoshida, T.
The JAERI Tandem Accelerator
Symposium of Heavy Ion Science on the Fields of Tandem Accelerator
(Joyo Geibun Center, Mito, January 12-13, 1999)

NUCLEAR STRUCTURE

Journal/proceedings

Ahmad, I., Back, B.B., Chasman, R.R., Greene, J.P., Ishii, T., Morss, L.R., Berg, G.P.A., Bacher, A.D., Foster, C.C., Lozowski, W.R., Schmitt, W., Stephenson, E.J. and Yamanaka, T.
Possible Observation of the $1/2^+[880]$ Orbital in ^{249}Cm
Nucl. Phys. A646(1999)175.

Asai, M., Ichikawa, S., Tsukada, K., Sakama, M., Shibata, M., Kojima, Y., Osa, A., Nishinaka, I., Nagame, Y., Kawade, K. and Tachibana, T.
β-decay Half-lives of New Neutron-rich Isotopes $^{167,168}Tb$ and Levels in $^{167,168}Dy$
Phys. Rev. C59(1999)3060.

Hossain, I., Ishii, T., Makishima, A., Asai, M., Ichikawa, S., Itoh, M., Ishii, M., Kleinheinz, P. and Ogawa, M.
Lifetime Measurement of the $\pi g_{9/2}$ Isomer in ^{79}As
Phys. Rev. C58(1998)1318.

Ichikawa, S., Tsukada, K., Nishinaka, I., Hatsukawa, Y., Iimura, H., Hata, K., Nagame, Y., Osa, A., Asai, M., Kojima, Y., Hirose, T., Shibata, M., Kawade, K. and Oura, Y.
Identification of ^{161}Sm and ^{165}Gd
Phys. Rev. C58(1998) 1239.

Ichikawa, S., Tsukada, K., Asai, M., Osa, A., Sakama, M., Kojima, Y., Shibata, M., Nishinaka, I., nagame, Y., Oura, Y. and Kawade, K.
β-decay Half-lives of New Neutron-rich Lanthanide Isotopes
Proc. 2nd Int. Conf. on Exotic Nuclei and Atomic Masses, AIP No.455(1998)540.

Iimura, H., Ichikawa, S., Sekine, T., Oshima, M. and Miyaji, M.
Conversion Electron Measurements in $^{125,127}Ba$
ENAM 98 Exotic Nuclei and Atomic Masses, AIP Conference Proceedings

Fall Meeting of the Physical Society of Japan, Akita(Oct. 5, 1998).

Asai, M., Sakama, M., Tsukada, K., Ichikawa, S., Oura, Y., Sueki, K., Nakahara, H., Nishinaka, I., Nagame, Y., Osa, A., Shibata, M., Kojima, Y. and Kawade, K.
Isotope Separation of EC Decaying Actinides and Measurement of their Atomic Masses
Spring Meeting of the Physical Society of Japan, Hiroshima(March 31, 1999).

Hatsukawa, Y., Hayakawa, T., Shinohara, N. and Oshima, M.
Application of Multidimensional Spectrum for Analytical Chemistry
International Conference on Experimental Nuclear Physics in Europe, Sevilla, Spain(June 21, 1999).

Hayakawa, T., Oshima, M., Hatsukawa, Y., Katakura, J., Iimura, H., Mitarai, S., Shimizu, Y., Outsubo, S., Shimizu, T., Sugawara, M. and Kusakari, H.
Identical Band of N=91 Isotone
Fall Meeting of the Physical Society of Japan, Akita(Oct. 4, 1998).

Hayakawa, T.
Rotational Bands of $^{155,156}Gd$
The Workshop on Frontier of Gamma-Ray Spectroscopy, JAERI(July 23, 1998).

Ichikawa, S., Asai, M., Tsukada, K., Osa, A., Nishinaka, I., Nagame, Y., Kojima, Y., Shibata, M., Oura, Y., Sakama, M. and Kawade, K.
Search for New Neutron-rich Lanthanide Isotopes Using an Isotope Separator.
The 42nd Symposium on Radiochemistry, Sendai(Sept. 16, 1998).

Iimura, H., Yonezawa, C., Matsue, H. Shinohara, N. and Raman, S.
Efficiency Calibration of a Ge Detector in the 0.1-11.0 MeV Region
Spring Meeting of the Physical Society of Japan, Hiroshima(March 29, 1999).

Ishii, T., Asai, M., Hossain, I., Kleinheinz, P., Ogawa, M., Makishima, A.,

Ichikawa, S., Itoh, M., Ishii, M. and Blomqvist, J.
The ($\nu g_{9/2} \pi p_{3/2}$)$_{19/2^-}$ Isomer in ^{69}Cu
Fall Meeting of the Physical Society of Japan, Akita(Oct. 4, 1998).

Ishii, T., Asai, M., Makishima, A., Hossain, I., Ogawa, M., Ichikawa, S. and Hasegawa, J.
Nuclear Structure of Neutron-rich Ni Region
Spring Meeting of the Physical Society of Japan, Hiroshima(March 31, 1999).

Sakama, M., Tsukada, K., Asai, M., Ichikawa, S., Oura, Y., Nagame, Y., Nishinaka, I., Sueki, K., Ebihara, M., Nakahara, H., Osa, A., Shibata, M. and Kawade, K.
Half-lives of New Neutron Deficient Actinides Isotopes ^{235}Am and ^{236}Am.
Spring Meeting of the Chemical Society of Japan, Yokohama(March 28-31, 1999).

Sakama, M., Tsukada, K., Asai, M., Ichikawa, S., Oura, Y., Nagame, Y., Nishinaka, I., Sueki, K., Nakahara, H., Kojima, Y., Shibata, M. Osa, A. and Kawade, K.
Improvement of Overall Efficiency of the Gas-jet Coupled JAERI-ISOL System and Search for New Americium Isotopes
1998 Symposium on Radiochemistry, Sendai(Sept. 16-18, 1998).

Sugawara, M., Kusakari, H., Murakami, T. and Kohno, T.
Lifetime Measurement of the (11/2) Isomer in ^{125}Cs
The Workshop on the Frontier of γ-ray Spectroscopy , JAERI(July 23, 1998).

Sugawara, M., Kusakari, H., Mitarai, S., Oshima, M., Hayakawa, T. and Hatsukawa, Y.
Dipole Bands in the Mass～130 and 80 Regions
Symposium on the Heavy Ion Science in the Tandem Energy Region, Mito(January 12, 1999).

Yamazaki, A., Nakagawa, T., Yamaya, T., Kumagai, K., Hirai, M., Kuzumaki, T., Yahata, H., Kato, M., Tojima, J., Suehiro, T., Kato, S.,

Ishiyama, H., Tanaka, M.H., Kubono, S., Sugiyama, Y. and Hamada, S.
Nuclear Structure in Light Nuclei via the Three-Nucleon Transfer Reactions
Fall Meeting of the Physical Society of Japan, Akita(Oct. 5, 1998).

NUCLEAR REACTIONS

Journal/Proceedings

Chadwick, M.B., Young, P.G., Chiba, S., Frankle, S.C., Hale, G.M., Hughes, G., Koning, A.J., Little,R.C., MacFarlane, R.E., Prael, R.E. and Waters, L.S.
Cross Section Evaluations to 150MeV for Accelerator-Driven Systems and Implementation in MCNPX
Nucl. Sci. Eng. 131(1999)293.

Chiba, S., Togasaki, K., Ibaraki, M., Baba, M., Matsuyama, S., Shibata, K., Iwamoto, O., Koning, A.J., Hale, G.M. and Chadwick, M.B.
Measurement and Theoretical Analysis of Neutron Elastic Scattering and Inelastic Reactions Leading to 3-body Final State for ^{6}Li at 10 to 20 MeV Region
Phys. Rev. C58(1998)2205.

Chiba, S.
Los Alamos Activiry on High Energy Nuclear Data Evaluation
JAERI-Conf . 98-016(1998)86.

Chiba, S.
Status of the Neutron Nuclear Physics Studies in the World
JAERI-Conf. 99-003(1999)184.

Harada, M., Yamamoto, A., Tanaka, Y., Watanabe, Y., Shin, K., Meigo, S., Iwamoto, O., Nakashima, H., Takada, H., Chiba, S., Fukahori, T., Sasa, T. and Tanaka, S.
Study of Secondary Charged-Particle Production by Proton-Induced Reaction at Several Tens of MeV
JAERI-Conf 99-002(1999)268.

Ibaraki, M., Baba, M., Matsuyama, S., Chiba, S., Togasaki, K., Shibata, K., Iwamoto, O., Koning, A.J. Hale, G.M. and Chadwick, M.B.
Mearurement and Theoretical Analysis of Neutron-Induced Neutron-

Emission Reactions of ^{6}Li at 10 to20 MeV Region
JAERI-Research 98-032(1998).

Iga, K., Ishibashi, K., Shigyo, N., Matsufuji, S., Nakamoto, T., Maehata, K., Numajiri, M., Meigo, S., Takada, H., Chiba, S., Nakamura, T. and Watanabe, Y.
Measurement of Gamma-Ray Production Double-Differential Cross Section for the Spallation Reaction Induced by 0.8, 1.5 and 3.0 GeV Protons
J. Nucl. Sci. Technol. 35(1998)329.

Lee, Y.O., Chang, J., Fukahori, T. and Chiba, S.
Evaluation of Neutron- and Proton-induced Cross Sections of ^{27}Al up to 2 GeV
JAERI-Conf. 99-002(1999)246.

Maruyama, Tomoyuki and Chiba, S.
Relationship between the Isovector Optical Potential and Direct Urca Process in High-density Neutron Star Matter in the Relastivistic Mean-field Theory
JAERI-Research 99-006(1999).

Meigo, S., Chiba, S. and Shin, K.
Analysis of Neutron Spectra from Thick Tagets Bombaded with 710-MeV Alpha Particles by Quantum Molecular Dynamics plus Statistical Decay Model
J. Nucl. Sci. Technol. 36(1999)250.

Sugiyama, Y., Napoli, D.R., Stefanini, A.M., Corradi, L., Signorini, C., Scarlassara, F., Tomita, Y., Ikezoe, H., Ideno, K., Yamanouchi, Y., Nagashima, Y., Sugimitsu, T. and Pollarolo, C.
Elastic and Inelastic Scattering of $^{58}Ni+^{90,94}Zr$
Eur. Phys. J. A4(1999)157.

Sukhovitskij, E.S., Chiba, S., Iwamoto, O. and Porodzinskij, Y.V.
Nucleon Interaction with ^{12}C Studied by the Soft-Rotator Model and a Limit on the Charge-Symmetry Breaking in the Nuclear Mean Field

Nucl. Phys. A640(1998)47.

Sukhoviskij, E.S., Chiba, S. and Iwamoto, O.
Coupled-Channels Optical Model Calculation with Account of Nuclear Volume Conservation
Nucl. Phys. A646(1999)19.

Sukhoviskij, E.S., Porodzinskij, Y.V., Iwamoto, O., Chiba, S. and Shibata, K.
Programs OPTMAN and SHEMMAN Version 5(1998)-Coupled Channels *Optical Model and Collective Nuclear Structure Calculation-*
JAERI-Data/Code 98-019(1998).

Titarenko, Yu.E., Shvedov, O.V., Batyaev, V.F., Karpikhin, E.I. Zhivum, V.M., Koldobsky, A.B., Igumnov, M.M., Sklokin, I.S., Mulambetov, R.D., Sosnin, A.N., Yasuda, H., Takada, H., Chiba, S., Kasugai, Y., Mashnik, S.G., Prael, R.E., Chadwick, M.B., Gabriel,T.A. and Blann, M.
Experimental and Computer Simulation Study of Radionuclide yields in the ADT materials Irradiated with Intermediate Energy Protons
JAERI-Conf. 98-016(1998)125.

Zhao, Y.L., Nagame, Y., Nishinaka, I., Tsukada, K., Sueki, K., Oura, Y., Nakahara, H., Ichikawa, S., Ikezoe, H., Tanikawa, M., Ohtsuki, T. and Kudo, H.
Experimental Verification of Two Deformation Paths in Mass Division Process of Actinides
J. Alloys and Comp. 271(1998)327.

Zhao, Y.L., Nishinaka, I., Nagame, Y., Tanikawa, M., Tsukada, K., Ichikawa, S., Sueki, K., Oura, Y., Ikezoe, H., Mitsuoka, S., Ohtsuki, T., Kudo, H. and Nakahara, H.
Symmetric and Asymmetric Scission Properties: Identical Shape Elongations of Fissioning Nuclei
Phys. Rev. Lett. 82(1999)3408.

Zhao, Y.L., Ohtsuki, T., Nagame, Y., Nishinaka, I., Tsukada, K., Ichikawa, S., Ikezoe, H., Hatsukawa, Y., Hata, H., Tanikawa, M., Oura, Y., Sueki, K.,

Kudo, H. and Nakahara, H.
Characteristics of Binary Scission Configurations in Proton Induced Fission of Actinides
J. Radioanal. Nucl. Chem. 239(1999)113.

Meetings

Nishinaka, I., Zhao, Y., Nagame, Y., Tsukada, K., Ichikawa, S., Ikezoe, H., Oura, Y., Sueki, K., Nakahara, H. and Tanikawa, M.
Correlation between Two Mass Division Modes and Fragment Shell Effects in Proton-Induced Fission of ^{232}Th
The 42nd Symposium on Radiochemistry, Sendai, (Sept. 16, 1998).

Nishinaka, I., Zhao, Y., Nagame, Y., Tsukada, K., Ichikawa, S., Ikezoe, H., Oura, Y., Sueki, K., Nakahara, H. and Tanikawa, M.
Correlation between Two Mass Division Modes and Deformability of Fragments in Proton-induced Fission of ^{232}Th
Fall Meeting of the Physical Society of Japan, Akita(Oct. 3, 1998).

Nishio, K., Ikezoe, H., Lu, J. and Mitsuoka, S.
Experimental Study of Fusion-Fission Reaction for $^{32}S+^{182}W$ at Sub-barrier Energy Region.
Spring Meeting of the Physical Society of Japan, Hiroshima(March 28, 1999).

Sugiyama, Y., Hamada, S., Ikuta, T. and Yamazaki, A.
Pair Neutron Transfer Reactions in the Nickel Region and a Possible Existance of the Nuclear Josephson Effect
International Nuclear Physics Conference, Paris(August 24-28, 1998).

Sugiyama, Y., Hamada, S., Ikuta, T. and Yamazaki, A.
Two-Neutrons Transfer Reactions in the Ni+Ni System around the Coulomb Barrier
Fall Meeting of the Physical Society of Japan, Akita(Oct. 5, 1998).

Sugiyama, Y.

Heavy-ion Nuclear Reaction around the Coulomb Barrier
Nuclear Physics Seminar at RCNP, Osaka(Oct. 9, 1998).

Sugiyama, Y.
Nuclear Josephson Effect in the Heavy-Ion Collision
Symposium on Heavy-Ion Science in the Tandem Energy Region, Mito(January 13, 1999).

Yamazaki, A., Sugiyama, Y. Hamada, S. et at.
Three-Nucleons Cluster Structure in Light Nuclei
Fall Meeting of the Physical Society of Japan, Akita(Oct. 5, 1998).

Zhao, Y.L., Nishinaka, I., Nagame, Y., Tanikawa, M., Nakahara, H., Tsukada, K., Sueki, K. Oura, Y., Ichikawa, S., Mitsuoka, S. and Ikezoe, H.
The Study of Deformation Properties of Scission Nucleus
Fall Meeting of the Physical Society of Japan, Akita(Oct. 3-6, 1998).

Zhao, Y.L., Nishinaka, I., Nagame, Y., Tanikawa, M., Sueki, K., Oura, Y., Nakahara, H., Tsukada, K., Ichikawa, S., Mitsuoka, S., Ikezoe, H., Ohtsuki, T. and Kudo, H.
Systematic Study on Bimodal Fission Phenomena
The 42nd National Conference on Nucl. Radiochem. Sendai (Sept. 16-18, 1998).

455(1998) p544.

Ikezoe, H., Ikuta, T., Mitsuoka, S., Nagame, Y., Nishinaka, I. Tsukada, Y. Ohtsuki, T., Kuzumaki, T. and Lu, J.
First Evidence for a New Spontaneous Fission Decay produced in the Reaction $^{30}Si+^{238}U$
The European Physical Journal A2(1998)379-382.

Ishida, Y., Iimura, H., Ichikawa, S. and Horiguchi, T.
Mean-Square Nuclear Charge Radius of Radioactive ^{144}Ce by Laser Spectroscopy
Phys. Rev. C59(1999)1794.

Ishii, T., Asai, M., Hossain, I., Kleinheinz, P., Ogawa, M., Makishima, A., Ichikawa, S., Itoh, M., Ishii, M. and Blomqvist, J.
The $(\nu g_{9/2} \pi p_{3/2})_{19/2^-}$ Isomer in ^{71}Cu and the Prediction of its E2 Decay from the Shell Model
Phys. Rev. Lett. 81(1998)4100.

Sekine, T., Ichikawa, S., Osa, A., Koizumi, M., Iimura, H., Tsukada, K., Nishinaka, I., Hatsukawa, Y., Nagame, Y., Asai, M., Kojima, Y., Hirose, T., Shibata, M., Yamamoto,H. and Kawade, K.
Recent Studies of Unstable Nuclei far from Stability with the On-line Isotope Separators of JAERI.
J. Radional. Nucl. Chem. 239(1999)127.

Sugawara, M., Kusakari, H., Murakami, T. and Kohno, T.
Lifetime Measurement of the (11/2) Isomer in ^{125}Cs
Eur. Phys. J. A2(1998)237.

Meetings

Asai, M., Ichikawa, S., Tsukada, K., Sakama, M., Shibata, M., Kojima, Y., Osa, A., Nishinaka, I., Nagame, Y., Kawade, K. and Tachibana, T.
Beta-decay Half-lives of Neutron-rich Nuclei ^{167}Tb and ^{168}Tb

NUCLEAR THEORY

Journal/proceedings

Iwamoto, A., Kondratyev, V.N. and Bonasera, A.
Vlasov Treatment of Spontaneous Fission and Sub-Barrier Fusion Reactions
Proc. Tours Symposium on Nuclear Physics Ⅲ AIP Proc. 425(1998)pp.222-230

Iwamoto, A., Kondratyev, V.N. and Bonasera, A.
Effect of nuclear Exchange in Heavy-Ion Fusion Reactions
Proc. RIKEN Symposium on "Dynamics in Hot Nuclei", (1998)217.

Kondratyev, V.N., Iwamoto, A. and Bonasera, A.
Mean-Field Simulation of Heavy-Ion Fusion at near-Barrier Energies
Proc. XVII RCNP International Symposium on Innovative Computational Methods in Nuclear Many-Body Problem (1998) pp.492-494.

Maruyama, Toshiki, Niita, K., Oyamatsu, K., Maruyama, Tomoyuki, Chiba, S. and Iwamoto, A.
Quantum Molecular Dynamics Approach to the Nuclear Matter below the Saturation Density
Proc. XVII RCNP International Symposium on Innovative Computational Methods in Nuclear Many-Body Problem (1998) pp.481-483.

Wu, X., Gu, J. and Iwamoto, A.
Statistical Properties of Quasiparticle Spectra in Deformed Nuclei
Phys. Rev. C 59(1999) 215.

Meetings

Chikazumi, S., Maruyama, T., Niita, K. and Iwamoto, A.
Dynamical Simulation of Nuclear Matter(I)
Fall Meeting of the Physical Society of Japan, Akita(Oct. 3-6, 1998)

Chikazumi, S., Maruyama, T., Niita, K. and Iwamoto, A.

Dynamical Simulation of Nuclear Matter(II)
Annual Meeting of the Physical Society of Japan, Hiroshima(March 28-31, 1999)

Iwamoto, A.
Effect of Nucleon Exchange Sub- and Above-Barrier Fusion
A Symposium in Honor of Ray Nix "Nuclear Shapes and Motion", Santa Fe(Oct. 25-27, 1998)

Maruyama, Toshiki, Niita, K., Maruyama, Tomoyuki, Chiba, S. and Iwamoto, A.
Nuclear Matter Structure Studied with Quantum Molecular Dynamics
International Nuclear Physics Conference 98, Paris(Aug. 24-28, 1998)

ATOMIC PHYSICS, SOLID STATE PHYSICS AND IRRADIATION EFFECTS IN MATERIALS

Journal/Proceedings

Chimi, Y., Iwase, A. and Ishikawa, N.
Electronic Exciattion Effects on Defect Production and Radiation Annealing in Fe Irradiated at ~80 K with Energetic Particles
Mat. Res. Soc. Symp. Proc. 504(1998)221.

Chimi, Y., Iwase, A. and Ishikawa, N.
Defect Accumulation Behavior in Iron Irradiated with Energetic Ions and Electrons at ~80 K
J. Nucl. Mater. 271&272(1999)236.

Huang, D.H. Sasaki, Y., Okayasu, S., Aruga, T., Hojou, K. and Ikuhara, Y.
Damage Morphology along Ion Trace in Au-Irradiated $Bi_2Sr_2CaCu_2O_x$
Phys. Rev. B 57(1998)13907.

Huang, D.H., Sasaki, Y. and Ikuhara, Y.
Influence of Ion Velocity on Damage Efficiency in the Single Ion-Target *Irradiation System:Au- $Bi_2Sr_2CaCu_2O_x$*
Phys. Rev. B 59(1999)13862.

Ishikawa, N., Chimi, Y., Iwase, A., Maeta, H., Tsuru, K., Michikami, O., Kambara, T., Mitamura, T., Awaya, Y. and Terasawa, M.
Electronic Excitation Effects in Ion-Irradiated High-Tc Superconductors
Nucl. Mater. Methods B135(1998)184.

Ishikawa, N., Chimi, Y., Iwase, A., Tsuru, K. and Michikami, O.
Defect Production and Recovery in High-Tc Superconductors Irradiated with Electrons and Ions at Low Temperature
J. Nucl. Mater. 258-263(1998)1924.

Ishikawa, N., Chimi, Y., Iwase, A., Tsuru, K. and Michikami, O.
Defect Production and Annealing in High-Tc Superconductor $EuBa_2Cu_3O_y$

Irradiated with Energetic Ions at Low-Temperature
Mat. Res. Soc. Symp. Proc. Vol.504(1999)171.

Iwase, A., Ishikawa, N., Chimi, Y., Tsuru, K., Wakana, H., Michikami, O. and Kambara, T.
High Energy Heavy Ion Irradiation Damage in Oxide Superconductor $EuBa_2Cu_3O_y$
Nucl. Instru. Meth.in Phys. Res. B146(1998)557.

Iwase, A.
Current Studies on Low Temperature Irradiation Experiments
Materia(in Japanese), Japan 37(1998)470.

Iwata, T. and Iwase, A.
Effects of Primary Recoil (PKA) Energy Spectrum on Radiation Damage in FCC Metals
Rad. Eff. Defects Solids 144(1998)27.

Itaka, K., Yasugaki, Y., Shibauchi, T., Tamegai, T. and Okayasu, S.
Novel Asymmetric Critical State in $YBa_2Cu_3O_{7-\delta}$ *with Columnar Defects*
J. Low Temperat. Phys. (Proceedings for Physics and Chemistry of Molecular and Oxide Superconductors(MOS99)).

Kawatsura, K., Imai, M., Sataka, M., Kitazawa, S., Komaki, K., Yamazaki, Y., Shibata, H., Azuma, T., Kanai, Y., Tawara, H. and Stolterfort, N.
Electron Spectra from Fast Projectile Si and S Ions Studied by Zero Degree Electron Spectroscopy
J. Electron Spectrosc. 88-91(1998)87.

Kawatsura, K., Sataka, M., Kitazawa, S., Komaki, K., Yamazaki, Y., Shibata, H., Azuma, T., Kanai, Y. Imai, Y., Tawara, H., Hansen, J.E. Kadar, I. and Stolterfort, N.
High Resolution L Auger Electron Spectra from Fast Projectile Ions Studied by Zero Degree Electron Spectroscopy
J. Electron Spectrosc. 88-91(1998)83.

Kuboyama, S., Sugimoto, S., Shugyo, S., Matsuda, S. and Hirao, T.
Single-Event Burnout of Epitaxial Transistors
IEEE Trns. Nucl. Sci. Vol. NS-45, No.6.(1998)pp. 2527-2533.

Ogikubo, K., Kobayashi, T., Terai, T. and Tanaka, S.
Effect of High-Energy Heavy-Ion Irradiation on the Superconducting Properties of Bi-2212 Single Crystals
Proceedings of the 4th International Summer School on High Temperature Superconductivity(1998) 35.

Sasase, M., Okayasu, S., Kurata, H. and Hojou, K.
Effect of Au^{24+} Ion Irradiation on the Superconductive Properties and Microstructure of $EuBa_2Cu_3O_x$ Thin Films
Surface and Coating Technology Vol. 103-104(1998)pp.360-364.

Sueyoshi, T., Ishikawa, N., Iwase, A., Chimi, Y., Kiss, T., Fujiyoshi, T. and Miyahara, K.
Transport Characteristics near the Glass-Liquid Transition Temperature Before and After Heavy-Ion Irradiation in a $YBa_2Cu_3O_y$ Thin Film
Physica C 309(1998)79.

Yuya, H., Matsui, T., Maeta, H., Ohutsuka, H. and Sugai, H.
Defect Clusters in High-Energy Ion-Irradiated Ni and Dilute Ni Alloys investigated by Diffuse X-ray Scattering
Nucl. Instru. Methods in Phys. Res. B 148(1999)891.

Meetings

Chimi, Y., Iwase, A. and Ishikawa, N.
Electronic Excitation and Atomic Displacement Induced by High-Energy Heavy Ion Irradiation in Fe
Fall Meeting of the Physical Society of Japan, Okinawa(Sept. 25, 1998).

Fujiyoshi, T., Sueyoshi, T., Ishikawa, N., Iwase, A., Chimi, Y., Kiss, T. and Miyahara, K.

Optical Response and Transport Properties of Epitaxial $YBa_2Cu_3O_y$ Thin Films with Columnar Defects
The 12th International Symposium on Superconductivity , Fukuoka(Nov. 18, 1998).

Ishikawa, N., Chimi, Y., Kuroda, N., Iwase, A. and Kambara, T.
Ion-Velocity Effects on Defects Production in High-Tc Superconductors and Metals
IX International Conference on the Physics of Highly-Charged Ions, Benzheim(Sept. 14, 1998).

Ishikawa, N., Sueyoshi, T., Iwase, A., Chimi, Y., Kiss, T., Fujiyoshi, T. and Miyahara, K.
Transport Properties in $YBa_2Cu_3O_y$ Thin Film Irradiated with Heavy Ions
Fall Meeting of Physical Society of Japan, Okinawa (Sept. 25, 1998)

Ishikawa, N., Iwase, A., Chimi, Y., Tsuru, K., Wakana, H., Michikami, O. and Kambara, T.
Defect Production through Electronic Excitation in Oxide Superconductors Irradiated with Swift Heavy Ions
Spring Meeting of the Physical Society of Japan, Hiroshima(March 28, 1999).

Ishino, S., Morita, K., Tobita, T., Chimi, Y. Ishikawa, N. and Iwase, A.
Irradiation Effects of High Energy Heavy Ion on Fe-Cu Alloys
International Group for Radiation Damage in Materials, Nashvill(January 18, 1999).

Itaka, K., Yasugaki, Y., Shibauchi, T., Tamegai, T. and Okayasu, S.
Magnetization Anomaly near Zero Field in Heavily-Ion Irradiated $YBa_2Cu_3O_{7-\delta}$
Spring Meeting of the Physical Society of Japan, Hiroshima(March 28, 1999).

Iwase, A., Ishikawa, N., Chimi, Y., Tsuru, K., Wakana, H., Michikami, O. and Kambara, T.
High Energy Heavy Ion Irradiation Damage in Oxide Superconductor $EuBa_2Cu_3O_y$

The Fourth International Symposium on Swift Heavy Ions in Matter, Berlin(May 13, 1998).

Iwase, A.
Atomic Displacements Induced by Electronic Excitation in Solids
Radiation Physics Symp. on "Electron Excitation in Solids by Ion Bombardment"
Fall Meeting of the Physical Society of Japan, Okinawa(Sept. 26, 1998).

Morita, K., Ishino, S., Tobita, T., Chimi, Y., Ishikawa, N. and Iwase, A.
Heavy Ion Irradiation Effects of Fe-Cu Model Alloys (II)
Spring Meeting of Atomic Energy Society of Japan, Hiroshima(March 25, 1998).

Morita, K., Ishino, S., Tobita, T., Chimi, Y., Ishikawa, N. and Iwase, A.
Heavy Ion Irradiation Effects of Fe-Cu Model Alloys
Fall Meeting of Atomic Energy Society of Japan, Fukui(Sept. 25, 1998).

Ogikubo, K., Kobayashi, T., Terai, T., Tanaka, S., Shimomura, J., Kishio, K., Okayasu, S. and Hojou, K.
Effect of High-Energy Heavy-Ion Irradiation on the Superconducting Properties of Bi-2212 Single Crystals
1998 International Workshop on Superconductivity, Okinawa(July 12-15, 1998).

Ogikubo, K., Kobayashi, T., Terai, T. and Tanaka, S.
Effect of High-Energy Heavy-Ion Irradiation on the Superconducting Properties of Bi-2212 Single Crystals
The 4th International Summer School on High Temperature Superconductivity, Eger., Hungary(July 18-26, 1998).

Sasase, M., Okayasu, S., Kurata, H. and Hojou, K.
Effect of Au^{24+} Ion Irradiation on the Jc of $EuBa_2Cu_3O_x$ Thin Films
Spring Meeting of the Japan Society of Applied Physics, Tokyo(March 31, 1998)

Sasase, M. Kurata, H. and Hojou, K.
Defect Structure of $EuBa_2Cu_3O_x$ Thin Films by High-Energy Heavy Ion Irradiation
The 11th International Conference on Ion Beam Modification of Materials(IBMM'98), Amsterdam(Sept. 1, 1998).

Sataka, M., Imai, M., Yamazaki, Y., Komaki, K., Kawatsura, K., Kanai, Y. Tawara, H., Schultz, D.R. and Reinhold, C.O.
Binary Electron Production by Highly Charged Heavy Ions
Symposium on Heavy-Ion Science in the Tandem Energy Region, Mito(January 13, 1999).

Sataka, M.
Zero-degree Electron Spectroscopy of Ion-Atom Collisions
Symposium on Heavy-Ion Science in the Tandem Energy Region, Mito(January 13, 1999).

Sueyoshi, T., Ishikawa, N., Iwase, A., Chimi, Y., Kiss, T., Fujiyoshi, T. and Miyahara, K.
Critical Scaling Analysis of Transport Characteristics before and after Heavy-Ion Irradiation in a $YBa_2Cu_3O_y$ Thin Film
The 12th International Symposium on Superconductivity , Fukuoka(Nov. 18, 1998).

Suzuki, T., Sugimoto, K., Shugo, S., Kuboyama, S., Matsuda, S., Hirao, T., Nashiyama, I., Hirose, T. and Ohira, H.
Tolerance for Single-Event Effect of Bipolar Transistors for Space and Commercial System Application
The Institute of electronics, Information and Communication Engineers, Tokyo (March 13, 1998).

Suzuki, T., Kuboyama, s., Matsuda, S., Hirao, T., Nashiyama, I., Hirose, T. and Ohira, H.
Evaluation of SEB in Power Transistors for Commercial System Application
The Institute of Electronics, Information and Communication Engineers, Yamanashi (Sept. 30, 1998).

This is a blank page.

7. Personnel and Committees

This is a blank page.

(1) Personnel (FY 1998)

Department of Materials Science

Hiroshi	Katsuta	Director
Akira	Iwamoto	Deputy Director
Satoshi	Takemori	Administrative Manager

Accelerator Division

Scientific Staff

Tadashi	Yoshida*
Suehiro	Takeuchi
Susumu	Hanashima
Makoto	Matsuda

Technical Staff

Susumu	Kanda
Isao	Ohuchi
Katsuzo	Horie
Shinichi	Abe
Nobuhiro	Ishizaki
Hidekazu	Tayama

Materials Innovation Laboratory

Akira	Iwamoto*
Tetsuya	Nakazawa
Daijyu	Yamaki
Akihiro	Iwase
Norito	Ishikawa
Yasuhiro	Chimi
Naoshi	Kuroda
Kenji	Morita

Solid State Physics Laboratory

Kiichi	Hojou*
Masao	Sataka
Satoru	Okayasu
Sin-iti	Kitazawa
Hideo	Ohtsuka

Teruo Kato
Masato Sasase

Nuclear Chemistry Laboratory

Toshiaki Sekine*
Nobuo Shinohara
Yuichi Hatsukawa
Hideki Iimura
Kentaro Hata

Advanced Science Research Center

Research Group for Exotic Heavy Nuclei

Hiroshi Ikezoe*
Yasuharu Sugiyama
Tetsuro Ishii
Shin-ichi Mitsuoka

Research Group for Hadron Science

Satoshi Chiba*
Toshiki Maruyama

Research Group for Inverse Compton Gamma-ray Spectroscopy

Masumi Oshima
Michiaki Sugita

Research Group for Nuclear Chemistry of Heavy Elements

Yuichiro Nagame*
Shin-ichi Ichikawa
Kazuaki Tsukada
Ichiro Nishinaka

Department of Nuclear Energy System

Nuclear Data Center

Akira Hasegawa*
Jun-ichi Katakura
Tokio Fukahori

Osamu Iwamoto

Department of Radioisotopes

Isotope Research and Development Division

Hiroyuki Sugai

Department of Health Physics

Radiation Control Division II

Yukihiro Miyamoto

Yuuichi Takaba

Tohru Tayama

Advanced Photon Research Center

Free Electron Laser Research Group

Takehito Hayakawa

* Head

(2)Tandem Consultative Committee

(Chairman)	Shinzo	Saito	(Director General, Tokai Research Establishment)
(Vice Chairman)	Kunihisa	Soda	(Deputy Director General, Tokai Research Establishment)
(Vice Chairman)	Hiroshi	Katsuta	(Director, Department of Materials Science)
	Hiroyasu	Ejiri	(Professor, Osaka University)
	Kohei	Furuno	(Professor, Tsukuba University)
	Naohiro	Hirakawa	(Professor, Tohoku University)
	Jun	Imasato	(Professor, National Laboratory for High Energy Physics)
	Masayasu	Ishihara	(Professor, The University of Tokyo, Research Scientist, Institute of Physics and Chemical Research)
	Yasuo	Ito	(Associate professor, The University of Tokyo)
	Kenji	Katori	(Professor, Osaka University)
	Hisaaki	Kudo	(Associate professor, Niigata University)
	Hiroshi	Kudo	(Professor, Tsukuba university)
	Kohzoh	Masuda	(Professor emeritus, University of Tsukuba)
	Shunpei	Morinobu	(Professor, Kyushu University)
	Kenji	Morita	(Professor, Nagoya University)
	Hiroshi	Nakahara	(Professor, Tokyo Metropolitan University)
	Masaharu	Nakazawa	(Professor, The University of Tokyo)
	Naoto	Sekimura	(Associate professor, The University of Tokyo)
	Akito	Takakahashi	(Professor, Osaka University)
	Hiroyuki	Tawara	(Professor, Institute of Plasma Physics, Nagoya University)
	Hiroshi	Maekawa	(Head, Division of Collaborative Activities)
	Akira	Iwamoto	(Deputy Director, Department of Materials

			Science)
	Masao	Sataka	(Solid State Physics Laboratory)
(Secretary)	Satoshi	Takemori	(Administrative Manager, Department of Materials Science)
(Secretary)	Suehiro	Takeuchi	(Accelerator Division)
(Secretary)	Tadashi	Yoshida	(Head, Accelerator Division)

(3)Program Advisery Committee

(a) Sub-committee for Nuclear Physics and Nuclear Chemistry

	Akira	Iwamoto	(Deputy Director, Department of Materials Science)
	Kenji	Katori	(Professor, Osaka University)
	Hiromichi	Nakahara	(Professor, Tokyo Metropolitan University)
	Shunpei	Morinobu	(Professor, Kyushu University)
	Kouhei	Furuno	(Professor, Tsukuba University)
	Hiroshi	Ikezoe	(Head, Research Group for Fusion of Heavy Deformed Nuclei)
	Toshiaki	Sekine	(Head, Nuclear Chemistry Laboratory)
(Secretary)	Suehiro	Takeuchi	(Accelerator Division)
(Secretary)	Tadashi	Yoshida	(Head, Accelerator Division)

(b) Sub-committee for Materials and Radiation Damage

	Akira	Iwamoto	(Deputy Director, Department of Materials Science)
	Naoto	Sekimura	(Associated Professor, Tokyo University)
	Hiroyuki	Tawara	(Professor, National Institute for Fusion Science)
	Kenji	Morita	(Professor, Nagoya University)
	Hiroshi	Kudo	(Professor, Tsukuba University)
	Kiichi	Hojou	(Head, Solid State Physics)
	Akihiro	Iwase	(Materials Innovation Laboratory)
(Secretary)	Suehiro	Takeuchi	(Accelerator Division)
(Secretary)	Tadashi	Yoshida	(Head, Accelerator Division)

This is a blank page.

8. Cooperative Researches

This is a blank page.

Title	Contact person Organization
1. Systematic Investigation on Magnetic Rotation in Atomic Nucleus	Masahiko SUGAWARA Department of Natural science Chiba Institute of Technology
2. Study of Electromagnetic Properties of Nuclear High-spin State through Crystal Ball (II)	Tetsuro KOMATSUBARA Tandem Accelerator Center, University of Tsukuba
3. Investigation on Anomalous Phenomena of Electromagnetic transitions between Multipole Deformed State	Hideshige KUSAKARI Faculty of Education Chiba University
4. Nuclear Structure of Neutron-rich Nuclei through Deep Inelastic Collisions	Masao OGAWA Department of Energy Science, Tokyo Institute of Technology
5. Dependence of Bimodal Fission on Excitation Energy	Hiromichi NAKAHARA Faculty of Science, Tokyo Metropolitan University
6. Precise measurement of Gamma-ray Emission Probability for Proton-rich nuclides	Hiroshi MIYAHARA Department of Radiological Technology School of Health Science Nagoya University
7. α-cluster Structure in Heavy Nuclei	Takemi NAKAGAWA Faculty of Science, Tohoku University

8. Correlation between Fragment Deformation and Mass Division Modes in Actinide Fission	Tadashi SAITOH Faculty of Science, Osaka University
9. Study of Single-events Induced by High Energy Ions	Sumio MATSUDA NASDA
10. High-energy Ion Beam Irradiation of Functional Electronic Materials	Takayuki TERAI Engineering Research Institute, School of Engineering, University of Tokyo
11. Study of Sputtering due to electronic Excitation by Heavy ion bombardments	Mititaka TERASAWA Faculty of Engineering, Himeji Institute of Technology
12. Study of Electron spectra due to Collision of Highly Charged Ions	Ken-ichiro KOMAKI Graduate School of Arts and Science, University of Tokyo
13. Study of the Property and Microstructure on the Oxide Superconductors Irradiated with High Energy Ions	Yukichi SASAKI Japan Fine Ceramics Center
14. Vortex Motion of High Tc Superconductors Irradiated by Heavy ions	Tsuyoshi TAMEGAI Associated Professor Department of Applied Physics University of Tokyo
15. Study of Vortex State for High Tc Superconductors with Columnar Defects	Kazuo KADOWAKI Professor of Materials Science University of Tsukuba

16. Electron Wave Interference Effects in the Ballistic conductive Region due to Defects induced by Heavy Ion Irradiation

Yuuichi OCHIAI
Professor
Department of Materials Technology
Chiba University

This is a blank page.

国際単位系 (SI) と換算表

表 1　SI 基本単位および補助単位

量	名称	記号
長さ	メートル	m
質量	キログラム	kg
時間	秒	s
電流	アンペア	A
熱力学温度	ケルビン	K
物質量	モル	mol
光度	カンデラ	cd
平面角	ラジアン	rad
立体角	ステラジアン	sr

表 2　SI と併用される単位

名称	記号
分，時，日	min，h，d
度，分，秒	°，′，″
リットル	l，L
トン	t
電子ボルト	eV
原子質量単位	u

1 eV = 1.60218 × 10^{-19} J

1 u = 1.66054 × 10^{-27} kg

表 3　固有の名称をもつ SI 組立単位

量	名称	記号	他の SI 単位による表現
周波数	ヘルツ	Hz	s^{-1}
力	ニュートン	N	$m\cdot kg/s^2$
圧力，応力	パスカル	Pa	N/m^2
エネルギー，仕事，熱量	ジュール	J	N·m
工率，放射束	ワット	W	J/s
電気量，電荷	クーロン	C	A·s
電位，電圧，起電力	ボルト	V	W/A
静電容量	ファラド	F	C/V
電気抵抗	オーム	Ω	V/A
コンダクタンス	ジーメンス	S	A/V
磁束	ウェーバ	Wb	V·s
磁束密度	テスラ	T	Wb/m^2
インダクタンス	ヘンリー	H	Wb/A
セルシウス温度	セルシウス度	℃	
光束	ルーメン	lm	cd·sr
照度	ルクス	lx	lm/m^2
放射能	ベクレル	Bq	s^{-1}
吸収線量	グレイ	Gy	J/kg
線量当量	シーベルト	Sv	J/kg

表 4　SI と共に暫定的に維持される単位

名称	記号
オングストローム	Å
バーン	b
バール	bar
ガル	Gal
キュリー	Ci
レントゲン	R
ラド	rad
レム	rem

1 Å = 0.1 nm = 10^{-10} m

1 b = 100 fm^2 = 10^{-28} m^2

1 bar = 0.1 MPa = 10^5 Pa

1 Gal = 1 cm/s^2 = 10^{-2} m/s^2

1 Ci = 3.7 × 10^{10} Bq

1 R = 2.58 × 10^{-4} C/kg

1 rad = 1 cGy = 10^{-2} Gy

1 rem = 1 cSv = 10^{-2} Sv

表 5　SI 接頭語

倍数	接頭語	記号
10^{18}	エクサ	E
10^{15}	ペタ	P
10^{12}	テラ	T
10^{9}	ギガ	G
10^{6}	メガ	M
10^{3}	キロ	k
10^{2}	ヘクト	h
10^{1}	デカ	da
10^{-1}	デシ	d
10^{-2}	センチ	c
10^{-3}	ミリ	m
10^{-6}	マイクロ	μ
10^{-9}	ナノ	n
10^{-12}	ピコ	p
10^{-15}	フェムト	f
10^{-18}	アト	a

（注）

1. 表 1 − 5 は「国際単位系」第 5 版，国際度量衡局 1985 年刊行による。ただし，1 eV および 1 u の値は CODATA の 1986 年推奨値によった。
2. 表 4 には海里，ノット，アール，ヘクタールも含まれているが日常の単位なのでここでは省略した。
3. bar は，JIS では流体の圧力を表わす場合に限り表 2 のカテゴリーに分類されている。
4. EC 閣僚理事会指令では bar，barn および「血圧の単位」mmHg を表 2 のカテゴリーに入れている。

換　算　表

力	N(=10^5 dyn)	kgf	lbf
	1	0.101972	0.224809
	9.80665	1	2.20462
	4.44822	0.453592	1

粘度　1 Pa·s(N·s/m^2) = 10 P(ポアズ)(g/(cm·s))

動粘度　1 m^2/s = 10^4 St(ストークス)(cm^2/s)

圧力	MPa(=10 bar)	kgf/cm^2	atm	mmHg(Torr)	lbf/in^2(psi)
	1	10.1972	9.86923	7.50062 × 10^3	145.038
	0.0980665	1	0.967841	735.559	14.2233
	0.101325	1.03323	1	760	14.6959
	1.33322 × 10^{-4}	1.35951 × 10^{-3}	1.31579 × 10^{-3}	1	1.93368 × 10^{-2}
	6.89476 × 10^{-3}	7.03070 × 10^{-2}	6.80460 × 10^{-2}	51.7149	1

エネルギー・仕事・熱量	J(=10^7 erg)	kgf·m	kW·h	cal(計量法)	Btu	ft·lbf	eV
	1	0.101972	2.77778 × 10^{-7}	0.238889	9.47813 × 10^{-4}	0.737562	6.24150 × 10^{18}
	9.80665	1	2.72407 × 10^{-6}	2.34270	9.29487 × 10^{-3}	7.23301	6.12082 × 10^{19}
	3.6 × 10^6	3.67098 × 10^5	1	8.59999 × 10^5	3412.13	2.65522 × 10^6	2.24694 × 10^{25}
	4.18605	0.426858	1.16279 × 10^{-6}	1	3.96759 × 10^{-3}	3.08747	2.61272 × 10^{19}
	1055.06	107.586	2.93072 × 10^{-4}	252.042	1	778.172	6.58515 × 10^{21}
	1.35582	0.138255	3.76616 × 10^{-7}	0.323890	1.28506 × 10^{-3}	1	8.46233 × 10^{18}
	1.60218 × 10^{-19}	1.63377 × 10^{-20}	4.45050 × 10^{-26}	3.82743 × 10^{-20}	1.51857 × 10^{-22}	1.18171 × 10^{-19}	1

1 cal = 4.18605 J（計量法）

= 4.184 J　（熱化学）

= 4.1855 J　（15 °C）

= 4.1868 J（国際蒸気表）

仕事率　1 PS（仏馬力）

= 75 kgf·m/s

= 735.499 W

放射能	Bq	Ci
	1	2.70270 × 10^{-11}
	3.7 × 10^{10}	1

吸収線量	Gy	rad
	1	100
	0.01	1

照射線量	C/kg	R
	1	3876
	2.58 × 10^{-4}	1

線量当量	Sv	rem
	1	100
	0.01	1

（86 年 12 月 26 日現在）